Departamento de Electromagnetismo y Física de la Materia
Universidad de Granada

Fluctuaciones fuera del Equilibrio en Sistemas Difusivos

Carlos Pérez Espigares

Directores: Pablo I. Hurtado Fernández y Pedro L. Garrido Galera
–

– Granada, noviembre de 2012 –

Editor: Editorial de la Universidad de Granada
Autor: Carlos Pérez Espigares
D.L.: GR 867-2013
ISBN: 978-84-9028-459-9

D. Pablo I. Hurtado Fernández y D. Pedro L. Garrido Galera,
CERTIFICAN que la presente memoria, *Fluctuations out of Equilibrium in Diffusive Systems* (*Fluctuaciones fuera del Equilibrio en Sistemas Difusivos*), ha sido realizada por D. Carlos Pérez Espigares bajo su dirección en el Departamento de Electromagnetismo y Física de la Materia, así como que éste ha disfrutado de una estancia en el extranjero, durante un periodo de tres meses, en el Laboratoire de Physique et Mécanique des Milieux Hétérogènes.

Granada, 16 de Noviembre de 2012

Fdo: Pablo I. Hurtado Fernández y Pedro L. Garrido Galera

Agradecimientos

Tras haber concluido este trabajo, no queda más que expresar mi gratitud a todos aquellos que en estos años me han apoyado tanto. En primer lugar, mi más sincero agradecimiento a mis directores de tesis, Pablo Hurtado y Pedro Garrido, por todo lo que he aprendido y lo mucho que me han ayudado en todo momento. También quiero agradecer a todos los compañeros y amigos del departamento, con los que he tenido la suerte de compartir tanto tiempo, que con ellos, he pasado una de las mejores etapas de mi vida.

Finalmente, quiero darle las gracias a mi familia. Sin su constante apoyo y comprensión, este trabajo no hubiera sido posible.

Contents

Resumen de la Tesis

En las últimas dos décadas se ha experimentado un gran avance en en el entendimiento de los sistemas fuera del equilibrio. Sin embargo, a pesar de los esfuerzos en esta dirección, aún no se ha logrado establecer una teoría general que permita describir la física macroscópica de los sistemas de no-equilibrio a partir de sus propiedades microscópicas. Una teoría general para entender estos sistemas sería de gran importancia ya que la mayoría de procesos presentes en la naturaleza están lejos del equilibrio.

La física estadística del equilibrio trata de explicar las propiedades macroscópicas de la materia a partir de sus constituyentes microscópicos. Es una teoría que nos permite obtener el valor medio de observables macroscópicos y el de sus *fluctuaciones* a partir únicamente de la distribución de probabilidad de Gibbs, sin tener que resolver ninguna ecuación de movimiento para los constituyentes microscópicos. Consideremos por ejemplo un sistema en contacto con dos baños térmicos a temperaturas T_L y T_R. Se dice que el sistema está en equilibrio si las dos temperaturas son iguales ($T_L = T_R = T$). En este caso la probabilidad de encontrar al sistema en una configuración microscópica C viene dada por la distribución de Gibbs

$$P_{\text{equilibrium}}(C) = Z^{-1} \exp\left[\frac{-E(C)}{k_B T}\right] \tag{1}$$

donde $E(C)$ es la energía interna del sistema en la configuración C, k_B es la constante de Boltzmann y Z es la función de partición. La tarea de la mecánica estadística del equilibrio es pues derivar las propiedades macroscópicas (ecuaciones de estado, transiciones de fase, puntos críticos, etc) desde la Eq. (1) como punto de partida. Un aspecto simplificador de (1) es que no depende ni de la naturaleza del acoplamiento con los baños ni de los detalles de la dinámica. Todo lo que necesitamos saber es la energía de las configuraciones microscópicas.

Por el contrario, si las temperaturas de los baños son diferentes ($T_L \neq T_R$), el sistema alcanza en el límite de tiempos largos un estado estacionario de no-equilibrio y, a diferencia del sistema en equilibrio, no existe una expresión que generalice (1) para la probabilidad $P(C)$ de las configuraciones microscópicas en el estado estacionario

$$P_{\text{non-equilibrium}}(C) = ? \tag{2}$$

De hecho, para un sistema fuera del equilibrio, la medida $P(C)$ del estado estacionario depende en general de la dinámica del sistema y del acoplamiento

con los baños térmicos y su cálculo a partir de la diámica microscópica es un problema realmente difícil que solamente se ha resuelto para modelos muy sencillos [5, 6, 7]. Por eso, lejos del equilibrio, el objeto básico que permita definir equivalencias con la entropía y los potenciales termodinámicos para hacer así una extensin natural de la termódinámica, no es directamente accesible.

Sin embargo, la física estadística del equilibrio nos ofrece un camino alternativo a la teoría de colectividades para derivar los potenciales termódinaámicos. Esta alternativa consiste en estudiar el comportamiento macroscópico fluctuante del sistema. Esta observación fundamental se puede generalizar a sistemas fuera del equilibrio [8]-[20], donde no existe una teoría general capaz de predecir el comportamiento macroscópico y fluctuante en términos de la física micróspica.

Para el caso de equilibrio se puede demostrar que, conforme el volumen del sistema se hace más grande (pero finito), podemos expresar la probabilidad de observar una fluctuación de la densidad como la exponencial de una función multiplicada por el volumen, i.e.,

$$P(\rho) \sim \exp\left[+v\mathcal{I}\left(\rho\right)\right]. \tag{3}$$

Se dice entonces que dicha probabilidad sigue un principio de grandes desviaciones [23, 24]. A la función $\mathcal{I}(\rho)$ se le conoce como función de grandes desviaciones (LDF, por sus siglas en inglés) y nos da una idea del ritmo al que se concentra la probabilidad alrededor del valor medio conforme el volumen crece. En equilibrio se demuestra (véase la introducción de la tesis) que esta LDF está unívocamente relacionada con la energía libre del sistema, a partir de la cual podemos describir todas las propiedades macroscópicas del mismo.

Esta conexión bien establecida en equilibrio entre fluctuaciones de observables macroscópicos y potenciales termódinamícos, es la que ha motivado el estudio de tales fluctuaciones en sistemas fuera del equilibrio. Por tanto, uno de los objetivos más importantes de la física estadística del no-equilibrio, es encontrar el observable macróscopico adecuado que permita, a través del estudio de sus fluctuaciones, definir el equivalente a un potencial termódinámico, desde el cual se puedan derivar las propiedades macrosópicas del sistema, como ocurre en el caso de equilibrio. Para poder establecer esa equivalencia, es necesario expresar la probabilidad de las fluctuaciones del observable como un principio de grandes desviaciones, lo que nos lleva a centrarnos en el estudio de la LDF que es la que caracteriza dicha probabilidad.

Por un lado, como extensión natural del caso de equilibrio, uno de los observables macroscópicos a estudiar para sistemas de no-equilibrio es la densidad. Esto ha conducido a resultados muy interesantes [32] en los que la LDF de la densidad ha permitido describir propiedades macroscópicas del sistema (como por ejemplo las correlaciones de largo alcance, una de las propiedades ms relevantes de los sistemas fuera del equilibrio).

Sin embargo, nosotros estamos interesados en sistemas caracterizados por

algún observable macroscópico que se conserva localmente (e.g. energía, densidad de partículas, momento). En este tipo de sistemas es razonable pensar que el observable macroscópico más relevante es la corriente que se forma cuando ponemos a dicho sistema fuera del equilibrio mediante la acción de un campo externo, o aplicando un gradiente en sus extremos. Esta es la razón por la que el estudio de la estadística de la corriente en términos de la física microscópica se ha convertido en uno de los principales focos de atención de la física estadística del no-equilibrio en las últimas dos décadas [8]-[20]. Esta actividad ha llevado a un gran número de resultados interesantes válidos arbitrariamente lejos del equilibrio. Probablemente el resultado más importante obtenido hasta ahora, es el llamdo teorema de fluctuación de Gallavotti-Cohen [8, 9, 12], que manifiesta las sutiles consecuencias de la reversibilidad temporal a nivel macroscópico. La lista de reultados continúa sin embargo con la igualdad de Jarzynski [25] o el teorema de fluctuación de Crooks [26], hasta la relación de Hatano-Sasa [27] o la reciente extensión de la desigualdad de Clausius a estados estacionarios fuera del equilibrio [28].

En esta tesis nos hemos centrado en el estudio de las fluctuaciones de la corriente en sistemas difusivos. Como hemos visto, la corriente puede ser un buen observable macroscópico con el que caracterizar a los sistemas fuera del equilibrio. En concreto, nuestro objetivo es calcular la LDF de varios sistemas y tratar de derivar a partir de ella propiedades generales de los sistemas de no-equilibrio. El marco teórico en el que nos hemos basado, es la llamada teoría macroscópica fluctante (MFT, por sus siglas en inglés), desarrollada por Bertini y colaboradores en los últimos diez años [15]-[18]. Esta teoría, descrita en el capítulo 1, describe en detalle las fluctuaciones dinámicas en sistemas difusivos, ofreciendo predicciones para la LDF a partir del conocimiento de la ecuación de evolución macróscopica (o hidrodinmica) del sistema y sólo dos coeficientes de transporte. La MFT es un marco teórico muy general y de amplia aplicación que normalmente desemboca en un problema variacional complicado cuya solución exacta es difícil en la mayoría de los casos. Como consecuencia, en el capítulo 3 de esta tesis, se suponen dos hipótesis simplificadoras que nos permiten resolver el problema variacional. Estas hipótesis consituyen la "conjetura de aditividad", cuyo nombre se debe a que su versión unidimensional es equivalente al Principio de Aditividad (Additivity Principle) postulado por Bodineau y Derridad en 2004 [34].

Para determinar la LDF de la corriente integrada en el tiempo aplicando la MFT dados los coeficientes de transporte, es necesario minimizar un funcional sobre los campos de corriente y de densidad, que en general, pueden depender del tiempo y el espacio. Estos campos están relacionados por la ecuación de continuidad. Esto, como hemos señalado anteriormente, es un problema variacional muy complicado pero que, suponiendo la "conjetura de aditividad" sí se puede resolver. La citada conjetura supone lo siguiente:

i Los campos óptimos de densidad y de corriente que minimizan el funcional, responsables de producir una fluctuación de la corriente, son independientes del tiempo.

ii El campo de corriente, a su vez, no tiene estructura espacial, con lo

que es constante.

Con estas dos hipótesis, somos capaces de calcular explícitamente la función de grandes desviaciones de la corriente integrada en el tiempo, obteniendo así la probabilidad de observar dicha corriente transcurrido un tiempo largo pero finito. Hay que resaltar que cuando estudiamos las fluctuaciones de la corriente integrada en el tiempo, dicho tiempo juega el mismo papel que el volumen para el caso de las fluctuaciones de la densidad. De ahí la necesidad de considerar tiempos largos para poder expresar las fluctuaciones de la corriente como un principio de grandes desviaciones. En el capítulo 3, se calcula de manera teórica la LDF de la corriente integrada en un modelo paradigmático de transporte difusivo. Este es el modelo de Kipnis-Marchioro-Presutti (KMP), descrito en detalle en el capítulo 2. Una vez que tenemos la predicción teórica de la LDF de la corriente suponiendo la conjetura de aditividad, comprobamos la validez de la misma realizando sofisticadas simulaciones numéricas. En este punto, es importante destacar el papel fundamental que desempeñan las dichas simulaciones, ya que representan el "laboratorio experimental" donde comprobar y acotar la validez de las aproximaciones que se realizan en la teoría. Analizando los resultados numéricos obtenidos para el modelo KMP, llegamos a la conclusión de que la conjetura de aditividad se cumple para un amplio rango de fluctuaciones de la corriente. Además, uno de los resultados a resaltar, es que el perfil de densidad (independiente del tiempo) que minimiza el funcional para una fluctación de la corriente dada, es de hecho el que medimos en las simulaciones. Esto indica que el sistema adopta precisamente ese perfil para producir dicha fluctuación.

Hay que decir que nos hemos centrado en el modelo KMP bidimensional [43]. De hecho la segunda hipótesis de la conjetura de aditividad tiene sentido para sistemas de más de una dimensión. El porqué de ir a dos dimensiones es debido a que una gran cantidad de nuevos fenómenos y simetrías aparecen para sistemas con dimensión mayor que uno. Este hecho se refleja en el capítulo 4, donde se deriva una nueva relación de fluctuación isómetrica (IFR) [10] para fluctuaciones de la corriente en sistemas d-dimensionales reversibles temporalmente y descritos por un único campo localmente conservado.. En general, un sistema con muchos grados de libertad transita un camino óptimo en el espacio mesoscópico (coarse-grained) de las fases para facilitar una fluctuación dada. Tal y como ha quedado demostrado en los tests de aditividad realizados en el capítulo 3, este camino óptimo es un observable físico bien definido. Usando las herramientas de la MFT, se puede demostrar que bajo condiciones muy generales y en dimensión arbitraria, este camino óptimo permanece invariante bajo ciertas transformaciones de simetría sobre el vector corriente [10]. Usando esta invariancia, se demuestra que en un sistema d-dimensional reversible temporalmente y descrito por un único campo localmente conservado, la probabilidad de observar una fluctuación dada del vector corriente empírico (promediado en espacio y tiempo) obedece la siguiente relación de fluctuación isométrica (IFR, por sus siglas

en inglés)

$$\lim_{\tau\to\infty} \frac{1}{\tau} \ln\left[\frac{\mathrm{P}_\tau(\mathbf{J})}{\mathrm{P}_\tau(\mathbf{J}')}\right] = \boldsymbol{\epsilon}\cdot(\mathbf{J}-\mathbf{J}')\,, \tag{4}$$

para cualquier par de vectores corriente isométricos, $|\mathbf{J}| = |\mathbf{J}'|$. $P_\tau(\mathbf{J})$ es la probabilidad de observar una fluctuación de la corriente $\mathbf{J}$ integrada en un tiempo τ. En la ecuación anterior $\boldsymbol{\epsilon} = \boldsymbol{\varepsilon} + \mathbf{E}$ es un vector constante directamente relacionado con el ritmo de producción de entropía en el sistema, y que depende de los baños térmicos del borde a través de $\boldsymbol{\varepsilon} = (\rho_R^{-1} - \rho_L^{-1})\hat{\mathbf{n}}$ siendo $\hat{\mathbf{n}}$ el versor que apunta en la dirección del gradiente externo y ρ_L, ρ_R la temperatura de los baños térmicos. La ecuación anterior, que incluye como caso particular el teorema de Gallavotti y Cohen cuando $\mathbf{J}' = -\mathbf{J}$, relaciona de una manera sorprendentemente sencilla la probabilidad de una flctuación de corriente $\mathbf{J}$ con la de cualquier otro vector corriente en la misma hiperesfera d-dimensional de radio $\mathbf{J}$, proyectando el problema complicado de determinar la distribución de probabilidad $P_\tau(\mathbf{J})$ en d-dimensiones en un problema muchos más sencillo en sólo una dimensión. Al contrario de lo que sucede con la relación de Gallavotti y Cohen, que es una simetría no diferenciable que implica el cambio de signo de la corriente, la IFR es válida para cambios de orientación arbitrarios del vector corriente. Esto hace que la verificación experimental de esta relación sea plausible, al contrario de lo que sucede con el teorema de Gallavotti y Cohen, ya que podemos generar suficiente estadística para fluctuaciones isométricas alrededor de la corriente media y así garantizar la precisión del experimento. Es importante subrayar que la IFR se cumple para fluctuaciones arbitrariamente grandes, incluso en las colas no gaussianas de la distribución.

Cabe destacar, que la relación de fluctuación isométrica se demuestra de manera sencilla en el marco de la MFT, una vez suplementada con el conjetura de aditividad. Además, se puede comprobar que el perfil óptimo de densidad depende de $\mathbf{J}^2$, con lo que solo depende exclusivamente del módulo de $\mathbf{J}$ y no se su orientación. De esta forma, todas las fluctuaciones de corriente isométricas entre sí (esto es, caracterizadas por un módulo $|\mathbf{J}|$ constante) tendrán asociado el mismo perfil óptimo de densidad, independientemente de si el vector $\mathbf{J}$ apunta en la dirección del gradiente externo, en contra del gradiente o en cualquier otra dirección. En otras palabras, el perfil óptimo es invariante frente a rotaciones del vector corriente. En el capítulo 4 se demuestra que esta invarianza no es más que una consecuencia de la reversibilidad temporal de la dinámica.

La relación de fluctuación isométrica tiene implicaciones profundas en las propiedades de no-equilibrio de un sistema. En particular, la IFR implica una familia sorprendente de jerarquías en los cumulantes de la distribución de corriente y los coeficientes de respuesta no-lineal del sistema, válidas arbitrariamente lejos del equilibrio, y que van mucho más allá que las relaciones de reciprocidad de Onsager y las fórmulas de Green-Kubo.

Es importante señalar que la relación de fluctuación isométrica, un avance derivado en el marco de la teoría macroscópica fluctuante, ha sido confirmada con todo detalle en simulaciones a gran escala de dos modelos de no-equilibrio diferentes: (i) El modelo KMP de transporte en dos dimensiones, y (ii) un fluido de discos duros en un gradiente de temperatura [10]. En este

último caso el sistema de interés obedece las ecuaciones de la hidrodinámica, estando caracterizado por cuatro campos localmente conservados diferentes, lo que claramente se sale del rango de aplicabilidad de la MFT. La validez de la IFR en este contexto sugiere por tanto esta relación de fluctuación, basada en la invariancia de los perfiles óptimos frente a transformaciones de simetría, es de hecho un resultado muy general válido para sistemas hidrodinámicos mesoscópicos arbitrarios.

Como hemos visto, la teoría macroscópica fluctuante nos permite estudiar fluctuaciones dinámicas en sistemas difusivos, ofreciendo predicciones concretas para la función de grandes desviaciones del observable de interés y el camino óptimo en el espacio de las fases mesoscópico responsable de una fluctuación dada. Este camino óptimo es en general un objeto dinámico que puede depender del tiempo, aunque ya hemos visto que en la práctica, y de acuerdo con el conjetura de aditividad, el camino óptimo resulta ser independiente del tiempo para un rango amplio de fluctuaciones (ver capítulo 3). Sin embargo, para sistemas periódicos la MFT indica que el camino óptimo pasa a ser dependiente del tiempo a partir de un valor crítico de la fluctuación de la corriente. Esto se interpreta como una transición de fase dinámica. En el capítulo 5 se observa esta transición de fase para otro modelo difusivo paradigmático: el proceso de exclusión simple débilmente asimétrico (WASEP, por sus siglas en inglés). Se hace en una y dos dimensiones. En este caso se observa que los perfiles adoptan una estructura de tipo onda viajera que se mueve a velocidad constante. Otro aspecto sorprendente es que el para el régimen dependiente del tiempo, la IFR se sigue cumpliendo, haciendo así extensiva su validez para perfiles dependientes del tiempo con estructura tipo onda viajera.

Por último, en el capítulo 6, nos salimos del marco de la MFT y explotamos la anteriormente citada relación de Hatano-Sasa [27]. Esta relación generaliza la igualdad de Jarzynski [25] generalizando de esta forma la segunda ley para transiciones entre estados estacionarios. Sin embargo, para poder aplicar la relación de Hatano-Sasa hemos de conocer *a priori* la distribución estacionaria de probabilidad. En lugar de esto, lo que se propone en el capítulo 6 es usar con distribuciones de probabilidad arbitrarias "de referencia" que sean suaves, de manera que uno pueda tratar sistemas cuya distribución estacionaria es demasiado difícil de calcular, como generalmente ocurre en los sistemas fuera del equilibrio con muchos grados de libertad. Haciendo esto, demostramos [29] que cada conjunto de distribuciones de referencia da lugar a una desigualdad que juega el papel de una generalización de la segunda ley. Cuanto mejor es la aproximación de la distribución de referncia a la estacionaria, más restringida es la desigualdad. Esto da lugar a un procedimiento de optimización de la distribución de referencia que puede ser implementado numérica o experimentalmente.

Introduction

Fluctuations arise universally in Nature as a reflection of the discrete microscopic world at the macroscopic level. Despite their apparent noisy origin, fluctuations encode fundamental aspects of the physics of the system at hand. One of the first examples of the importance of fluctuations is given by Einstein's paper on brownian motion [1]. From the study of fluctuations in the movement of a mesoscopic particle suspended in a liquid, Einstein was able to determine the size of the molecules of the liquid, thus confirming the molecular hypothesis. Another relevant examples range from the role of fluctuations to understand critical phenomena beyond mean-field phenomenological theories [2] to the study of fluctuations of spatio-temporal correlations in glasses and amorphous materials, which has revealed the existence of universal dynamical heterogeneities [3]. Particularly interesting are the fluctuations of the measured cosmic background radiation temperature in cosmology [4], whose origin goes back to the presence of small inhomogeneities in the matter distribution of the primordial universe, offering a framework to understand the origin of the universe structure at a macroscale. In addition, fluctuations inherit the microscopic symmetries, reflecting them at the macroscopic level. Examples of these symmetries at the fluctuating level are the Gallavotti-Cohen Fluctuation Theorem [8], or the recently introduced Isometric Fluctuation Relation [10], which are deep statements on the subtle consequences of time-reversal symmetry of microscopic dynamics at the macroscopic, irreversible level.

Equilibrium statistical mechanics attempts to explain the macroscopic properties of matter in terms of the interaction of its microscopic constituents. The basic paradigm of this theory states that in order to obtain the typical value of macroscopic observables and their *fluctuations* we do not have to solve any equation of motion of the microscopic constituents and the calculations can be performed by using the Gibbs distribution. Let us consider for instance a sytem in contact with two heat baths at temperature T_L and T_R, see figure 1.d. The system is in equilibrium when the heat baths are at the same temperature ($T_L = T_R = T$). In this case, the probability of finding the system in a certain microscopic configuration C is given by the Gibbs distribution

$$P_{\text{equilibrium}}(C) = Z^{-1} \exp\left[\frac{-E(C)}{k_B T}\right] \tag{5}$$

where $E(C)$ is the internal energy of the system in configuration C, k_B is Boltzmann's constant and Z is the partition function. Then the task of equilibrium statistical mechanics is to derive macroscopic properties (equations of states, phase transitions, critical points, etc) from (5) as a starting point. A very simplifying aspect of (5) is that it depends neither on the precise nature of the coupling with the heat baths nor on the details of the dynamics. All we need to know are the energies of the microscopic configurations.

However, most of the systems we find in Nature are out of equilibrium: they are open, hysteric systems, subject to thermal gradients, mass and/or energy fluxes, which suffer the action of external agents, or are subject to several sources of non-thermal noise. Non-equilibrium processes are also essential for cell functioning, brain processing, etc. For instance, in the interior of a cell there is a complex chemical activity, mediated by enzimes and motor proteins, which is far from equilibrium. It can be stated that all living organisms are non-equilibrium structures. In addition, non-equilibrium phenomena appear at all scales. Examples range from gravitational collapse of a star to the escape of metastable electrons in nanoelectronic devices, mutations in DNA or conformational changes in proteins. In fact, non-equilibrium phenomena are the rule, being equilibrium systems a rather unlikely exception. It seems that nonequilibrium is a fundamental ingredient for the observed structure in Nature. As in equilibrium systems, those systems out of equilibrium also show instabilities which give rise to spatio-temporal patterns, dissipative structures, self-organization, spontaneus-symmetry breaking, etc., all of them commonly observed in Nature. Since the physics of the above examples is rather different, we will concentrate on the simplest situation in a non-equilibrium system, i.e., on the steady state.

Let us come back to our first example consisting of a system in contact with two heat baths. If the two temperatures T_L and T_R are different, the system reaches in the long-time limit a non-equilibrium steady state (NESS) [11] and, unlike the equilibrium system, there does not exist an expression which generalizes (5) for the steady state weights $P(C)$ of the microscopic configurations

$$P_{\text{non-equilibrium}}(C) =? \tag{6}$$

In fact, for a non-equilibrium system, the steady state measure $P(C)$ depends in general on the dynamics of the system and on its coupling with heat baths and its computation from microscopic dynamics is a really difficult problem which has been successfully carried out in very few simple models [5, 6, 7]. Therefore the basic object to define analogs of entropy or thermodynamic potentials which we need to construct a natural extension of thermodynamics, is not immediately available.

Nevertheless, equilibrium statistical mechanics offers an alternative derivation of thermodynamic potentials by studying the *fluctuating* macroscopic behavior of the system at hand. This crucial observation can be generalize to non-equilibrium systems [8]-[20], where no general theory exists up to date capable of predicting macroscopic and fluctuating behavior in terms of

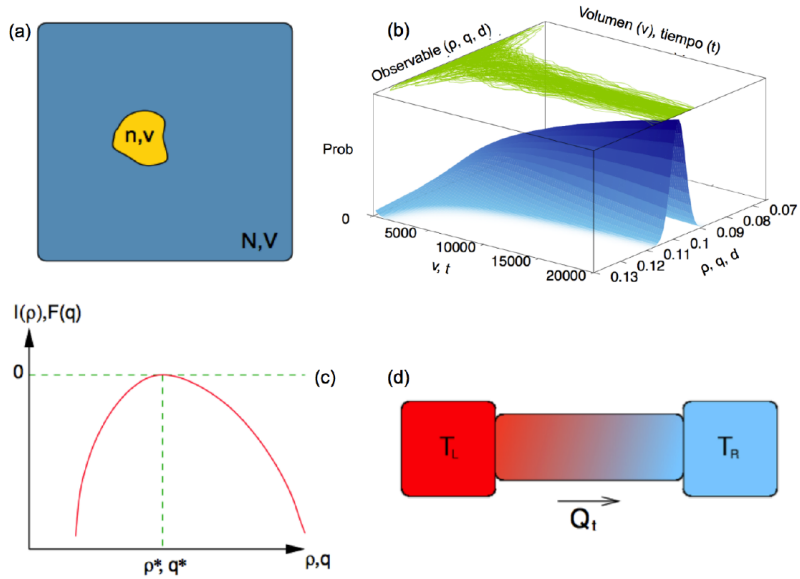

Figure 1: (a) Density fluctuations in a large subvolume v in an equilibrium system. (b) Concentration of the probability of observing a certain observable (e.g., density in a large subvolume, averaged current in long time interval t, etc). (c) Typical form of a large deviation function (LDF). (d) System in contact with two heat baths. If $T_L \neq T_R$ the system is out of equilibrium due to a gradient temperature and we can measure current fluctuations.

microscopic physics, in a way similar to equilibrium statistical mechanics. In this way, the study of fluctuations out of equilibrium may open the door to such a general theory. Actually, as we shall see, the large deviation function (LDF) which characterizes the fluctuations of macroscopic observables, can be identified as the non-equilibrium analog of the free-energy functional in equilibrium systems, from which macroscopic properties of a nonequilibrium system can be obtained (including its most prominent features, as for instance the ubiquitous long range correlations [21, 22], etc). Thus, understanding large deviation functions in out of equilibrium systems has become one of the main objectives of non-equilibrium statistical physics.

In order to understand what a large deviation is, let us start with a simple example. If one considers a box of volume V containing N particles, as in figure 1.a, the probability $P_v(n)$ of observing n particles in a subsystem of volume v has the following large v dependence

$$P_v(n) \sim \exp\left[+v\mathcal{I}\left(\frac{n}{v}\right)\right] \tag{7}$$

This equation follows a large deviation principle [23, 24], and the function $\mathcal{I}(\rho) \leq 0$ is the large deviation function. The approximation sign "$\sim$" de-

notes logarithmic equivalence as $v \to \infty$,

$$\lim_{v\to\infty} \frac{1}{v} \ln P_v(n) = \mathcal{I}\left(\frac{n}{v}\right)$$

Eq. (7) tells us that the probability of observing in our subsystem a density fluctuation $\rho = n/v$, different from the average density $\rho^* = N/V$, decays exponentially with the volume v of the subsystem. In this way, the LDF $\mathcal{I}(\rho)$ measures the rate at which the probability $P_v(n)$ concentrates around the mean ρ^* as v grows[1], see figure 1.b. One advantage of expressing $P_v(n)$ in a large deviation form is that the LDF $\mathcal{I}(\rho)$ gives a direct and complete picture of the deviations or *fluctuations* of ρ around its typical value. In what follows, we briefly list some general properties which characterize LDF's. They are negative in the whole domain except for the mean value of the observable where they are null, $\mathcal{I}(\rho^*) = 0$ see figure 1.c, reaching their maximum, $\mathcal{I}'(\rho^*) = 0$. Around the mean value ρ^*, LDF's are quadratic. This yields by approximating $\mathcal{I}(\rho)$ up to the first quadratic term around ρ^*,

$$\mathcal{I}(\rho) \approx \mathcal{I}(\rho^*) + \mathcal{I}'(\rho^*) + \frac{1}{2}\mathcal{I}''(\rho^*)(\rho-\rho^*)^2 = \frac{1}{2}\mathcal{I}''(\rho^*)(\rho-\rho^*)^2, \quad (8)$$

leading to the Gaussian approximation

$$P_v(n) \sim \exp\left[+v\frac{1}{2}\mathcal{I}''(\rho^*)(\rho-\rho^*)^2\right], \quad (9)$$

which can be thought of as a weak form of the Central Limit Theorem. This explains the meaning of the name large deviations. On the one hand, a *small* deviation, ρ, is a value for which the quadratic approximation to $\mathcal{I}(\rho)$ is a good approximation of $\mathcal{I}(\rho)$, and for which, therefore, the Central Limit Theorem yields essentially the same information as the large deviation principle. On the other hand, a *large* deviation, ρ, is a value for which $\mathcal{I}(\rho)$ departs sensibly from its quadratic approximation, and for which, therefore, the Central Limit theorem yields no useful information about the large fluctuations of ρ away from its mean ρ^*. In this sense, large deviation theory can be seen as a generalization of the Central Limit Theorem characterizing the small as well as the large fluctuations of a random variable. For a further study of large deviation theory see Ref. [24].

For equilibrium systems, the LDF is also closely related to the free energy. In fact, if the volume v is sufficiently large, for short range interactions and in the absence of external potential, the LDF is given by [14]

$$\mathcal{I}(\rho) = -\frac{f(\rho) - f(\rho^*) - (\rho-\rho^*)f'(\rho^*)}{k_B T}, \quad (10)$$

where $f(\rho)$ is the free energy per unit volume at density ρ, $\rho^* = N/V$ and T is the temperature. This can be seen by noticing that, if $v \ll V$ and $v^{1/d}$ is much larger than the range of the interactions (being d the dimension), on has

$$P_v(n) = \frac{Z_v(n) Z_{V-v}(N-n)}{Z_V(N)} \exp O(v^{(\frac{d-1}{d})}), \quad (11)$$

[1] For that reason, the LDF is also known in the mathematical literaure as rate function.

where $Z_V(N)$ is the partition function of N particles in a volume V and the term $\exp[O(v^{\frac{d-1}{d}})]$ respresents the interactions between all pairs of particles, one of which is in the subsystem v and the other is in the rest of the system $V - v$. Then taking the ln of (11) and using the definition of the free energy per unit of volume, $f(\rho) \equiv -k_B T V^{-1} \ln Z_V(V\rho)$, one gets Eq. (10). A similar calculation allows to show that the probability for the system to adopt a density profile $\rho(\mathbf{r})$ obeys a large deviation principle, $P[\rho(\mathbf{r})] \sim \exp[+V\mathcal{I}[\rho(\mathbf{r})]]$, where the large deviation functional $\mathcal{I}[\rho(\mathbf{r})]$ is fully determined by the knowledge of the density free energy $f[\rho(\mathbf{r})]$,

$$\mathcal{I}[\rho(\mathbf{r})] = -\frac{1}{k_B T} \int_\Lambda d\mathbf{r}[f[\rho(\mathbf{r})] - f(\rho^*)]. \tag{12}$$

Where Λ is the space domain, $\Lambda \in [0,1]^d$. Notice that, as expected for an equilibrium system, the functional $\mathcal{I}[\rho(\mathbf{r})]$ depends *locally* on the density profile $\rho(\mathbf{r})$, as well as being a convex functional of $\rho(\mathbf{r})$.
It is remarkable that if one expands (10) near ρ^* and one replaces it into (7) one gets that the distribution of the number n of particles in the subvolume v is Gaussian (if v is large enough)

$$P_v(n) \sim \exp\left[-v\frac{f''(\rho^*)}{2k_B T}(\rho - \rho^*)^2\right] = \exp\left[-v\frac{f''(\rho^*)}{2vk_B T}(n - v\rho^*)^2\right], \tag{13}$$

and its variance, as predicted by Smoluchowski and Einstein, is given by

$$\langle n^2\rangle - \langle n\rangle^2 = v\frac{k_B T}{f''(\rho^*)} = vk_B T\kappa(\rho^*) \tag{14}$$

where the compressibility is defined by $\kappa(\rho) \equiv \rho^{-1} d\rho/dp$ (and the pressure is given as usual by $p = -(d/dV)[Vf(N/V)] = \rho^* f'(\rho^*) - f(\rho^*))$).

Thus, we have just shown how by studying the fluctuations of macroscopic observables (e.g. the density) in equilibrium systems, we are able to relate univocally the LDF characterizing these fluctuations to the free energy of the system. Note that key to do this, is to express the probability of a fluctuation as a large deviation principle.

Far from equilibrium, we may also study the fluctuations of macroscopic observables with the hope for LDF's to be related to the non-equilibrium analogs of thermodynamic potentials in equilibrium systems. A crucial point to start working within this framework, is to identify the essential macroscopic observables which characterize the behavior of non-equilibrium systems. We are usually interested in system having a locally conserved magnitude (e.g. energy, number of particles, charge, momentum). Hence, the essential macroscopic observable is the *current* or flux which is established when a system is driven out of equilibrium by the action of an external field or by applying a gradient in its boundaries. This is why the understanding of current statistics in terms of microscopic dynamics has become one of the main objectives of non-equilibrium statistical physics in the last two decades [8]-[20]. This activity has led to a number of groundbreaking results valid arbitrarily far from equilibrium (and therefore not restricted to

the confining world of linear response), which are offering a glimpse of the long-sought general theory of nonequilibrium phenomena. A main example is the already mentioned Gallavotti-Cohen fluctuation theorem [8, 9, 12], which express the subtle but enduring consequences of microscopic time reversibility at the macroscopic level. The list continues however, with further breakthroughs ranging from the Jarzynski equality [25] or the Crooks fluctuation theorem [26] to the Hatano-Sasa relation [27] or the recent extension of Clausius inequality to nonequilibrium steady states [28], to mention just a few.

As we have already seen, a paradigmatic non-equilibrium system is the one in contact with two heat baths at different temperatures, see figure 1.d. In this case, as time increases, and provided that the system is ergodic, the time-averaged current $J = \tau^{-1} \int_0^\tau j(t)\, dt$ quickly converges toward its ensemble average $\langle J \rangle$. For large (but finite) times, the measured J may fluctuate and the probability of a given output follows in general a large-deviation principle for long times, $\mathrm{P}_\tau(J) \sim \exp[+\tau L^d G(J)]$. Here $G(J)$ is the current large deviation function (LDF), and measures the (exponential) rate at which $J \to \langle J \rangle$ as τ increases (notice that $G(J) \leq 0$, with $G(\langle J \rangle) = 0$). We then see that the current in non-equilibrium follows a large deviation principle similar to which the density does in equilibrium systems, see Eq. (7), with time playing the role of the volume v in equilibrium.

Computing large deviations in non-equilibrium systems starting from microscopic dynamics, is an extraordinary complicated task which has been successfully achieved in very few simple cases [5, 6, 7, 14]. However, L. Bertini, A. De Sole, D. Gabrielli, G. Jona-Lasinio and C. Landim have developed in the last ten years a macroscopic fluctuating theory (MFT) to describe in detail dynamical fluctuations in diffusive systems. This theory offers detailed predictions for relevant large deviations functions from the knowledge of the macroscopic (or hydrodynamic) evolution equation of the system at hand and two transport coefficients. It is worth noting that the theoretical laboratory to test this theory is provided by stochastic lattice gases. The dynamics of these stochastic lattice models is different from the Hamiltonian dynamics that one would assume for a classical real gas, but the hope is that the macroscopic behavior of a system, at least for certain intervals of time, be qualitatively independent of this assumption. One expects that general properties like the type and number of conservations laws should be the most relevant features. It is then here where computer simulations come into play, since they can be considered as the experimental laboratory to test the MFT predictions by implementing the dynamics of such stochastic lattice models and by measuring the observables in which one is interested. Thus, simulation results become of central importance in order to confirm and bound the validity of the MFT.

For all the reasons above exposed, the aim of this thesis is to investigate fluctuations in out of equilibrium systems. Particularly, we focus on diffusive systems, where there exists a locally conserved magnitude and where

the time-averaged current is the relevant macroscopic observable. Thus, we study the current large deviation function which is, as we have argued, the best candidate from which macroscopic properties of a non-equilibrium diffusive system can be obtained.

We start in chapter 1 by briefly introducing the MFT. The starting point is a continuity equation which describes the macroscopic evolution of diffusive systems. Then, by using a path integral formalism we get the large deviation function controlling the probability of observing a time-average current fluctuation. In that case, the MFT gives rise to a complex spatio-temporal variational problem whose solution remains challenging. Therefore we supplement the MFT with a simplifying additivity conjecture which leads to manageable equations.

In chapter 2, we describe several stochastic lattice models in which the MFT will be applied. We shall see how despite their different microscopic dynamics, they lead to a macroscopic diffusive behavior well characterized by their transport coefficients which are the two ingredients necessary to exploit the MFT. Particularly we concentrate on the Kipnis-Marchioro-Presutti (KMP) model and several exclusion models.

Chapter 3 is devoted to deeply analyze the additivity conjecture from which we get theoretical predictions for the current LDF in the KMP model. We test its range of validity of the additivity conjecture by measuring numerically not only the current LDF but also the density profiles the system adopts in order to sustain a given large current fluctuation. As we shall see, it is pretty surprising that these measured optimal profiles actually correspond to the theoretical profiles obtained by minimizing the functional resulting from the additivity conjecture. This confirms the idea that the system indeed modifies its density profile to facilitate the deviation of the current, validating the power of the additivity conjecture to compute both the current LDF and the associated optimal profiles.

In chapter 4 we show that by demanding invariance of optimal paths under symmetry transformations, new and general fluctuation relations valid arbitrarily far from equilibrium are unveiled. This opens an unexplored route toward a deeper understanding of nonequilibrium physics by bringing symmetry principles to the realm of fluctuations. We illustrate this concept studying symmetries of the current distribution out of equilibrium. In particular we derive an isometric fluctuation relation which links in a strikingly simple manner the probabilities of any pair of isometric current fluctuations. This relation, which results from the time-reversibility of the dynamics, includes as a particular instance the Gallavotti-Cohen fluctuation theorem in this context but adds a completely new perspective on the high level of symmetry imposed by time-reversibility on the statistics of nonequilibrium fluctuations. The new symmetry implies remarkable hierarchies of equations for the current cumulants and the nonlinear response coefficients, going far beyond Onsager's reciprocity relations and Green-Kubo formulas. We confirm the validity of the new symmetry relation in extensive numerical simulations, and suggest that the idea of symmetry in fluctuations as invariance of optimal paths has far-reaching consequences in diverse fields.

Another recent discovery concerns the existence of *coherent structures*

associated to large, rare fluctuations which enhance their probability [39, 40]. Such coherent, self-organized patterns emerge via a dynamical phase transition at the fluctuating level, which is accompanied by spontaneous symmetry breaking event. In chapter 5 we investigate in detail this last phenomenon in the weakly-asymmetric simple exclusion process, where we study fluctuations of the time-averaged current. As we also analyze the two-dimensional case, we have observed that the isometric fluctuation relation still holds in the time-dependent regime.

Finally, in chapter 6 we derive a natural extension of the already mentioned Hatano-Sasa theorem. This theorem, which is in turn an extension of the Jarzynski equality, gives rise to a generalization of the second law which holds for transitions between steady states. However, it relies on the a priori knowdlege of the stationary probability distribution. Instead, arbitrary 'trial' smooth distributions can be used, thus allowing one to treat systems whose stationary distribution is too difficult to calculate, as generically occurs in out of equilibrium systems with many degrees of freedom. We show here [29] that every set of trial distributions yields an inequality playing the role of a generalization of the Second Law. The better the approximation, the more constraining the inequality becomes: this suggests a criterion for its accuracy, as well as an optimization procedure that may be implemented numerically and even experimentally. As an illustration, we numerically approximate the stationary distribution of a paradigmatic non-equilibrium driven system with many degrees of freedom, the Simple Symmetric Exclusion Process in one dimension.

Chapter 1

Macroscopic fluctuation theory

1.1 Introduction

Recent years are witnessing a quiet revolution in nonequilibrium statistical physics. At the core of this revolution is the realization of the essential role played by macroscopic fluctuations to understand the fully nonequilibrium behavior of a system of interest. This activity has led to a number of groundbreaking results valid arbitrarily far from equilibrium (and therefore not restricted to the confining world of linear response), which are offering a glimpse of the long-sought general theory of nonequilibrium phenomena [8]-[20]. One of the main contributions along the last ten years has been done by L. Bertini, A. De Sole, D. Gabrielli, G. Jona-Lasinio and C. Landim, which have developed the Macroscopic Fluctuation Theory (MFT) [15]-[18]. In this chapter we briefly introduce the MFT and its main results.

In general, this theory offers detailed predictions for relevant large deviations functions (LDF's) from the knowledge of the macroscopic (or hydrodynamic) evolution equation of the system at hand and two transport coefficients. It has been inspired by and tested on stochastic models of interacting particles systems (stochastic lattice gases).

One of the most important tasks in out of equilibrium systems, is to identify the relevant macroscopic observable whose LDF plays the role of a thermodynamic potential. In nonequilibrium diffusive systems where there exits a locally conserved magnitude (e.g. energy, particle density, charge, momentum, etc), this good macroscopic observable may be the current. However, the density could also play a fundamental role, as it does in equilibrium systems (see Introduction). The MFT was firstly developed for the density as the relevant observable [15] and later for the current [16]. Note that these two observables are related by the continuity equation

$$\partial_t \rho(\mathbf{r}, t) = -\boldsymbol{\nabla} \cdot \mathbf{j}(\mathbf{r}, t) \tag{1.1}$$

One of the starting points of this theory is to assume *local equilibrium* in the following sense: Locally on a macroscopic scale it is possible to define

thermodynamic variables like density, temperature, chemical potentials, etc, which vary smoothly on the same scale. Microscopically this implies for the system to reach local equilibrium in a shorter time compared to the times typical of the macroscopic evolutions, as described for example by hydrodynamic equations. So what characterizes situations in which this description applies is a separation of scales both in space and time.

As mentioned above, a theoretical laboratory where to test this theory is provided by stochastic lattice gases. For several models local equilibrium has been proved and hydrodynamic evolution equations have been derived. The microscopic dynamics of these models is different from the Hamiltonian dynamics that one would assume for a classical real gas but the hope is that the macroscopic behavior of a system, at least for certain intervals of time, be qualitatively independent of this assumption

The microscopic evolution of each stochastic model from which the macroscopic theory has been developed, is given by a Markov process X_t which represents the configuration of the system at time t. If the system is in equilibrium, the stationary state is an equilibrium state. However, if the system is driven out of equilibrium through the interaction with boundary reservoirs and/or under the action, one assumes that the system reaches in the long-time limit a non-equilibrium stationary state (NESS) characterized by a probability distribution P_{st} over the trajectories of X_t invariant with respect to time shifts.

Before introducing the basic assumptions of the MFT, recall that for non-equilibrium systems by expressing the probability of macroscopic fluctuations of a relevant observable as a large deviation principle one naturally identifies the large deviation function (LDF) with a non-equilibrium thermodynamic function (see Introduction). Thus, the goal of the MFT is to derive relevant LDF's.

The MFT assumes the following basic axioms

- The macroscopic state is completely described by the local density $\rho(\mathbf{r}, t)$ and the associated current $\mathbf{j}(\mathbf{r}, t)$
- The macroscopic evolution is given by the following continuity equation,

$$\partial_t \rho(\mathbf{r}, t) = -\boldsymbol{\nabla} \cdot \Big(\mathbf{Q}_{\mathbf{E}}[\rho(\mathbf{r}, t)] + \boldsymbol{\xi}(\mathbf{r}, t) \Big) . \tag{1.2}$$

This equation describes the macroscopic evolution of a wide class of d-dimensional systems characterized by a locally-conserved magnitude (e.g. energy, particle density, momentum, etc.) and derives from the underlying microscopic dynamics through an appropriate scaling limit in which the microscopic time and space coordinates $\tilde{t}$, $\tilde{\mathbf{r}}$ are rescaled diffusively: $t = \tilde{t}/L^2$, $\mathbf{r} = \tilde{\mathbf{r}}/L$ where L is the linear size of the system. The macroscopic coordinates are then $(\mathbf{r}, t) \in \Lambda \times [0, \tau]$. Where Λ is the spatial domain, $\Lambda \in [0, 1]^d$, being d the dimensionality of the system In Eq. (1.2), $\rho(\mathbf{r}, t)$ is the density field and

$$\mathbf{j}(\mathbf{r}, t) \equiv \mathbf{Q}_{\mathbf{E}}[\rho(\mathbf{r}, t)] + \boldsymbol{\xi}(\mathbf{r}, t) \tag{1.3}$$

is the fluctuating current, with local average $\mathbf{Q}_{\mathbf{E}}[\rho(\mathbf{r},t)]$, and $\boldsymbol{\xi}(\mathbf{r},t)$ is a Gaussian white noise which scales as $L^{-d/2}$. This noise is characterized by a variance (or *mobility*) $\sigma[\rho(\mathbf{r},t)]$, i.e.,

$$\begin{aligned}\langle \boldsymbol{\xi}(\mathbf{r},t)\rangle &= 0\\ \langle \boldsymbol{\xi}(\mathbf{r},t)\boldsymbol{\xi}(\mathbf{r}',t')\rangle &= L^{-d}\sigma[\rho]\delta_{ij}\delta(\mathbf{r}-\mathbf{r}')\delta(t-t')\end{aligned} \tag{1.4}$$

being $i,j \in [0,d]$ the components of the spatial coordinates. This (conserved) noise term accounts for microscopic random fluctuations at the macroscopic level. This noise source represents the many fast microscopic degrees of freedom which are averaged out in the coarse-graining procedure resulting in Eq. (1.2), and whose net effect on the macroscopic evolution amounts to a Gaussian random perturbation according to the central limit theorem. Since $\boldsymbol{\xi}(\mathbf{r},t)$ scales as $L^{-d/2}$, in the limit $L \to \infty$ we recover the deterministic hydrodynamic equation, but as we want to study the fluctuating behavior, we consider large (but finite) system sizes, i.e., we are interested in the limit $\boldsymbol{\xi} \to 0$. Notice that the current functional includes in general the effect of a conservative external field,

$$\mathbf{Q}_{\mathbf{E}}[\rho(\mathbf{r},t)] = \mathbf{Q}[\rho(\mathbf{r},t)] + \sigma[\rho(\mathbf{r},t)]\mathbf{E}. \tag{1.5}$$

Examples of systems described by Eq. (1.2) range from diffusive systems [14, 15, 16, 17, 34, 36, 37, 39], where $\mathbf{Q}[\rho(\mathbf{r},t)]$ is given by Fourier's (or equivalently Fick's) law,

$$\mathbf{Q}[\rho(\mathbf{r},t)] = -D[\rho]\boldsymbol{\nabla}\rho(\mathbf{r},t), \tag{1.6}$$

to most interacting-particle fluids [2, 33], characterized by a Ginzburg-Landau-type theory for the locally-conserved particle density. To completely define the problem, the above evolution equation (1.2)-(1.5) must be supplemented with appropriate boundary conditions, which are either periodic when Λ is the torus or the the non-homogeneous condition

$$\varphi(\rho(\mathbf{r},t)) = \varphi_0(\mathbf{r}), \qquad \mathbf{r} \in \partial\Lambda \tag{1.7}$$

in the case of boundary-driven systems in which the driving is due to an external gradient. Here $\partial\Lambda$ is the boundary of Λ and φ_0 is the chemical potential of the boundary reservoirs. Finally the initial condition for (1.2) is the limiting empirical density of the chosen microscopic configuration of particles. The diffusion coefficient $D[\rho]$ and the mobility $\sigma[\rho]$, can be readily obtained experimentally and satisfy the local Einstein relation

$$D[\rho] = \kappa[\rho]^{-1}\sigma[\rho] \tag{1.8}$$

where $\kappa[\rho]$ is the compressibility: $\kappa[\rho]^{-1} = f_0''[\rho]$, being f_0 the equilibrium free energy of the system.

We obtain an equilibrium model either if Λ is the torus and there is no external field or in the case of boundary-driven systems in which the external field in the bulk matches the driving from the boundary. We are also in equilibrium if the chemical potentials of the boundaries are the same. In the other cases the stationary state yields a non-vanishing current and the system is out of equilibrium.

1.2 Large deviation of the density and current

We consider now the probability that the system follows a particular trajectory during a time τ for the density and current fields, $\{\rho(\mathbf{r},t),\mathbf{j}(\mathbf{r},t)\}_0^\tau$, which can be different from the hydrodynamic trajectory. This probability can be written as a path integral over all possible noise realizations, $\{\boldsymbol{\xi}(\mathbf{r},t)\}_0^\tau$, weighted by its Gaussian measure and restricted to those realizations compatible with Eq. (1.2)

$$\mathrm{P}\left(\{\rho,\mathbf{j}\}_0^\tau\right)=\int\mathcal{D}\boldsymbol{\xi}\,\exp\left[-L^d\int_0^\tau dt\int_\Lambda d\mathbf{r}\frac{\boldsymbol{\xi}^2}{2\sigma[\rho]}\right]\prod_t\prod_{\mathbf{r}}\delta\Big[\boldsymbol{\xi}-(\mathbf{j}-\mathbf{Q}_{\mathbf{E}}[\rho])\Big], \tag{1.9}$$

with $\rho(\mathbf{r},t)$ and $\mathbf{j}(\mathbf{r},t)$ coupled via the continuity equation,

$$\partial_t\rho+\boldsymbol{\nabla}\cdot\mathbf{j}=0. \tag{1.10}$$

Notice that this coupling does not determine univocally the relation between ρ and $\mathbf{j}$. For instance, the fields $\tilde{\rho}(\mathbf{r},t)=\rho(\mathbf{r},t)+\chi(\mathbf{r})$ and $\tilde{\mathbf{j}}(\mathbf{r},t)=\mathbf{j}(\mathbf{r},t)+\mathbf{g}(\mathbf{r},t)$, with $\chi(\mathbf{r})$ arbitrary and $\mathbf{g}(\mathbf{r},t)$ divergenceless, satisfy the same continuity equation. This means that from a density field we can determine the current field up to a divergence free vector field. This freedom can be traced back to the loss of information during the coarse-graining from the microscale to the macroscale [16]. Eq. (1.9) naturally leads to

$$\mathrm{P}\left(\{\rho,\mathbf{j}\}_0^\tau\right)=\exp\left(+L^dI_\tau[\rho,\mathbf{j}]\right), \tag{1.11}$$

which has the form of a large deviation principle. Here the rate functional $I_\tau[\rho,\mathbf{j}]$ is given by

$$I_\tau[\rho,\mathbf{j}]=-\int_0^\tau dt\int_\Lambda d\mathbf{r}\frac{(\mathbf{j}(\mathbf{r},t)-\mathbf{Q}_{\mathbf{E}}[\rho])^2}{2\sigma[\rho]}. \tag{1.12}$$

This functional plays a fundamental role because starting from this form we can compute the large deviation of one of the most relevant observables in nonequilibrium systems: The time-averaged current $\mathbf{J}$.

1.2.1 Large deviations of the time-averaged current

Nonequilibrium systems typically exhibit currents of different observables (e.g., mass or energy) which characterize their macroscopic behavior. Understanding how micoscopic dynamics determine the long-time averages of these currents and their fluctuations is one of the main objectives of nonequilibrium statistical physics [8]-[20]. Therefore we focus now on the probability $P_\tau(\mathbf{J})$ of observing an averaged current $\mathbf{J}=\tau^{-1}\int_0^\tau dt\int_\Lambda d\mathbf{r}\mathbf{j}(\mathbf{r},t)$. This probability can be written as

$$\mathrm{P}_\tau(\mathbf{J})=\int^*\mathcal{D}\rho\mathcal{D}\mathbf{j}\;\mathrm{P}\left(\{\rho,\mathbf{j}\}_0^\tau\right)\;\delta\left(\mathbf{J}-\tau^{-1}\int_0^\tau dt\int_\Lambda d\mathbf{r}\,\mathbf{j}(\mathbf{r},t)\right),$$

where the asterisk means that this path integral is restricted to histories $\{\rho,\mathbf{j}\}_0^\tau$ coupled via Eq. (1.10). As the exponent of $\mathrm{P}\left(\{\rho,\mathbf{j}\}_0^\tau\right)$ is extensive in

both τ and L^d [43], see Eq. (1.11), for long times and large system sizes the above path integral is dominated by the associated saddle point, resulting in the following large deviation principle

$$\mathrm{P}_\tau(\mathbf{J}) \sim \exp[+\tau L^d G(\mathbf{J})], \tag{1.13}$$

where the rate functional $G(\mathbf{J})$ is the current *large deviation function* (LDF) given by

$$G(\mathbf{J}) = \lim_{\tau\to\infty} \frac{1}{\tau} \max_{\rho(\mathbf{r},t),\mathbf{j}(\mathbf{r},t)} I_\tau[\rho,\mathbf{j}] \tag{1.14}$$

with the constraints $\mathbf{J} = \tau^{-1}\int_0^\tau dt \int_\Lambda d\mathbf{r}\, \mathbf{j}(\mathbf{r},t)$ and $\partial_t\rho + \boldsymbol{\nabla}\cdot\mathbf{j} = 0$. The optimal density and current fields solution of this variational problem, denoted here as $\rho_0(\mathbf{r},t;\mathbf{J})$ and $\mathbf{j}_0(\mathbf{r},t;\mathbf{J})$, can be interpreted in mesoscopic phase space as the optimal path the system follows in order to sustain a long-time current fluctuation $\mathbf{J}$. It is worth emphasizing here that the existence of an optimal path rests on the presence of a selection principle at play, namely a long time, large size limit which selects, among all possible paths compatible with a given fluctuation, an optimal one via a saddle point mechanism.

1.2.2 Large deviations of the density field

Beside the current, there is another interesting observable which is the density field. In equilibrium, we have seen that the density LDF is univocally related to the free energy of the system (see Eq. (10) in the Introduction). In addition, this LDF depends *locally* on the density profile $\rho(\mathbf{r})$, as well as being a convex functional of $\rho(\mathbf{r})$. In non-equilibrium systems it may be non-local, reflecting the presence of long range correlations. Hence, we are now interested in the probability of a particular trajectory during a time interval $[0,\tau]$ for the density profile, $\{\rho\}_0^\tau$, starting in the initial state $\rho(\mathbf{r},0)$. To compute this probability we start from Eq. (1.2)

$$\partial_t\rho(\mathbf{r},t) = -\boldsymbol{\nabla}\cdot\mathbf{Q}_\mathbf{E}[\rho(\mathbf{r},t)] + \boldsymbol{\nu}(\mathbf{r},t)\,, \tag{1.15}$$

where the new random variable is $\boldsymbol{\nu}(\mathbf{r},t) = -\boldsymbol{\nabla}\cdot\boldsymbol{\xi}(\mathbf{r},t)$. After some calculations one can show that the probability distribution of $\boldsymbol{\nu}(\mathbf{r},t)$ starting from the gaussian measure for the noise field $\boldsymbol{\xi}(\mathbf{r},t)$ is given by the following quadratic form

$$\mathrm{P}_\tau(\boldsymbol{\nu}(\mathbf{r},t)) = \exp\left[-\frac{1}{2}\int_0^\tau dt \int_\Lambda d\mathbf{r}d\mathbf{r}'\boldsymbol{\nu}(\mathbf{r},t)\mathcal{M}(\mathbf{r},\mathbf{r}';t)^{-1}\boldsymbol{\nu}(\mathbf{r}',t)\right], \tag{1.16}$$

where $\mathcal{M}(\mathbf{r},\mathbf{r}';t) = L^{-d}\partial_{r_i}\partial_{r_i'}\sigma[\rho(\mathbf{r},t)]\delta(\mathbf{r}-\mathbf{r}')$. Thus, the probability of a particular trajectory exclusively for the density, $\{\rho\}_0^\tau$, is now written as a path integral over all realizations of the noise field $\boldsymbol{\nu}(\mathbf{r},t)$,

$$\mathrm{P}\left(\{\rho\}_0^\tau\right) = \int \mathcal{D}\boldsymbol{\nu}\, \mathrm{P}_\tau(\boldsymbol{\nu}(\mathbf{r},t)) \prod_t \prod_\mathbf{r} \delta\Big[\boldsymbol{\nu} - (\partial_t\rho + \boldsymbol{\nabla}\cdot\mathbf{Q}_\mathbf{E}[\rho])\Big], \tag{1.17}$$

Using Eq. (1.16) into Eq. (1.17) we get that

$$\mathrm{P}\left(\{\rho\}_0^\tau\right) \sim \exp[L^d\mathcal{I}_\tau[\rho]], \tag{1.18}$$

with

$$\mathcal{I}_\tau[\rho] = -\frac{1}{2L^d}\int_0^\tau dt \int_\Lambda d\mathbf{r}d\mathbf{r}' \left(\partial_t\rho + \boldsymbol{\nabla}\cdot\mathbf{Q}_\mathbf{E}[\rho]\right)\mathcal{M}(\mathbf{r},\mathbf{r}';t)^{-1}\left(\partial_t\rho + \boldsymbol{\nabla}\cdot\mathbf{Q}_\mathbf{E}[\rho]\right) \tag{1.19}$$

$\mathcal{I}_\tau[\rho]$ is a functional which vanishes in the stationary state, ρ_{st}, and represents the cost necessary to follow the trajectory $\{\rho\}_0^\tau$ [15].

Now we consider the following situation. The system is macroscopically in the stationary state $\rho_{st} \equiv \rho_{st}(\mathbf{r})$, $\mathbf{r} \in \Lambda$ (a stationary solution to Eq. (1.2)) at $t = -\infty$, but at $t = 0$ we find it in the state $\hat{\rho}$. Thus, using Eq. (1.18), the probability of a trajectory connecting this two states is

$$\mathrm{P}(\{\rho\}_{-\infty}^0) \sim \exp\left[L^d\mathcal{I}_{[-\infty,0]}[\rho]\right] \tag{1.20}$$

We want to determine the most probable trajectory in the spontaneous creation of this fluctuation. According to (1.20) the most probable trajectory is the one that maximizes $\mathcal{I}$ among all trajectories $\rho(\mathbf{r},t)$ connecting ρ_{st} to $\hat{\rho}$ in the interval $t \in [0,-\infty]$,

$$G[\hat{\rho}] = \max_\rho \mathcal{I}_{[-\infty,0]}[\rho] \tag{1.21}$$

which can be interpreted as the non-equilibrium analog of the free energy, from which macroscopic properties of our nonequilibrium system can be obtained, including its most prominent features, as for instance the ubiquitous long range correlations [21, 22].

We have seen so far how the MFT offers predicitions for the density (1.21) as well as for the time-averaged current (1.14). As we have already mentioned, we shall focus on the study of the current LDF in several diffusive models which are described in next chapter. It is worth noting that the MFT predicts in general time-dependent optimal profiles, $\rho(\mathbf{r},t)$ and $\mathbf{j}(\mathbf{r},t)$, in order to sustain a large current fluctuation $\mathbf{J}$. These time-dependent profiles result from the maximization of the functional given by Eq. (1.12). However, this variational problem is a complex spatio-temporal problem whose solution remains challenging in most cases. Therefore, in chapter 3 we shall see how by doing two simplifying hypotheses we are able to obtain explicit predictions for the current LDF in a paradigmatic diffusive model: the Kipnis-Marchioro-Presutti Model (KMP) [35]. These hypotheses consitute the additivity conjecture and consist in assuming that the optimal current and density fields are time independent and that the current field is, in particular, constant across the space. Furthermore, we test the validity of this additivity conjecture in extensive numerical simulations. We concentrate on the current LDF of the 2D-KMP model and we shall derive that provided the additiviy conjecture, the optimal density profiles associated to a given current fluctuation only depend on the magnitud of the curret and not on its orientation with respect to the gradient direction. In chapter 4 we unveil a new fluctuation relation as a consequence of this invariance of the optimal density field under current rotations. The new fluctuation relation implies remarkable hierarchies of equations for the current cumulants and the non-linear response coefficients, going far beyond Onsager's reciprocity

relations and Green-Kubo formulas. Although the time independence of the optimal profiles, namely the additivity conjecture, holds in a broad regime, we show in chapter 5 that in some particular cases the optimal fields become time-dependent, as is predicted by the MFT in general (see Eq. (1.14)). This fact is interpreted as a dynamical phase transition.

Chapter 2

Models of transport out of equilibrium

In this chapter we describe some stochastic lattice models in which the MFT can be applied. Although the microscopic dynamics of these models is different from the Hamiltonian dynamics that one would assume for a classical real gas, it captures the most relevant features which characterize realistic systems. In these models local equilibrium has been proved and hydrodynamic diffusive macroscopic equations have been derived.

2.1 Kipnis-Marchioro-Presutti (KMP) model

In 1982, C. Kipnis, C. Marchioro and E. Presutti [35] proposed a simple lattice model in order to understand energy transport in systems with many degrees of freedom. This model has become one of the paradigmatic energy transport models of nonequilibrium statistical physics. In particular, KMP were able to show rigurously from microscopic dynamics that this model obeys Fourier's law. The KMP is then an optimal model to test the MFT and its extensions.

It is a one-dimensional chain with N sites in which each site models an harmonic oscillator mechanically uncoupled from its nearest neighbors but interacts with them through a random process which redistributes energy locally. The microscopic configuration of the system is defined by $C \equiv \{\rho_i, i = 1, ...L\}$, where $\rho_i \geq 0$ is the energy of the site $i \in [1, N]$. The system undergoes a stochastic dynamics proceeding through random energy exchanges between randomly chosen nearest-neighbors according to a random microcanonical procedure, i.e., the energy is kept constant. Hence, $(\rho_i, \rho_{i+1}) \rightarrow (\rho'_i, \rho'_{i+1})$ $\forall i$ such that,

$$\begin{aligned} \rho'_i &= p(\rho_i + \rho_{i+1}) \\ \rho'_{i+1} &= (1-p)(\rho_i + \rho_{i+1}) \end{aligned} \tag{2.1}$$

Figure 2.1: One dimensional KMP model with different temperatures with boundary gradient conditions ($T_L \neq T_R$)

where $p \in [0,1]$ is an uniform random number. In addition, we must complete the model with the appropriate boundary conditions. In the original paper [35], KMP consider open boundary conditions where extremal ($i \in 1, N$) sites of the chain are connected to thermal baths (see figure 2.1). In this case, the extremal sites ($i \in 1, N$) may interchange energy with thermal baths at temperatures T_L for $i = 1$ and T_R for $i = N$, i.e., $\rho_{1,N} \rightarrow \rho'_{1,N}$ such that

$$\rho'_{1,N} = p(\tilde{\rho}_{L,R} + \rho_{1,N}) \tag{2.2}$$

where $p \in [0,1]$ is again an uniform random number and $\tilde{\rho}_{L,R}$ is a random number drawn from a Gibbs distribution at the corresponding temperature, $P(\rho_k) = \beta_k \exp(-\beta_k)$, $k = L, R$. In the general case, as we mentioned above, Kipnis, Marchioro andPresutti showed [35] that the system reaches a nonequilibrium steady state described by Fourier's law in the hydrodynamic limit. In this case the average energy current is given by

$$\langle J \rangle = -D[\rho]\frac{\rho_{st}(x)}{dx}\ , \ x \in [0,1] \tag{2.3}$$

where $D[\rho] = \frac{1}{2}$ is the conductivity or diffusivity for the KMP model. It was also show that the stationary energy density profile is

$$\rho_{st}(x) = T_L + x(T_R - T_L) \tag{2.4}$$

In Ref. [35] it was also proved that in the hydrodynamic limit there is a convergence of the stationary probability distribution toward the local Gibbs measure. This means that ρ_i with $i \in [1, N]$ obeys locally an exponential distribution with local temperature $\rho_{st}(\frac{i}{L+1})$ in the thermodynamic limit. Despite this convergence, corrections to local equilibrium can be observed in the fluctuating behavior of this model [36, 37]. The macroscopic evolution equation for this model is

$$\partial_t \rho(x,t) = \partial_x(\frac{1}{2}\partial_x \rho(x,t)) \tag{2.5}$$

which is nothing but the dynamical expression of the Fourier's law. According to the MFT a second transport coefficient must be provided in order to complete the macroscopic description of this model. This second coefficient is the mobility, which measures the variance of local energy current fluctuations in equilibrium ($\rho_L = \rho_R$). For the KMP model $\sigma[\rho] = \rho^2$. It is also worth noting that the micrscopic dynamics in the KMP model obeys the local detailed balance condition [13], thus being time-reversible. In chapter 3 and 4 we shall study the macroscopic fluctuating behavior of the KMP model.

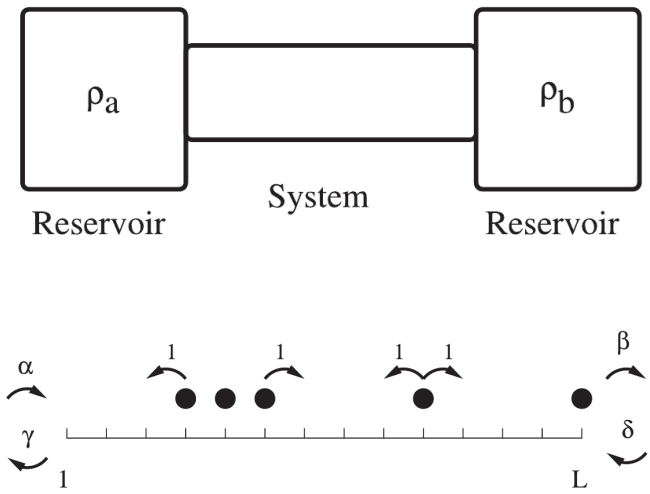

Figure 2.2: Top: Skecth of a system in contact with two reservoirs at densities ρ_a and ρ_b. Bottom: The symmetric simple exclusion process

2.2 Symmetric Simple Exclusion Process (SSEP)

We now set out to describe anoter paradigmatic nonequilibrium model: the symmetric simple exclussion process (SSEP) [30, 31, 32]. It is one of the simplest models of a system maintained out of equilibrium by contact with two reservoirs at densities ρ_a and ρ_b (see top sketch in figure 2.2). The model is defined as a one-dimensional lattice of L sites with open boundaries, see bottom skecth in figure 2.2. Sites are either occupied by a single particle or empty. A microscopic configuration is defined by the vector of occupation numbers $\mathbf{n} = (n_1, ..., n_L)$ where $n_i = 0$ or 1 is a binary variable indicating whether site $i \in [1, L]$ empty or occupied with. Each particle in the bulk independently attempts to jump to an empty site to its right or to its left site. At the two boundaries the dynamics is modified to mimic the coupling with the reservoirs of particles: at the left boundary each particle is injected at site 1 at rate α (if this site is empty) and removed from site 1 at rate γ (if this site is occupied). Similarly on site L, particles are injected at rate δ and removed at rate β. We will see below that these choices of the rates $\alpha, \gamma, \beta, \delta$ correspond to the left boundary being connected to a reservoir at density ρ_a and the right boundary to a reservoir at density ρ_b given by

$$\rho_a = \frac{\alpha}{\alpha + \gamma}; \qquad \rho_b = \frac{\delta}{\beta + \delta} \tag{2.6}$$

If $\rho_a = \rho_b = \rho$ the system is in equilibrium and the distribution is of product form: $\rho_{eq}(\mathbf{n}) = \prod_{i=1}^{L} \rho^{n_i}(1-\rho)^{1-n_i} = e^{\sum_{i=1}^{L} \mu n_i}/(1+e^{\mu})^L$, where $\mu = \log(\rho/(1-\rho))$ is the chemical potential. As soon as $\rho_a \neq \rho_b$, the system is out of equilibrium, a current is established, and the problem becomes non trivial, with long range correlations. For the SSEP, the calculation of the average profile or the correlation functions, can be done directly from the

definition of the model. One can write the time evolution of the average occupation $\langle n_i \rangle$ as,

$$\frac{d\langle n_1 \rangle}{dt} = \alpha - (\alpha + \gamma + 1)\langle n_1 \rangle + \langle n_2 \rangle$$

$$\frac{d\langle n_i \rangle}{dt} = \langle n_{i-1} \rangle - 2\langle n_i \rangle + \langle n_{i+1} \rangle \qquad \text{for} \;\; 2 \leq i \leq L-1$$

$$\frac{d\langle n_L \rangle}{dt} = \langle n_{L-1} \rangle - (1 + \beta + \delta)\langle n_L \rangle + \delta.$$

It has been shown that this model reaches a steady state density profile (obtained by writing that $d\langle n_i \rangle / dt = 0$) given by [32]

$$\langle n_i \rangle = \frac{\rho_a (L + \frac{1}{\beta+\delta} - i) + \rho_b (i - 1 + \frac{1}{\alpha+\gamma})}{L + \frac{1}{\alpha+\gamma} + \frac{1}{\beta+\delta} - 1}. \tag{2.7}$$

with ρ_a and ρ_b defined as in (2.6). Notice that for large L, if one introduces a macroscopic coordinate $i = Lx$, the above equation becomes

$$\langle n_i \rangle = \rho_{st}(x) = (1 - x)\rho_a + x\rho_b \tag{2.8}$$

which is the is the stationary density profile. Remarkably for large L one also obtains $\langle n_1 \rangle \to \rho_a$ and $\langle n_L \rangle \to \rho_b$, indicating that ρ_a and ρ_b defined by 2.6 represent the densities of the left and right reservoirs. The average current in the steady state is given by

$$\langle J \rangle = \langle n_i (1 - n_{i+1}) - n_{i+1}(1 - n_i) \rangle = \langle n_i - n_{i+1} \rangle = \frac{\rho_a - \rho_b}{L + \frac{1}{\alpha+\gamma} + \frac{1}{\beta+\delta} - 1}. \tag{2.9}$$

This shows that for large L, the current $\langle J \rangle \simeq (\rho_a - \rho_b)/L$ is prportional to the gradient of the density (with a coefficient of proportionality which is simply one) and therefore follows Fick's law,

$$\langle J \rangle = -D[\rho] \frac{\rho_{st}(x)}{dx}\,, \; x \in [0, 1], \tag{2.10}$$

with $D[\rho] = 1$. One can write down the equations which generalize (2.7) and govern the time evolution of the two-point correlation function or higher correlations. For example one finds [32, 33] in the steady state for $1 \leq i < j \leq L$

$$\langle n_i n_j \rangle_c = \frac{-(\rho_0 - \rho_1)^2 (\frac{1}{\alpha+\gamma} + i - 1)(\frac{1}{\beta+\delta} + L - j)}{(\frac{1}{\alpha+\gamma} + \frac{1}{\beta+\delta} + L - 1)^2 (\frac{1}{\alpha+\gamma} + \frac{1}{\beta+\delta} + L - 2)}. \tag{2.11}$$

For large L, introducing macroscopic coordinates $i = Lx$ and $j = Ly$, this becomes for $x < y$, $\langle n_{Lx} n_{Ly} \rangle_c = -x(1-y)(\rho_0 - \rho_1)^2 / L$. As stated in [32], one may think that these weak, but long range, correlations play no role in the macroscopic limit. However, they are responsible for a leading contribution in the variance of a macroscopic quantity such as the number of particles.

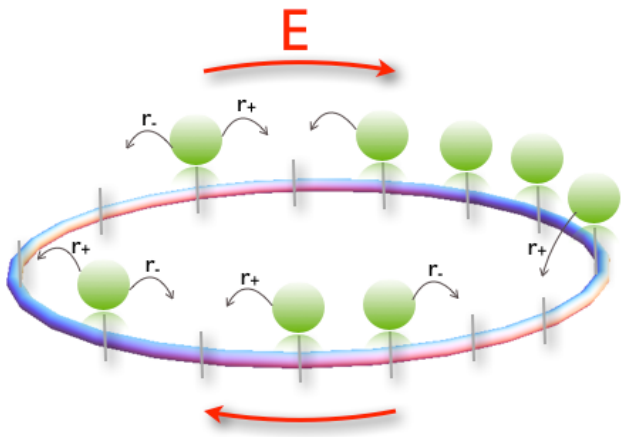

Figure 2.3: Top: Skecth of the weakly assymetric exclusion process with a weak external field, E, to the right

In chapter 6 we shall measure numerically the two-point correlation function (2.11) to test the quality of the approximated SSEP non-equilibrium stationary distribution obtained by using an optimization procedure. It is remarkable that all the correlation functions can be derived by knowing the non-equilibrium steady state measure of the SSEP. This distribution may be computed analytically through the so-called matrix method [6].

Finally the macroscopic equation for the SSEP is given by [33]

$$\partial_t \rho(x,t) = -\partial_x(\partial_x \rho(x,t)) \tag{2.12}$$

which corresponds to the dynamical expression of the Fick's law with $D[\rho] = 1$. In order to apply the MFT to this model, one also needs to know the mobility which, for the SSEP [33], is $\sigma[\rho] = 2\rho(1-\rho)$. It is remarkable that if each particle jumps to its right at rate $\frac{1}{2}$ (instead of at rate 1) and to its left at rate $\frac{1}{2}$ (instead of at rate 1), then $D[\rho] = \frac{1}{2}$ and $\sigma[\rho] = \rho(1-\rho)$.

2.3 Weakly Assymmetric Exclusion Process (WASEP)

Finally, we consider the weakly assymetric exclusion process (WASEP). This model is analogous to SSEP except that one introduces a weak external field, E, to any direction (e.g. to the right). In this case we consider periodic boundary conditions. Thus, this model is one-dimensional ring of N sites with $P = N\rho$ particles, being ρ the density of the system. The number of particles is then fixed because there are no density reservoirs at the boundaries, see figure 2.3. In the absence of the external field this model corresponds the SSEP. We have seen for this model that, if each particle jumps at rate $\frac{1}{2}$ to its right or to its left site (whenever they are empty), the transport coefficients become $D = \frac{1}{2}$ and $\sigma[\rho] = \rho(1-\rho)$. If one one

introduces a weak field, E, to the right, the model becomes the WASEP and the rates become $r_+ = \frac{1}{2} + E/2L$ to the right and $r_- = \frac{1}{2} - E/2L$, see figure 2.3. It has been shown [33] that the average current for the WASEP is given by $\langle J \rangle = \sigma[\rho]E$ and that the macroscopic evolution takes the form

$$\partial_t \rho(x,t) = \partial_x(-D[\rho]\partial_x \rho(x,t) + \sigma[\rho]E) \tag{2.13}$$

with $D[\rho] = \frac{1}{2}$ and $\sigma[\rho] = \rho(1-\rho)$. In chapter 5 we shall derive the current LDF by applying the MFT for this model and we shall observe how a dynamical phase transition emerges at the fluctuating level.

Chapter 3

Additivity of current fluctuations

3.1 Introduction

As we have seen, large deviation functions measure the rate at which the empiric average of an observable converges toward its asymptotic value. Think for instance on the time-averaged current in a d-dimensional system of linear size L. As time increases, and provided that the system is ergodic, the time-averaged current $\mathbf{J} = \tau^{-1} \int_0^\tau \mathbf{j}(t)\, dt$ quickly converges toward its ensemble average $\langle \mathbf{J} \rangle$, given for instance by Fourier's law, $\langle \mathbf{J} \rangle = -D[\rho_{st}] \boldsymbol{\nabla} \rho_{st}$, with ρ_{st} being the stationary profile. For finite times, the measured $\mathbf{J}$ may fluctuate and the probability of a given output follows in general a large-deviation principle [23, 24] for long times, $\mathrm{P}_\tau(\mathbf{J}) \sim \exp[+\tau L^d G(\mathbf{J})]$. Here $G(\mathbf{J})$ is the current large deviation function (LDF), and measures the (exponential) rate at which $\mathbf{J} \to \langle \mathbf{J} \rangle$ as τ increases (notice that $G(\mathbf{J}) \leq 0$, with $G(\langle \mathbf{J} \rangle) = 0$). The MFT provides a variational principle (see Eq. (1.14)) to get this LDF in which the only input parameters are the transport coefficients $D[\rho]$ and $\sigma[\rho]$. The solution of this variational problem yields the optimal path for the density and current fields associated to a given current fluctuation, which might be in general time-dependent. Thus, in order to obtain explicit predictions for the current LDF, we assume the following hypotheses

1. We assume that the optimal profiles responsible of a given current fluctuation are time-independent, $\rho_0(\mathbf{r}; \mathbf{J})$ and $\mathbf{j}_0(\mathbf{r}; \mathbf{J})$. This, together with the continuity equation 1.10, implies that the optimal current vector field is divergence-free, $\boldsymbol{\nabla} \cdot \mathbf{j}_0(\mathbf{r}; \mathbf{J}) = 0$.

2. A further simplification consists in assuming that this optimal current field has no spatial structure, i.e. is constant across space, so $\mathbf{j}_0(\mathbf{r}; \mathbf{J}) = \mathbf{J}$.

These hypothesis constitute the additivity conjecture. It allow us to make the initial variational problem (1.14) manageable and get explicit predictions for the current LDF given the diffusivity and the mobility. In this chapter we

assumes this additivity conjecture to predict the current LDF in the KMP model (already introduced in chapter 2) when subject to a boundary gradient. In addition, we test and bound its validity using extensive numerical simulations. In chapter 4 we shall see the importance of this conjecture to unveil a new fluctuation relation for the d-dimensional systems with d higher than one.

Provided that these hypotheses hold, the current LDF (1.14) can be written as

$$G(\mathbf{J}) = -\min_{\rho(\mathbf{r})} \int_\Lambda \frac{\left(\mathbf{J} - \mathbf{Q}_\mathbf{E}[\rho]\right)^2}{2\sigma[\rho(\mathbf{r})]} d\mathbf{r}\,, \tag{3.1}$$

which expresses the *locally*-Gaussian nature of fluctuations [10, 14]. In this way the probability $\mathrm{P}_\tau(\mathbf{J})$ is simply the Gaussian weight associated to the optimal density profile responsible of such fluctuation. Note however that the minimization procedure gives rise to a nonlinear problem which results in general in a current distribution with non-Gaussian tails [14, 15, 16, 36]. As opposed to the general problem in Eq. (1.14), its simplified version, Eq. (3.1), can be readily used to obtain quantitative predictions for the current statistics in a large variety of non-equilibrium systems. This minimization procedure yields a partial differential equation for the optimal density profile $\rho_0(\mathbf{r};\mathbf{J})$. This optimal profile is solution of the following equation

$$\frac{\delta\omega_2[\rho(\mathbf{r})]}{\delta\rho(\mathbf{r}')} - 2\mathbf{J}\cdot\frac{\delta\boldsymbol{\omega}_1[\rho(\mathbf{r})]}{\delta\rho(\mathbf{r}')} + \mathbf{J}^2\frac{\delta\omega_0[\rho(\mathbf{r})]}{\delta\rho(\mathbf{r}')} = 0\,, \tag{3.2}$$

which must be supplemented with appropriate boundary conditions. In the above equation, $\frac{\delta}{\delta\rho(\mathbf{r}')}$ stands for functional derivative, and

$$\boldsymbol{\omega}_n[\rho(\mathbf{r})] \equiv \int_\Lambda d\mathbf{r}\,\mathbf{W}_n[\rho(\mathbf{r})] \qquad \text{with} \qquad \mathbf{W}_n[\rho(\mathbf{r})] \equiv \frac{\mathbf{Q}^n_\mathbf{E}[\rho(\mathbf{r})]}{\sigma[\rho(\mathbf{r})]}\,. \tag{3.3}$$

For a diffusive system without external field for which $\mathbf{Q}_{\mathbf{E}=0}[\rho] = -D[\rho]\boldsymbol{\nabla}[\rho]$, the resulting differential equation (3.2) for the optimal profile, $\rho_0 \equiv \rho_0(\mathbf{r};\mathbf{J})$, takes the form

$$\mathbf{J}^2 a'[\rho_0] - c'[\rho_0](\boldsymbol{\nabla}\rho_0)^2 - 2c[\rho_0]\boldsymbol{\nabla}^2\rho_0 = 0, \tag{3.4}$$

where $a[\rho_0] = (2\sigma[\rho_0])^{-1}$ and $c[\rho_0] = D^2[\rho_0]a[\rho_0]$. Here $'$ denotes the derivative. Multiplying the above equation by $\boldsymbol{\nabla}\rho_0$, we obtain after one integration

$$(\boldsymbol{\nabla}\rho_0)^2 = \frac{\mathbf{J}^2 + 2\sigma[\rho_0]K}{D^2[\rho_0]} \tag{3.5}$$

where K is a constant of integration which guarantees the correct boundary conditions. Eqs. (3.1) and (3.5) completely determine the current distribution $\mathrm{P}_\tau(\mathbf{J})$, which is in general non-Gaussian (except for very small current fluctuations).

One observes that the optimal density profile solution of Eq. (3.5) only depends on the magnitude of $\mathbf{J}$ via $\mathbf{J}^2$. Hence it remains invariant under arbitrary rotations of the current vector, i.e., $\rho_0(\mathbf{r};\mathbf{J}) = \rho_0(\mathbf{r};|\mathbf{J}|)$ providing

a detailed example of the recently introduced Isometric Fluctuation Relation (IFR) [10]. In chapter 4 we shall study the origin of this invariance and its important consequences.

It is worth noting that in 2004 Bodineau and Derrida [34] conjectured an *additivity principle* for current fluctuations in 1D diffusive systems which can be readily applied to obtain quantitative predictions. As can be seen in appendix A, this additivity principle is equivalent to assume time-independent optimal energy density profiles within the MFT. Interestingly, for 1D systems the conjecture of time-independent optimal profiles implies that the optimal current profile must be constant, because they are coupled via the continuity equation $\partial_t \rho + \partial_x j = 0$. This is no longer true in higher dimensions, as any divergence-free current field with spatial integral equal to $\mathbf{J}$ is compatible with the continuity equation $\partial_t \rho + \boldsymbol{\nabla} \cdot \mathbf{j} = 0$. This gives rise to a variational problem with respect to the (time-independent) energy density and current fields which still poses many technical difficulties. Therefore an additional assumption is needed, namely the constancy of the optimal current vector field across space. Hence, the hypotheses (1) and (2) are the straightforward generalization to d-dimensional systems of the additivity principle conjectured by Bodineau and Derrida for one-dimesional diffusive systems.

Before studying the current LDF for the 2D-KMP model within the additivity scenario, we firstly describe the previous results obtained by Hurtado and Garrido [36, 37] for the one-dimensional case by assuming the addivity principle.

3.2 Current LDF for 1D diffusive systems

In this section, we are interested in computing the probability of observing a time-averaged current fluctuation, $J = \tau^{-1} \int_0^\tau dt \int_0^1 dx\, j(x,t)$, in a one-dimensional diffusive system subject to a boundary gradient, i.e., $\rho(0) = \rho_L$ and $\rho(1) = \rho_R$ with $\rho_L \neq \rho_R$. In general, the MFT shows that the current LDF can be written as Eq. (1.14) particularized for a one-dimensional system obeying the Fourier's law and without external field, namely with $Q[\rho]_{E=0} = Q[\rho] = -D[\rho]\rho'(x)$. Thus,

$$G(J, \rho_L, \rho_R) = -\lim_{\tau \to \infty} \frac{1}{\tau} \min_{\rho(x,t), j(x,t)} \left\{ \int_0^\tau dt \int_0^1 \frac{[j(x,t) + D[\rho]\rho'(x)]^2}{2\sigma[\rho]} dx \right\}, \tag{3.6}$$

with the constraints $J = \tau^{-1} \int_0^\tau dt \int_0^1 dx\, j(x,t)$ and $\partial_t \rho + \partial_x j = 0$. We have made explicit in (3.6) the dependence of G on the boundary baths, ρ_L and ρ_R, for convenience. By using now the additivity conjecture this complex variational problem is greatly simplified, and Eq. (3.6) takes the form

$$G(J, \rho_L, \rho_R) = -\min_{\rho(x)} \left\{ \int_0^1 \frac{[J + D[\rho]\rho'(x)]^2}{2\sigma[\rho]} dx \right\}, \tag{3.7}$$

This expression is the same as the one obtained assuming the additivity principle by Bodineau and Derrida [34] (see appendix A). The variational

problem (3.7) gives rise to the following differential equation for the optimal energy density profile $\rho_0(x;J)$

$$\left(\frac{d\rho_0(x;J)}{dx}\right)^2 = \frac{J^2\left(1+2K\rho_0^2(x;J)\right)}{D^2[\rho_0]}, \tag{3.8}$$

which corresponds to the one-dimensional version of Eq. (3.5). In the sequel we drop the dependence on J for the optimal profile. Notice that the optimal energy density profile, solution of Eq. (3.8), only depends on the magnitude of the current fluctuation via J^2 whatever its sign is, i.e, $\rho_0(x;J) = \rho_0(x;-J)$, reflecting the Gallavotti-Cohen symmetry [8]. Actually, using this invariance of the energy density profile under the current sign into Eq. (3.7), one gets the GC fluctuation theorem for the current LDF,

$$G(J) - G(-J) = -2J\int_0^1 \frac{D[\rho_0]\rho_0'(x)}{\sigma[\rho_0]}dx = 2J\int_{\rho_R}^{\rho_L}\frac{D[\rho_0]}{\sigma[\rho_0]}d\rho_0 = 2J\varepsilon \tag{3.9}$$

where $\rho_L = \rho(0)$, $\rho_R = \rho(1)$ and $\varepsilon \equiv \int_{\rho_R}^{\rho_L}\frac{D[\rho]}{\sigma[\rho]}d\rho \geq 0$. Hence, the GC symmetry states that the odd part of $G(J)$ is linear with a universal coefficient ε.

3.3 Results for the 1D-KMP Model

In chapter 2 we have shown that in the KMP model is characterized by a diffusivity $D[\rho] = \frac{1}{2}$, and a mobility $\sigma[\rho] = \rho^2$ which characterizes the variance of energy current fluctuations in equilibrium ($\rho_L = \rho_R$). Recall that it is a microscopic stochastic lattice model of energy transport in which Fourier's law holds. Each site on the lattice models an harmonic oscillator which is mechanically uncoupled from its nearest neighbors but interacts with them through a random process which redistributes energy locally. The system is coupled to boundary heat baths. For $\rho_L \neq \rho_R$ the system reaches a nonequilibrium steady state with a nonzero rescaled average current $\langle \mathbf{J}\rangle = (\rho_L - \rho_R)/2$ and a stationary profile $\rho_{\rm st}(x) = \rho_L + x\,(\rho_R - \rho_L)$. Hence, in order to get the current LDF one just have to substitute the transport coefficients into Eq. (3.8)

$$\left(\frac{d\rho_0(x)}{dx}\right)^2 = 4J^2\left(1+2K\rho_0^2(x)\right), \tag{3.10}$$

where K is a constant which guarantees the correct boundary conditions, $\rho_0(0) = \rho_L$ and $\rho_0(1) = \rho_R$. In this case the GC symmetry holds,

$$G(J) - G(-J) = 2J\varepsilon, \tag{3.11}$$

with $\varepsilon = \frac{1}{2}(\rho_R^{-1} - \rho_L^{-1})$.

According to Eq. (3.10), two different scenarios appear. On one hand, for large enough K the rhs of Eq. (3.10) does not vanish $\forall x \in [0,1]$ and the

resulting profile is monotone. In this case, and assuming $\rho_L > \rho_R$ henceforth without loss of generality,

$$\frac{d\rho_0(x)}{dx} = -2|J|\sqrt{1+2\rho_0^2(x)K}\,. \tag{3.12}$$

On the other hand, for $K < 0$ the rhs of Eq. (3.10) may vanish at some points, resulting in a $\rho_0(x)$ that is non-monotone and takes an unique value $\rho_0^* \equiv \sqrt{-1/2K}$ in the extrema. Notice that the rhs of Eq. (3.10) may be written in this case as $4|J|^2[1-(\rho_0(x)/\rho_0^*)^2]$. It is then clear that, if non-monotone, the profile $\rho_0(x)$ can only have a single maximum because: (i) $\rho_0(x) \leq \rho_0^*\ \forall x \in [0,1]$ for the profile to be a real function, and (ii) several maxima are not possible because they should be separated by a minimum, which is not allowed because of (i). Hence for the non-monotone case (recall $\rho_L > \rho_R$)

$$\frac{d\rho_0(x)}{dx} = \begin{cases} +2|J|\sqrt{1-\left(\dfrac{\rho_0(x)}{\rho_0^*}\right)^2}\,, & x < x^* \\ \\ -2|J|\sqrt{1-\left(\dfrac{\rho_0(x)}{\rho_0^*}\right)^2}\,, & x > x^* \end{cases} \tag{3.13}$$

where x^* locates the profile maximum. This leaves us with two separated regimes for current fluctuations, with the crossover happening for $|J| = \frac{\rho_L}{2}\left[\frac{\pi}{2} - \sin^{-1}\left(\frac{\rho_R}{\rho_L}\right)\right] \equiv |J_c|$. This crossover current can be obtained from Eq. (3.16) below by letting $\rho_0^* \to \rho_L$

3.3.1 Region I: Monotonous Regime ($|J| < |J_c|$)

Notice that, for $\rho_0(x)$ to be monotone, $1 + 2K\rho_0^2 > 0$ being $K > -(2\rho_L^2)^{-1}$. Integrating now Eq. (3.12) we obtain the following implicit equation for $\rho_0(x)$ in this regime

$$2x|J| = \begin{cases} \dfrac{1}{\sqrt{2K}} \ln\left[\dfrac{\rho_L + \sqrt{\rho_L^2 + \frac{1}{2K}}}{\rho_0(x) + \sqrt{\rho_0(x)^2 + \frac{1}{2K}}}\right]\,, & K > 0 \\ \\ \dfrac{\sin^{-1}\left[\rho_L\sqrt{-2K}\right] - \sin^{-1}\left[\rho_0(x)\sqrt{-2K}\right]}{\sqrt{-2K}}\,, & -\dfrac{1}{2\rho_L^2} < K < 0 \end{cases} \tag{3.14}$$

Making $x = 1$ and $\rho_0(x=1) = \rho_R$ in the previous equation, we obtain the implicit expression for the constant K. To get a feeling on how it depends on $|J|$, note that in the limit $K \to (-1/2\rho_L^2)$, the current $|J| \to |J_c|$, while for $K \to \infty$ one gets $|J| \to 0$. In addition, from Eq. (3.14) we see that for $K \to 0$ we find $|J| = (\rho_L - \rho_R)/2 = \langle J \rangle$. Thus, Eq. (3.14) allows us to compute the optimal profiles in the monotone regime.

3.3.2 Region II: Non-Monotonous Regime ($|J| > |J_c|$)

In this case the optimal profile has a single maximum $\rho_0^* \equiv \rho_0(x = x^*)$ with $\rho_0^* = 1/\sqrt{-2K}$ and $-1/2\rho_L^2 < K < 0$. Integrating Eq. (3.13) one gets an implicit equation for the non-monotone optimal profile

$$2x|J| = \begin{cases} \rho_0^* \left[\sin^{-1}\left(\dfrac{\rho_0(x)}{\rho_0^*}\right) - \sin^{-1}\left(\dfrac{\rho_L}{\rho_0^*}\right)\right] & \text{for } 0 \le x < x^* \\ 2|J| + \rho_0^* \left[\sin^{-1}\left(\dfrac{\rho_R}{\rho_0^*}\right) - \sin^{-1}\left(\dfrac{\rho_0(x)}{\rho_0^*}\right)\right] & \text{for } x^* < x \le 1 \end{cases} \tag{3.15}$$

At $x = x^*$ both branches of the above equation must coincide, and this condition provides simple equations for both x^* and ρ_0^*

$$|J| = \frac{\rho_0^*}{2}\left[\pi - \sin^{-1}\left(\frac{\rho_L}{\rho_0^*}\right) - \sin^{-1}\left(\frac{\rho_R}{\rho_0^*}\right)\right];$$
$$x^* = \frac{\dfrac{\pi}{2} - \sin^{-1}\left(\dfrac{\rho_L}{\rho_0^*}\right)}{\pi - \sin^{-1}\left(\dfrac{\rho_L}{\rho_0^*}\right) - \sin^{-1}\left(\dfrac{\rho_R}{\rho_0^*}\right)}. \tag{3.16}$$

The above equations are the implicit expressions for the constant K in the non-monotone regime. In figure 3.1 we show the value of constant K as a function of $|J|$ for both regimes.

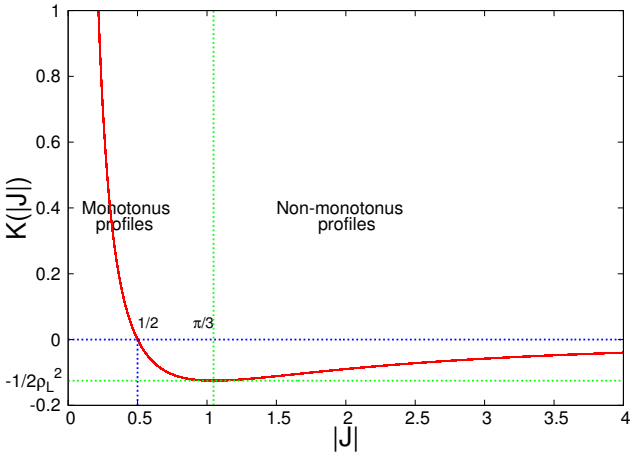

Figure 3.1: Constant K as a function of $|J|$ for $\rho_L = 2$ and $\rho_R = 1$.

In this way, given a value of K, such that $-1/2\rho_L^2 < K < 0$, we get ρ_0^*, $|J|$ and x^* from Eq. (3.16). Hence, we are able to obtain the optimal profile for the non-monotonous regime implicitely defined by (3.15). In figure 3.2 several optimal energy density profiles corresponding to different current fluctuations $|J|$ are displayed, both in the monotone and non-monotone regimes.

To calculate the LDF, $G(J)$, we insert Eq. (3.10) into Eq. (3.7) and do the

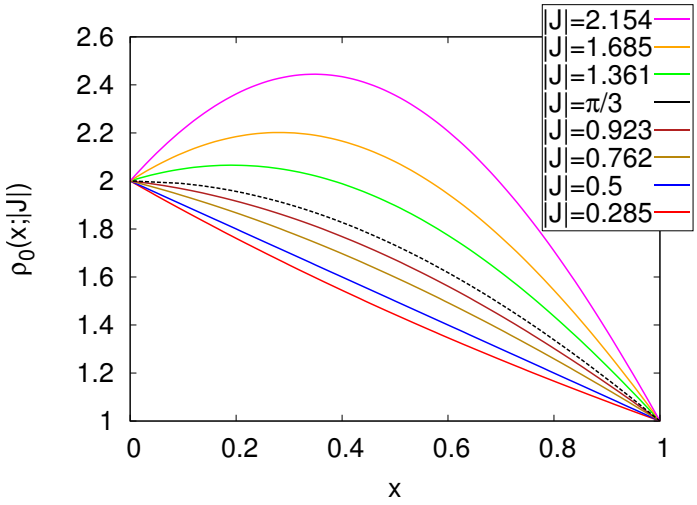

Figure 3.2: Optimal $\rho_0(x)$ with $\rho_L = 2$ and $\rho_R = 1$ and different $|J|$. The dash line ($|J| = |J_c| = \pi/3$) corresponds to the crossover between the monotone and non-monotone regimes.

integral. In the monotone regime, i.e. for $|J| < |J_c|$, we use particularly Eq. (3.12) into Eq. (3.7). Then, $G(J)$ reads

$$G(J) = \frac{J}{2}\left(\frac{1}{\rho_R} - \frac{1}{\rho_L}\right) - |J|^2 K + \frac{|J|}{2}\left[\frac{\sqrt{1+2K\rho_L^2}}{\rho_L} - \frac{\sqrt{1+2K\rho_R^2}}{\rho_R}\right], \tag{3.17}$$

whereas in the non-monotonous regime, i.e. for $|J| < |J_c|$, we split the integral in Eq. (3.7) at $x = x^*$ and use Eq. (3.13). Thus, $G(J)$ is given by

$$\begin{aligned} G(J) &= \frac{J}{2}\left(\frac{1}{\rho_R} - \frac{1}{\rho_L}\right) - \frac{|J|}{2}\left[\frac{1}{\rho_L}\sqrt{1-\left(\frac{\rho_L}{\rho_0^*}\right)^2} + \frac{1}{\rho_R}\sqrt{1-\left(\frac{\rho_R}{\rho_0^*}\right)^2}\right. \\ &- \left.\frac{1}{2\rho_0^*}\left(\pi - \sin^{-1}\left(\frac{\rho_L}{\rho_0^*}\right) - \sin^{-1}\left(\frac{\rho_R}{\rho_0^*}\right)\right)\right], \end{aligned} \tag{3.18}$$

where ρ_0^* is an implicit function of J, see Eq. (3.16). As expected, we can readily check that the GC symmetry (3.11) holds in the whole current interval. Figure 3.3 shows $G(J)$ in both regimes. Notice that the LDF is zero for $J = \langle J \rangle = (\rho_L - \rho_R)/2$ and negative elsewhere. For small current fluctuations, $J \approx \langle J \rangle$ (i.e. $K \to 0$), $G(J)$ obeys the following quadratic form

$$G(J) \approx -\frac{1}{2}\left(\frac{(|J| - (\rho_L - \rho_R)/2)^2}{\sigma^2}\right), \tag{3.19}$$

with $\sigma^2 = (\rho_L^2 + \rho_L\rho_R + \rho_R^2)/3$, resulting in Gaussian statistics for currents near the average as expected from the central limit theorem.

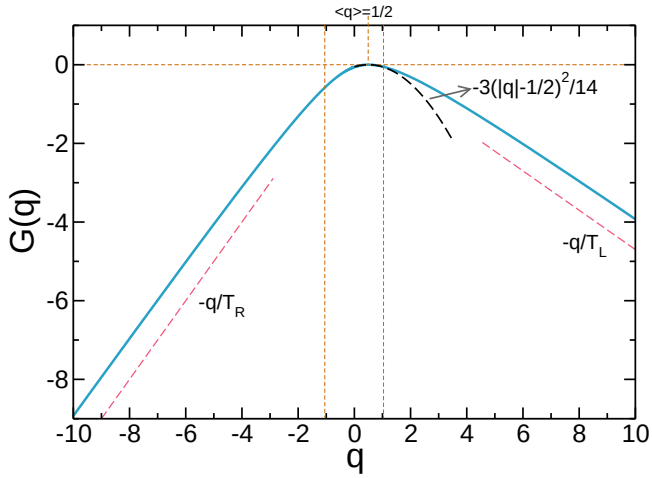

Figure 3.3: $G(J)$ ($q \equiv J$) for the 1D-KMP model as derived from the additivity principle, for $\rho_L = 2$ and $\rho_R = 1$. Notice the linear decay for large enough $|J|$. Vertical lines signal the crossover from monotone ($|J| < \pi/3$) to non-monotone ($|J| > \pi/3$) optimal profiles. The Gaussian approximation for $J \approx \langle J \rangle$, $G(J) \approx 3(|J| - \frac{1}{2})^2/14$, is also shown.

3.3.3 Numerical Test of the Additivity Conjecture in 1D

Large deviation functions are very hard to measure in experiments or simulations because they involve by definition exponentially-unlikely events, see Eq. (1.13). Recently, Giardina, Kurchan and Peliti [41] have introduced an efficient algorithm to measure the probability of a large deviation for observables such as the current or energy density in stochastic many-particle systems. The algorithm is based on a modification of the underlying stochastic dynamics so that the rare events responsible of the large deviation are no longer rare, and it requires the simulation of multiple *clones* of the system. This method, as well as its extension to systems with continuous-time stochastic dynamics [42], is described in Appendix B. This algorithm yields the Legendre transform of the large deviation function, which for a 1D system of linear size L is given by

$$\mu(\lambda) = \frac{1}{L} \max_J [G(J) + J\lambda] = \frac{1}{L}[G(J^*) + \lambda J^*], \tag{3.20}$$

where λ is the parameter conjugated to the current and $J^*(\lambda)$ is given by $\partial_J G(J)|_{J=J^*} + \lambda = 0$. Hence, using Eqs. (3.17) and (3.18) we get for both regimes

$$\mu(\lambda) = -\frac{K}{L}[J^*(\lambda)]^2, \tag{3.21}$$

In λ-space, monotone profiles are expected for $|\lambda + \varepsilon| \leq \frac{1}{2\rho_R}\sqrt{1 - (\rho_R/\rho_L)^2}$ with $\varepsilon = \frac{1}{2}(\rho_R^{-1} - \rho_L^{-1})$, whereas non-monotone profiles appear for $\frac{1}{2\rho_R}\sqrt{1 - (\rho_R/\rho_L)^2} \leq$

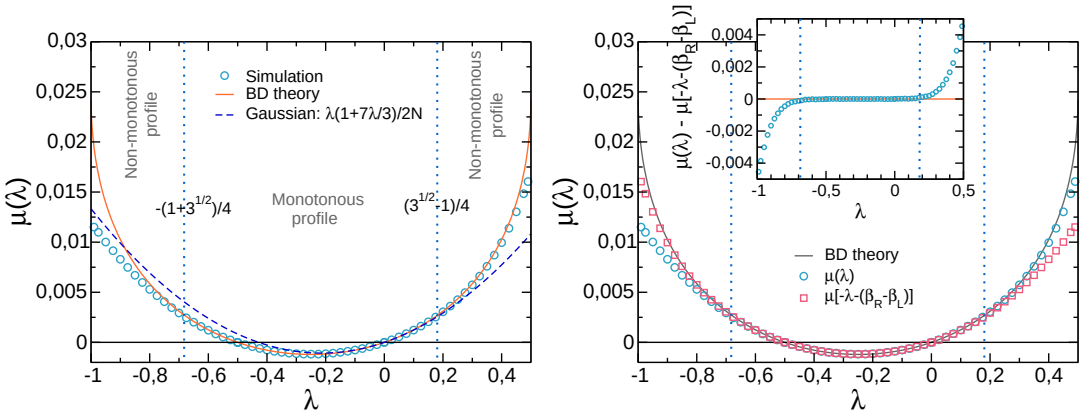

Figure 3.4: Left panel: Measured $\mu(\lambda)$ for the 1D-KMP model with for $\rho_L = 2$ and $\rho_R = 1$. Right panel: Measured $\mu(\lambda)$ and $\mu(\lambda - 2\varepsilon)$ superimposed. The GC symmetry is satisfied for a wide current interval. The inset shows the difference $\mu(\lambda) - \mu(\lambda - 2\varepsilon)$. Figure obtained from Refs. [36, 37]

$|\lambda + \varepsilon| \leq \frac{1}{2}\left(\frac{1}{\rho_L} + \frac{1}{\rho_R}\right)$. Notice that the GC symmetry (3.9) can be rewritten now as

$$\mu(\lambda) = \mu(-\lambda - 2\varepsilon) \tag{3.22}$$

Taking into account the equality (3.22) and Eq. (3.21) we arrive at

$$J^*(\lambda) = -J^*(-\lambda - 2\varepsilon). \tag{3.23}$$

Consequently, the invariance under the current sign for the energy profile turns into $\rho(x;\lambda) = \rho(x;-\lambda-2\varepsilon)$ in λ-space. For small current fluctuations, $\lambda \approx 0$, an expansion similar to (3.19) for $\mu(\lambda)$ yields

$$\mu(\lambda) \approx \frac{\lambda}{2}[(\rho_L - \rho_R) + \sigma^2 \lambda] \tag{3.24}$$

with $\sigma^2 = (\rho_L^2 + \rho_L\rho_R + \rho_R^2)/3$.

In Refs. [36, 37] Hurtado and Garrido carried out numerical simulations using the algorithm above described in order to test the additivity conjecture in the 1D-KMP model. The results they obtained for $\mu(\lambda)$ with $L = 50$, $\rho_L = 2$ and $\rho_R = 1$ are displayed in left panel of figure 3.4. It was shown, that the agreement with Bodineau and Derrida (BD) theory was excellent for a wide λ-interval, say $-0.8 < \lambda < 0.3$, which corresponded to a very large range of current fluctuations. Moreover, the deviations observed for extreme current fluctuations were due to known limitations of the algorithm [36, 37, 38, 41, 42], so no violations of additivity are observed. In fact, they used the Gallavotti-Cohen symmetry (3.22) to bound the range of validity of the algorithm: Violations of the fluctuation relation indicate a systematic bias in the estimations provided by the method of Ref. [41], see also [38]. Right panel of figure 3.4 shows that the Gallavotti-Cohen symmetry holds in the large current interval for which the additivity principle predictions agree with measurements, thus confirming its validity in this range. The

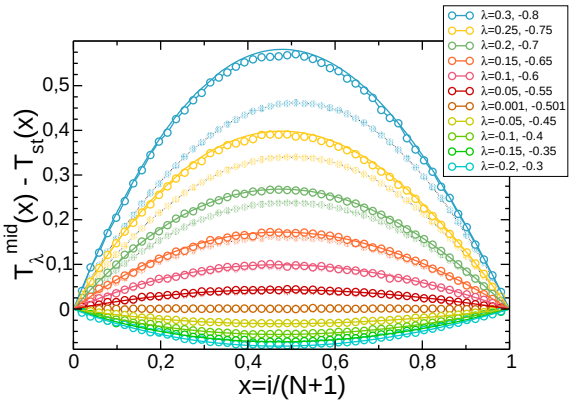

Figure 3.5: Excess energy density profiles for different current fluctuations for the 1D-KMP model with $\rho_L = 2$ and $\rho_R = 1$. Dotted symbols correspond to the measured midtime profiles, whereas solid lines correspond to the theoretical prediction. The invariance under current sign, $\rho_0(x;\lambda) = \rho_0(x;-\lambda-2\varepsilon)$. is observed for a wide current interval. Figure obtained from Refs. [36, 37]

additivity principle leads to the minimization of a functional of the energy density profile, $\rho(x)$, see Eqs. (3.7) and (3.10). A relevant question was whether this optimal profile is actually observable. One naturally defines empirically $\rho_0(x)$ as the average energy profile adopted by the system during a large deviation event of (long) duration τ and time-integrated current $J\tau$, measured at an *intermediate* time $0 \ll \tau \ll t$, i.e. $\rho_0(x) \equiv \rho_0^{\rm mid}(x)$. In Figure 3.5 they showed [36] the measured $\rho_0^{\rm mid}(x)$ for the nonequilibrium setting, and the agreement with BD predictions was again very good in all cases, with discrepancies appearing only for extreme current fluctuations, as otherwise expected. This confirmed the idea that the system indeed modifies its energy density profile to facilitate the deviation of the current, validating the additivity principle as a powerful conjecture to compute both the current LDF and the associated optimal profiles. The numerical results showed also that optimal profiles are indeed independent of the sign of the current, $\rho_0(x;\lambda) = \rho_0(x;-\lambda-2\varepsilon)$ or equivalently $\rho_0(x;J) = \rho_0(x;-J)$, a counter-intuitive symmetry resulting from the reversibility of microscopic dynamics.

3.4 Current fluctuations for 2D diffusive systems

We now set out to derive the current LDF in a two-dimensional diffusive system, particularly in the 2D-KMP model. We have seen that the expression for this LDF (3.1) in a d-dimensional diffusive system without external

field ($\mathbf{Q}_{\mathbf{E}=0}[\rho] = -D[\rho]\boldsymbol{\nabla}\rho$) is given by,

$$G(\mathbf{J}) = -\min_{\rho(\mathbf{r})} \int_\Lambda \frac{\left(\mathbf{J} + D[\rho]\boldsymbol{\nabla}\rho\right)^2}{2\sigma[\rho(\mathbf{r})]} d\mathbf{r}\,. \tag{3.25}$$

This variational problem gives rise to the following non-linear partial differential equation for the optimal profile (3.5) $\rho_0(\mathbf{r}, t; \mathbf{J})$ (in the sequel we drop the $\mathbf{J}$ dependence of the optimal profile)

$$\left(\boldsymbol{\nabla}\rho_0\right)^2 = \frac{\mathbf{J}^2 + 2\sigma[\rho_0]K}{D^2[\rho_0]}. \tag{3.26}$$

where K is a constant of integration which guarantees the correct boundary conditions. Notice that the time-independent optimal profile only depends on the magnitude of $\mathbf{J}$ via $\mathbf{J}^2$ and not on its orientation. Hence, all the isometric current fluctuations characterized by a constant $|\mathbf{J}|$ have the same associated optimal profile, $\rho_0(\mathbf{r}; \mathbf{J}) = \rho_0(\mathbf{r}; |\mathbf{J}|)$. We insist on that this observation will be further exploited in chapter 4.

We now investigate the current statistics in the 2D KMP model. In this case the system is coupled to boundary heat baths along the x-direction at temperatures ρ_L and ρ_R, whereas periodic boundary conditions hold in the y-direction. For $\rho_L \neq \rho_R$ the system reaches a nonequilibrium steady state with a nonzero rescaled average current $\langle \mathbf{J} \rangle = \hat{x}(\rho_L - \rho_R)/2$ and a stationary profile $\rho_{\text{st}}(x, y) = \rho_L + x\,(\rho_R - \rho_L)$. At the macroscopic level the KMP model is characterized by a diffusivity $D[\rho] = \frac{1}{2}$, and a mobility $\sigma[\rho] = \rho^2$ which measures the variance of local energy current fluctuations in equilibrium ($\rho_L = \rho_R$).

To study the statistics of the time-averaged current, we have to solve the partial differential equation (PDE) (3.26), subject to the aforementioned boundary conditions, to get the optimal energy density profile. In principle, this PDE may have several possible solutions. However, the symmetry of the problem suggests that the optimal energy density profile associated to a given current fluctuation depends exclusively on x, with no structure in the y-direction, i.e. $\rho_0(x, y) = \rho_0(x)$, compatible with the presence of an external gradient along the x-direction. This will be checked numerically below. Under these considerations, Eq. (3.26) becomes

$$\left(\frac{d\rho_0(x)}{dx}\right)^2 = 4\mathbf{J}^2\left(1 + 2K\rho_0^2(x)\right), \tag{3.27}$$

which corresponds to the same equation (3.10) for the optimal profile in the 1D case with $|J| = |\mathbf{J}|$. Here, K is the same constant which guarantees the correct boundary conditions, $\rho_0(0, y) = \rho_L$ and $\rho_0(1, y) = \rho_R \quad \forall y \in [0, 1]$. Hence, the optimal energy density profile associated to a fluctuation, $\mathbf{J}$, is the 1D optimal profile calulated in the previous section along the $\hat{x}$-direction, $\rho_0(x, y; |\mathbf{J}|) = \rho_0(x; |\mathbf{J}|)$. Figure 3.2 shows the x-dependence of optimal energy density profiles for different values of $|\mathbf{J}|$, including both the monotone and non-monotone regimes. Thus, Eq. (3.27) together with Eq. (3.25) completely determine the probability $P_\tau(\mathbf{J})$ of observing during a long time τ a time-averaged current $\mathbf{J}$. As in 1D, the optimal energy profile may be

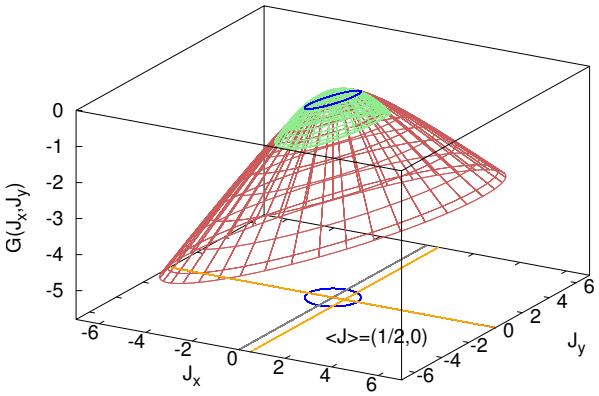

Figure 3.6: $G(\mathbf{J})$ for the 2D-KMP model for $\rho_L = 2$ and $\rho_R = 1$. The blue circle signals the crossover from monotone ($|\mathbf{J}| < |\mathbf{J}_c| \equiv \pi/3$) to non-monotone ($|\mathbf{J}| > \pi/3$) optimal profiles. The green surface corresponds to the Gaussian approximation for small current fluctuations.

now monotone or non-monotone, with a single maximum. In the former case, i.e. $|\mathbf{J}| < |\mathbf{J}_c|$, using Eq. (3.12) into Eq. (3.25) we have

$$G(\mathbf{J}) = \int_{\rho_L}^{\rho_R} d\rho_0 \frac{1}{4|\mathbf{J}|\rho_0^2\sqrt{1+2K\rho_0^2}} \left[\left(J_x - |\mathbf{J}|\sqrt{1+2K\rho_0^2} \right)^2 + J_y^2 \right], \tag{3.28}$$

with J_x and J_y the components of vector $\mathbf{J}$. This results in

$$G(\mathbf{J}) = \frac{J_x}{2}\left(\frac{1}{\rho_R} - \frac{1}{\rho_L}\right) - |\mathbf{J}|^2 K + \frac{|\mathbf{J}|}{2}\left[\frac{\sqrt{1+2K\rho_L^2}}{\rho_L} - \frac{\sqrt{1+2K\rho_R^2}}{\rho_R}\right]. \tag{3.29}$$

For the non-monotonous regime ($|\mathbf{J}| > |\mathbf{J}_c|$) we split the integral in Eq. (3.25) at x^*, and using Eq. (3.13) to change variables we arrive at

$$\begin{aligned} G(\mathbf{J}) &= \frac{J_x}{2}\left(\frac{1}{\rho_R} - \frac{1}{\rho_L}\right) - \frac{|\mathbf{J}|}{2}\left[\frac{1}{\rho_L}\sqrt{1-\left(\frac{\rho_L}{\rho_0^*}\right)^2} + \frac{1}{\rho_R}\sqrt{1-\left(\frac{\rho_R}{\rho_0^*}\right)^2}\right. \\ &- \left.\frac{1}{2\rho_0^*}\left(\pi - \sin^{-1}\left(\frac{\rho_L}{\rho_0^*}\right) - \sin^{-1}\left(\frac{\rho_R}{\rho_0^*}\right)\right)\right]. \end{aligned} \tag{3.30}$$

Recall that $\rho_0^* \equiv \rho_0(x = x^*)$ with $\rho_0^* = 1/\sqrt{-2K}$ which depends implicitely on $|\mathbf{J}|$. This constant can be calculated using Eqs. (3.16). In Figure 3.6 we show $G(\mathbf{J})$ for the 2D-KMP model with $\rho_L = 2$ and $\rho_R = 1$. Notice that the LDF is zero for $\mathbf{J} = \langle \mathbf{J} \rangle = ((\rho_L - \rho_R)/2, 0)$ and negative elsewhere. For

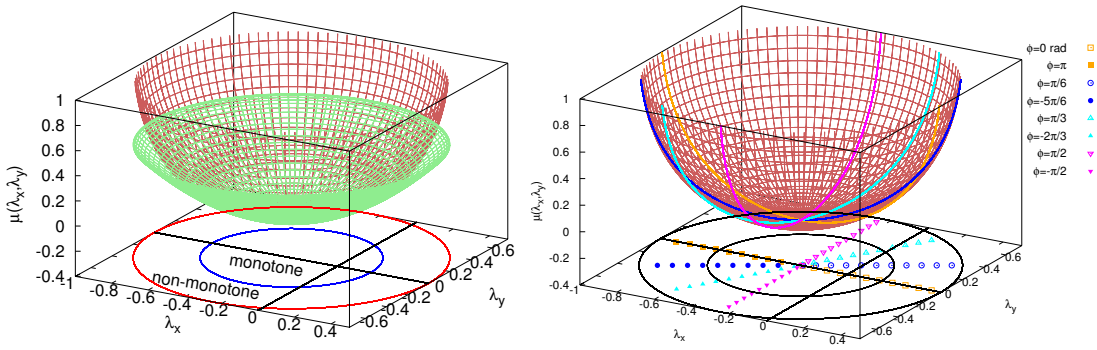

Figure 3.7: Left panel: Legendre transform of $G(\mathbf{J})$ (red) and its quadratic approximation around $\mathbf{J} \approx \langle \mathbf{J} \rangle$ (green) for $\rho_L = 2$ and $\rho_R = 1$, together with the projection in $\boldsymbol{\lambda}$-space of the crossover between monotonus and non-monotonous regime. Right panel: Theoretical $\mu(\boldsymbol{\lambda})$ with $\rho_L = 2$ and $\rho_R = 1$ together with the projection in $\boldsymbol{\lambda}$-space for different angles where measurements are taken.

small current fluctuations, $\mathbf{J} \approx \langle \mathbf{J} \rangle$, $G(\mathbf{J})$ obeys the following quadratic form

$$G(\mathbf{J}) \approx -\frac{1}{2}\left(\frac{(J_x - (\rho_L - \rho_R)/2)^2}{\sigma_x^2} + \frac{J_y^2}{\sigma_y^2} \right), \tag{3.31}$$

with $\sigma_x^2 = (\rho_L^2 + \rho_L\rho_R + \rho_R^2)/3$ and $\sigma_y^2 = \rho_L\rho_R$, resulting in Gaussian statistics for currents near the average as expected from the central limit theorem. Notice that beyond this restricted Gaussian regime, current statistics is in general non-Gaussian. In particular, for large enough current deviations, $G(\mathbf{J})$ decays linearly, meaning that the probability of such fluctuations is *exponentially* small in $|\mathbf{J}|$. Therefore large current fluctuations are far more probable than expected with Gaussian statistics. Sometimes it is interesting to work with the Legendre transform of the current LDF [15, 16, 36, 14],

$$\mu(\boldsymbol{\lambda}) = \max_{\mathbf{J}}[G(\mathbf{J}) + \boldsymbol{\lambda} \cdot \mathbf{J}] = G(\mathbf{J}^*) + \boldsymbol{\lambda} \cdot \mathbf{J}^*, \tag{3.32}$$

where $\boldsymbol{\lambda}$ is a vector parameter conjugate to the current and $\mathbf{J}^*(\boldsymbol{\lambda})$ can be derived from the equation $\partial G(\mathbf{J})/\partial J_\alpha|_{J_\alpha = J_\alpha^*} + \lambda_\alpha = 0$, with λ_α and J_α being the components of $\boldsymbol{\lambda}$ and $\mathbf{J}$ respectively ($\alpha = \hat{x}, \hat{y}$). Using the previous results for $G(\mathbf{J})$ it is easy to show that for both regimes

$$\mu(\boldsymbol{\lambda}) = -K[\mathbf{J}^*(\boldsymbol{\lambda})]^2, \tag{3.33}$$

where $\mathbf{J}^*(\boldsymbol{\lambda})$ is the current associated to a given $\boldsymbol{\lambda}$ and can be obtained using Eqs. (3.12) and (3.13) into Eq. (3.27) for the monotonous and non-monotonus regime respectively. Once we have λ_x and λ_y, one can readily show using (3.29) and (3.30) that for the monotonous regime the following

equality holds

$$|\boldsymbol{\lambda}+\boldsymbol{\varepsilon}| = \frac{1}{2}\left(\frac{\sqrt{1+2K\rho_L^2}}{\rho_L} - \frac{\sqrt{1+2K\rho_R^2}}{\rho_R}\right), \tag{3.34}$$

which in the non-monotonous regime reads

$$|\boldsymbol{\lambda}+\boldsymbol{\varepsilon}| = \frac{1}{2}\left(\frac{\sqrt{1+2K\rho_L^2}}{\rho_L} + \frac{\sqrt{1+2K\rho_R^2}}{\rho_R}\right), \tag{3.35}$$

where $\boldsymbol{\varepsilon} \equiv (\frac{1}{2}\left(\rho_R^{-1} - \rho_L^{-1}\right), 0)$ is a constant vector. Hence, since the constant K just depends on $|\mathbf{J}|$, we have that each value of $|\mathbf{J}|$ corresponds to a given value of $|\boldsymbol{\lambda}+\boldsymbol{\varepsilon}|$ in $\boldsymbol{\lambda}$-space. Note that, in $\boldsymbol{\lambda}$-space, monotone profiles are expected for $|\boldsymbol{\lambda}+\boldsymbol{\varepsilon}| \leq \frac{1}{2\rho_R}\sqrt{1-\left(\frac{\rho_R}{\rho_L}\right)^2}$, while non-monotone profiles appear for $\frac{1}{2\rho_R}\sqrt{1-\left(\frac{\rho_R}{\rho_L}\right)^2} \leq |\boldsymbol{\lambda}+\boldsymbol{\varepsilon}| \leq \frac{1}{2}\left(\frac{1}{\rho_L}+\frac{1}{\rho_R}\right)$ (in particular, for $\rho_L = 2$ and $\rho_R = 1$, see the blue and red circles in $\boldsymbol{\lambda}$-space of left panel of figure 3.7). For small current fluctuations, $\lambda \approx 0$, an expansion similar to (3.31) for $\mu(\boldsymbol{\lambda})$ yields

$$\mu(\boldsymbol{\lambda}) \approx \frac{\lambda_x}{2}\left[(\rho_L - \rho_R) + \sigma_x^2\lambda_x\right] + \frac{\sigma_y^2}{2}\lambda_y^2. \tag{3.36}$$

In left panel of figure 3.7 we show the Legendre transform of the theoretical LDF, $\mu(\boldsymbol{\lambda})$, as well as its gaussian approximation in $\boldsymbol{\lambda}$-space.

3.5 Testing additivity in two dimensions

Once we have derived the analytical predictions for the 2D-KMP model based on the additivity conjecture, we now compare them with results obtained from numerical simulations.

As we have already described in chapter 2, the 2D-KMP model is defined on a two-dimensional square lattice with L^2 sites. Each site is characterized by an energy e_i, $i \in [1, L^2]$, and models a harmonic oscillator which is mechanically uncoupled from its nearest neighbors but interact with them via a stochastic energy-redistribution process (see chapter 2). Dynamics thus proceeds through random energy exchanges between randomly-chosen nearest neighbors. In addition, left and right boundary sites may interchange energy with boundary baths at temperatures ρ_L and ρ_R, respectively, while periodic boundary conditions hold in the vertical direction. We performed a large number of steady-state simulations of long duration $\tau > L^2$ (the unit of time is the Monte Carlo step) for $L = 20$, $\rho_L = 2$ and $\rho_R = 1$. This is a diffusive time scale in which the hydrodynamic behavior should prevoil. These simulations have been performed using the same advanced Monte Carlo algorithm as we used for the 1D case [41], thus yielding the Legendre transform of the LDF of the space- and time-averaged current $\mathbf{J}$. First of all we measured the 2D structure of the optimal profiles for different current fluctuations to check that the optimal energy density profile has structure only along the gradient direction (see figure 3.8). As the gradient is along

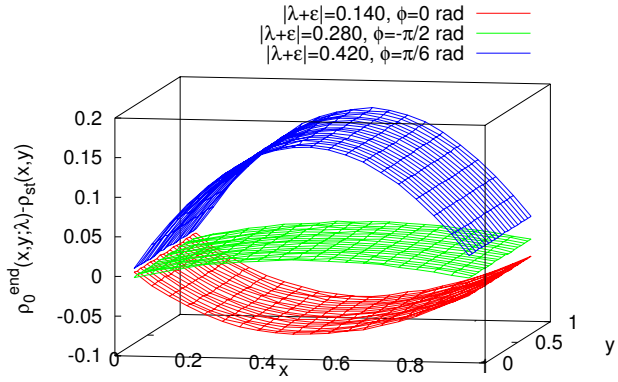

Figure 3.8: 2D excess optimal energy density profiles for different current fluctuations and different orientations with respect to the gradient direction with $L = 20$ and 1000 clones. In all cases no structure along the $\hat{y}$-direction is observed

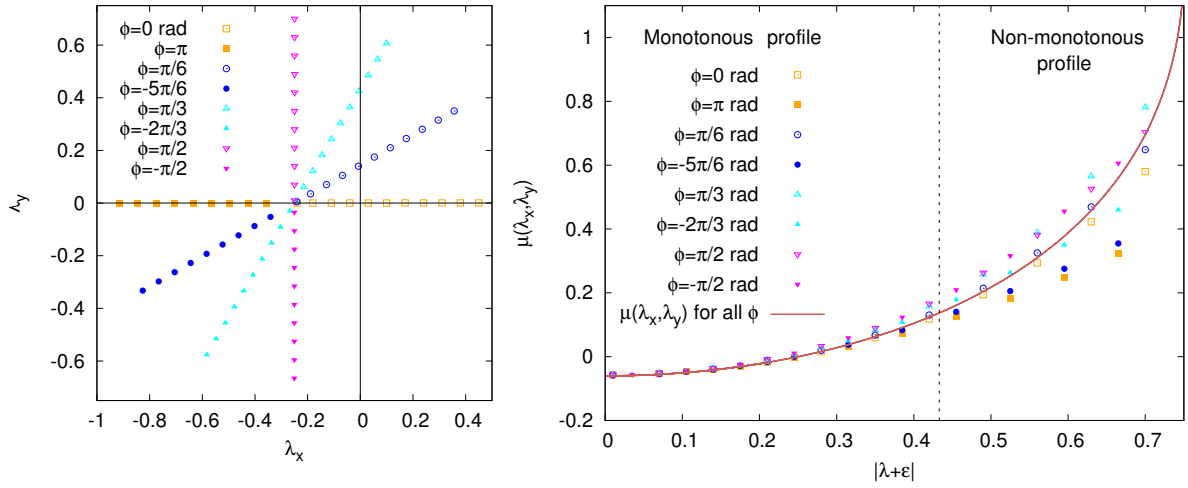

Figure 3.9: Left Panel: Points in $\boldsymbol{\lambda}$-space for different angles where measurements are taken. Right Panel: Measured $\mu(\boldsymbol{\lambda})$ with $\rho_L = 2$, $\rho_R = 1$ and $L = 20$ for different angles versus $|\boldsymbol{\lambda} + \boldsymbol{\varepsilon}|$. The solid line corresponds to the theoretical prediction.

the $\hat{x}$-direction, all current fluctuations with $\lambda_y \neq 0$ have a non-zero vertical component ($J_y \neq 0$). Furthermore, the angle ϕ formed by a current vector $\mathbf{J} = (J_x, J_y)$ with respect to the gradient direction, i.e. $\phi = \tan^{-1}\left(\frac{J_y}{J_x}\right)$, is

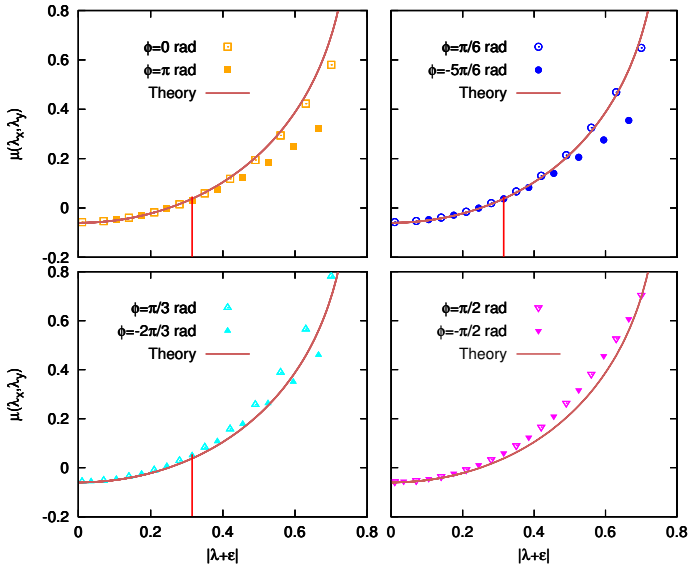

Figure 3.10: Measured $\mu(\boldsymbol{\lambda})$ with $\rho_L = 2$, $\rho_R = 1$, $L = 20$ and 1000 clones for opposite currents (see left panel figure 3.9). The red vertical line indicates the threshold value of $|\boldsymbol{\lambda} + \boldsymbol{\varepsilon}|$ up to which the GC symmetry holds.

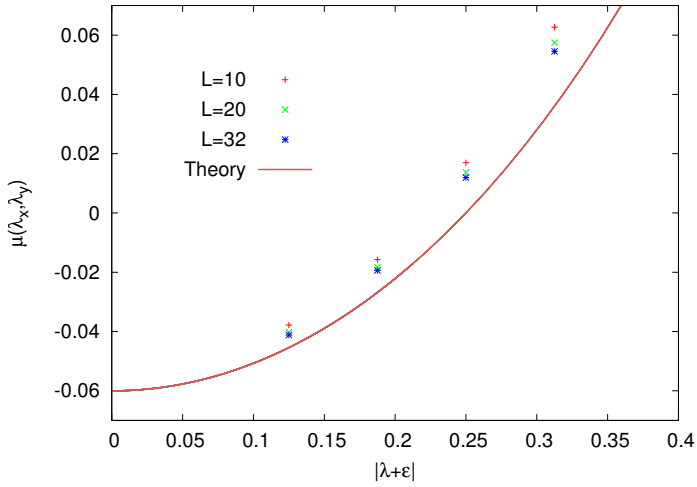

Figure 3.11: Measured $\mu(\boldsymbol{\lambda})$ with $\rho_L = 2$, $\rho_R = 1$, $L = 20$ and 1000 clones versus $|\boldsymbol{\lambda} + \boldsymbol{\varepsilon}|$ for $\phi = \pi/2$ and three different system sizes. The solid line is the theoretical prediction

given in $\boldsymbol{\lambda}$-space by

$$\phi = \tan^{-1}\left(\frac{\lambda_y}{\lambda_x + \varepsilon_x}\right) \tag{3.37}$$

In figure 3.8 we can see how optimal profiles associated to current fluctuations have structure only along the gradient direction, regardless of the orientation ϕ and modolus $|\mathbf{J}|$ of the current fluctuation, confirming the hypothesis $\rho(\mathbf{r};\mathbf{J}) = \rho(x;\mathbf{J})$.

Regarding now the Legendre transform of the LDF, we measured it for different angles with respect to the gradient direction (see right panel of figure 3.7). The theoretical prediction derived for $\mu(\boldsymbol{\lambda})$, Eq. (3.33), is based on the additivity conjecture and gives rise to a function which is independent of the angle ϕ. This is a consequence of the fact that $\mu(\boldsymbol{\lambda})$ depends exclusively on the *magnitude* of $\mathbf{J}$ via $\mathbf{J}^2$ (see Eq. (3.33)) and not on its orientation respect to the gradient direction. Since for each $|\mathbf{J}|$ there is an associated $|\boldsymbol{\lambda}+\boldsymbol{\varepsilon}|$ (see Eqs. (3.34) and (3.35)), we conclude that $\mu(\boldsymbol{\lambda})$ just depends on $|\boldsymbol{\lambda}+\boldsymbol{\varepsilon}|$ and not on ϕ. In the right panel of figure 3.9 we plot the measured $\mu(\boldsymbol{\lambda})$ versus $|\boldsymbol{\lambda}+\boldsymbol{\varepsilon}|$ together with the theoretical prediction for different angles. We observe that there is a good agreement for a broad interval current fluctuations such that $|\boldsymbol{\lambda}+\boldsymbol{\varepsilon}| \leq 0.25$, which corresponds to $|\mathbf{J}| \leq |\langle \mathbf{J} \rangle| = \frac{1}{2}$. From this value on we see that the measurements deviate from the theory and that these deviation depends on ϕ. The origin of such disagreement is twofold: *(i)* finite size effects, as the theory formally applies in the continuum limit but we are unable to simulate reliably systems with $L > 20$, and *(ii)* a different class of finite size effects related to the finite number of clones used to sample the large-deviation statistics [38]. As the Gallavotti-Cohen (GC) symmetry (3.22) is known to hold for any current fluctuation, we can state that numerical violations of this symmetry indicate that simulation results are biased and hence unreliable. The GC symmetry (3.22) implies that $\mu_{\phi}(|\boldsymbol{\lambda}+\boldsymbol{\varepsilon}|) = \mu_{-\pi+\phi}(|\boldsymbol{\lambda}+\boldsymbol{\varepsilon}|)$. Consequently, in figure 3.10 we plot the curves displayed in figure 3.9 in four different plots. In each plot we display the value of $\mu(\boldsymbol{\lambda})$ versus the magnitude of a fluctuation, $|\boldsymbol{\lambda}+\boldsymbol{\varepsilon}|$, for a fixed angle ($\phi$) and for the oppossite angle ($-\pi+\phi$) (see left panel of figure 3.9). This is equivalent to compare opposite current fluctuations which are coupled because of time reversibility. Looking at the top panels and the left bottom panel of figure 3.10, we see that GC holds to a good degree of accuray for $|\boldsymbol{\lambda}+\boldsymbol{\varepsilon}| \lesssim 0.3125$. As the right bottom panel corresponds to $\phi = \pi/2, -\pi/2$, the GC symmetry holds trivially for the whole current interval due to the $\pm y$ symmetry of the problem (recall that we have periodic boundary conditions along the $\hat{y}$-direction). Thus, we conclude that for $|\boldsymbol{\lambda}+\boldsymbol{\varepsilon}| \gtrsim 0.3125$ the algorithm results are biased due to the finite population of clones. On the other hand, the disagreement with the theory for $|\boldsymbol{\lambda}+\boldsymbol{\varepsilon}| \leq 0.3125$ is caused exclusively by finite size effects (small L). We corroborate this in figure 3.11 where we show $\mu(\boldsymbol{\lambda})$ versus $|\boldsymbol{\lambda}+\boldsymbol{\varepsilon}|$ for three system sizes ($L = 10, 20, 32$) and $\phi = \pi/2$. A clear convergence towards the theory as the system size increases is observed.

Attending now the optimal energy density profile, we compare the analytical predicitions with the measured profiles averaged along the y-direction. This comparison is done in figure 3.12, where we show the excess optimal energy density profiles ($\Delta\rho_0(x;\boldsymbol{\lambda}) = \rho_0(x;\boldsymbol{\lambda}) - \rho_{st}(x)$) given an angle for six

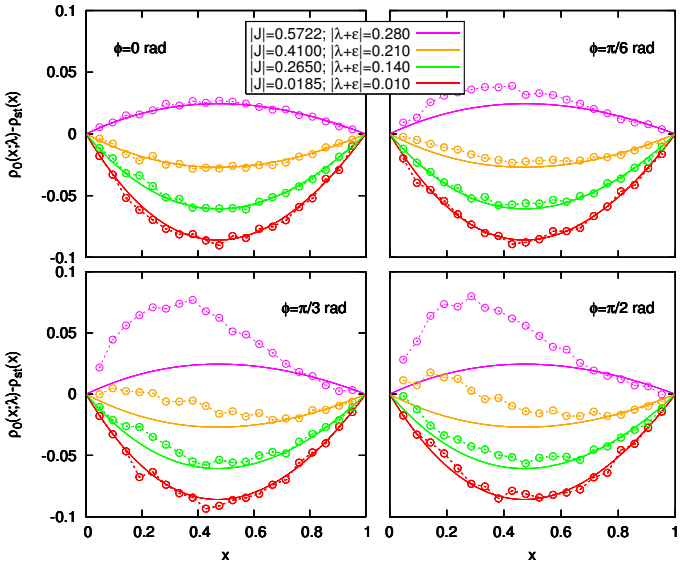

Figure 3.12: Measured optimal energy density profiles with $\rho_L = 2$, $\rho_R = 1$, $L = 20$ and 1000 clones for different angles versus $|\boldsymbol{\lambda} + \boldsymbol{\varepsilon}|$. The solid lines correspond to the theoretical profiles.

different values of $|\boldsymbol{\lambda} + \boldsymbol{\varepsilon}|$ which correspond to six different values of $|\mathbf{J}|$. We see how along the gradient direction ($\phi = 0$) the agreement with the theoretical profiles is perfect for all current fluctuations. However, as the current fluctuation deviates from the $\hat{x}$-direction, there is only good agreement for moderate current fluctuations, particularly for $|\mathbf{J}| = 0.265$ and $|\mathbf{J}| = 0.0185$. Although the additivity conjecture leads to the invariance of the optimal profiles under current rotations (see Eq. (3.26)), these violations here observed are a result of the finite, discrete character of the lattice system.

3.6 Conclusions

In this chapter, we have investigated the statistics of current fluctuations in a simple but very general model of diffusive energy transport in one and two dimensions, the KMP model [35].

We have derived theoretical predictions using the MFT, supplemented with an additivity conjecture which amounts to assume that (in d-dimensions)

(i) The optimal profiles responsible of a given current fluctuation are time-independent.

(ii) The resulting divergence-free optimal current profile is in fact constant across space.

In 1D this is equivalent to the additivity principle of Bodineau and Derrida [34] (see appendix A). In this case, it was shown [36, 37] that numerical sim-

ulations agree with theoretical predictions for a wide current interval. In the 2D case and provided that the additivity conjecture holds, we have obtained explicitely the current distribution for this model, which exhibits in general non-Gaussian tails. We have found good agreement for the theoretical LDF with numerical simulations. Furthermore, we also measured the optimal energy density profiles associated to a given current fluctuation finding again good agreement with the theoretical prediction. Profiles can be either monotone for small current fluctuations, or non-monotone with a single maximum for large enough fluctuations. It is remarkable that in this case, due to the periodicity in the vertical direction, these optimal profiles have structure only along the gradient direction. This symplifies considerably the calculations up to the point that the 2D optimal profiles associated to a given current fluctuation, $\mathbf{J}$, have the same structure along the $\hat{x}$-direction as in the 1D case (for $|J| = |\mathbf{J}|$). In addition, they are invariant under current rotations with respect to the gradient direction because they only depend on the magnitude of $|\mathbf{J}|$ and not on its orientation. In the next chapter we will see how this invariance has important consequences at the level of symmetries of the current distribution.

To conclude we can state that all the results here obtained strongly support the validity of the additivity conjecture in d-dimensional systems. However, assumption *(i)* is known to break down for extreme current fluctuations in some particular cases [16, 39, 40]. In chapter 5 we will study this breakdown for a periodic system in one and two dimensions, and we will observe the emergence of time-dependent optimal profiles. It could be also interesting to explore the range of validity of hypothesis *(ii)* in the time-independent regime. This could be achieved using a local stability analysis in the spirit of the results in [39].

Chapter 4

Symmetries in fluctuations far from equilibrium

4.1 Introduction

Large fluctuations, though rare, play an important role in many fields of science as they crucially determine the fate of a system [44]. Examples range from chemical reaction kinetics or the escape of metastable electrons in nanoelectronic devices to conformational changes in proteins, mutations in DNA, and nucleation events in the primordial universe. Remarkably, the statistics of these large fluctuations contains deep information on the physics of the system of interest [14, 17]. This is particularly important for systems far from equilibrium, where no general theory exists up to date capable of predicting macroscopic and fluctuating behavior in terms of microscopic physics, in a way similar to equilibrium statistical physics. The consensus is that the study of fluctuations out of equilibrium may open the door to such general theory. As most nonequilibrium systems are characterized by currents of locally conserved observables, understanding current statistics in terms of microscopic dynamics has become one of the main objectives of nonequilibrium statistical physics [8, 9, 11, 13, 14, 12, 15, 16, 17, 34, 36, 37, 39, 45, 46, 47]. Pursuing this line of research is both of fundamental as well as practical importance. At the theoretical level, the function controlling current fluctuations can be identified as the nonequilibrium analog of the free energy functional in equilibrium systems [14, 15, 16, 17], from which macroscopic properties of a nonequilibrium system can be obtained (including its most prominent features, as for instance the ubiquitous long range correlations [21, 22], etc.) On the other hand, the physics of most modern mesoscopic devices is characterized by large fluctuations which determine their behavior and function. In this way understanding current statistics in these systems is of great practical significance.

Despite the considerable interest and efforts on these issues, exact and general results valid arbitrarily far from equilibrium are still very scarce. The reason is that, while in equilibrium phenomena dynamics is irrelevant and the Gibbs distribution provides all the necessary information, in nonequilibrium

physics dynamics plays a dominant role, even in the simplest situation of a nonequilibrium steady state [14, 15, 16, 17]. However, there is a remarkable exception to this absence of general results which has triggered an important surge in activity since its formulation in the mid nineties. This is the fluctuation theorem, first discussed in the context of simulations of sheared fluids [9], and formulated rigorously by Gallavotti and Cohen under very general assumptions [8]. This theorem, which implies a relation between the probabilities of a given current fluctuation and the inverse event, is a deep statement on the subtle consequences of time-reversal symmetry of microscopic dynamics at the macroscopic, irreversible level. Particularly important here is the observation that symmetries are reflected at the fluctuating macroscopic level arbitrarily far from equilibrium. Inspired by this illuminating result, we explore in this chapter the behavior of the current distribution under symmetry transformations [48]. Key to our analysis is the observation that, in order to facilitate a given current fluctuation, the system traverses a well-defined optimal path in phase space [14, 15, 16, 17, 36, 37, 49]. This path is, under very general conditions, invariant under certain symmetry transformations on the current. Using this invariance we show that for d-dimensional, time-reversible systems described by a locally-conserved field and possibly subject to a boundary-induced gradient and an external field $\mathbf{E}$, the probability $\mathrm{P}_\tau(\mathbf{J})$ of observing a current $\mathbf{J}$ averaged over a long time τ obeys an *isometric* fluctuation relation (IFR)

$$\lim_{\tau\to\infty} \frac{1}{\tau} \ln\left[\frac{\mathrm{P}_\tau(\mathbf{J})}{\mathrm{P}_\tau(\mathbf{J}')}\right] = \boldsymbol{\epsilon}\cdot(\mathbf{J}-\mathbf{J}')\,, \tag{4.1}$$

for any pair of isometric current vectors, $|\mathbf{J}| = |\mathbf{J}'|$. Here $\boldsymbol{\epsilon} = \boldsymbol{\varepsilon} + \mathbf{E}$ is a constant vector directly related to the rate of entropy production in the system, which depends on the boundary baths via $\boldsymbol{\varepsilon}$ (see below).

The above equation, which includes as a particular case the Gallavotti-Cohen (GC) result for $\mathbf{J}' = -\mathbf{J}$, relates in a strikingly simple manner the probability of a given fluctuation $\mathbf{J}$ with the likelihood of any other current fluctuation on the d-dimensional hypersphere of radius $|\mathbf{J}|$, see figure 4.1, projecting a complex d-dimensional problem onto a much simpler one-dimensional theory. Unlike the GC relation which is a non-differentiable symmetry involving the inversion of the current sign, $\mathbf{J} \to -\mathbf{J}$, Eq. (4.1) is valid for arbitrary changes in orientation of the current vector. This makes the experimental test of the above relation a feasible problem, as data for current fluctuations involving different orientations around the average can be gathered with enough statistics to ensure experimental accuracy. It is also important to notice that the isometric fluctuation relation is valid for arbitrarily large fluctuations, i.e. even for the non-Gaussian far tails of current distribution. We confirm here the validity of the new symmetry in extensive numerical simulations of two different nonequilibrium systems: (i) A simple and very general lattice model of energy diffusion [36, 37, 35], and (ii) a hard-disk fluid in a temperature gradient [50].

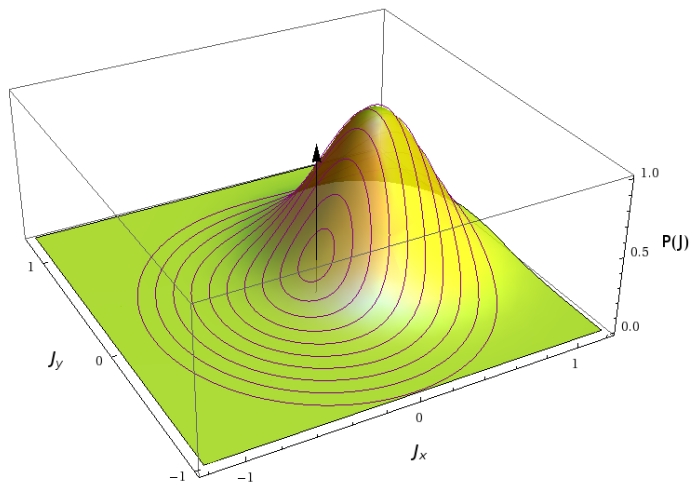

Figure 4.1: The isometric fluctuation relation at a glance. Sketch of the current distribution in two dimensions, peaked around its average $\langle \mathbf{J} \rangle_\epsilon$, and isometric contour lines for different $|\mathbf{J}|$'s. The isometric fluctuation relation, Eq. (4.1), establishes a simple relation for the probability of current fluctuations along each of these contour lines.

4.2 The Isometric Fluctuation Relation

Our starting point is the continuity equation given by Eq. (1.2), which describes the macroscopic evolution of a wide class of systems characterized by a locally-conserved magnitude (e.g. energy, particle density, momentum, etc.)

$$\partial_t \rho(\mathbf{r}, t) = -\boldsymbol{\nabla} \cdot \Big(\mathbf{Q}_\mathbf{E}[\rho(\mathbf{r}, t)] + \boldsymbol{\xi}(\mathbf{r}, t) \Big) \,. \tag{4.2}$$

We are interested in the probability $\mathrm{P}_\tau(\mathbf{J})$ of observing a space- and time-averaged empirical current $\mathbf{J}$, defined as

$$\mathbf{J} = \frac{1}{\tau} \int_0^\tau dt \int_\Lambda d\mathbf{r}\ \mathbf{j}(\mathbf{r}, t) \,. \tag{4.3}$$

where $\Lambda \in [0,1]^d$ is the space domain, being d the dimensionality of the system. This probability obeys a large deviation principle for long times [23, 24], $\mathrm{P}_\tau(\mathbf{J}) \sim \exp[+\tau L^d G(\mathbf{J})]$, where L is the system linear size and $G(\mathbf{J}) \leq 0$ is the current large-deviation function (LDF), meaning that current fluctuations away from the average are exponentially unlikely in time. According to macroscopic fluctuation theory described in chapter 1 we have

$$G(\mathbf{J}) = -\min_{\rho(\mathbf{r})} \int_\Lambda \frac{\big(\mathbf{J} - \mathbf{Q}_\mathbf{E}[\rho(\mathbf{r})]\big)^2}{2\sigma[\rho(\mathbf{r})]} d\mathbf{r} \,, \tag{4.4}$$

which expresses the *locally*-Gaussian nature of fluctuations [34, 36, 37]. The optimal profile $\rho_0(\mathbf{r}; \mathbf{J})$ solution of the above variational problem can be

interpreted as the density profile the system adopts to facilitate a current fluctuation $\mathbf{J}$ [36, 37, 49]. To derive Eq. (4.4) we assumed the additivity conjecture, namely that (i) the optimal profiles associated to a given current fluctuation are time-independent , and (ii) the optimal current field has no spatial structure. This last hypothesis, which greatly simplifies the calculation of current statistics, can be however relaxed for our purposes (as shown below). The probability $\mathrm{P}_\tau(\mathbf{J})$ is thus simply the *Gaussian* weight associated to the optimal profile. Note however that the minimization procedure gives rise to a nonlinear problem which results in general in a current distribution with non-Gaussian tails [14, 15, 16, 17, 34, 36, 37].

The optimal profile is solution of the following equation

$$\frac{\delta\omega_2[\rho(\mathbf{r})]}{\delta\rho(\mathbf{r}')} - 2\mathbf{J}\cdot\frac{\delta\boldsymbol{\omega}_1[\rho(\mathbf{r})]}{\delta\rho(\mathbf{r}')} + \mathbf{J}^2\frac{\delta\omega_0[\rho(\mathbf{r})]}{\delta\rho(\mathbf{r}')} = 0\,, \tag{4.5}$$

where $\frac{\delta}{\delta\rho(\mathbf{r}')}$ stands for functional derivative, and

$$\boldsymbol{\omega}_n[\rho(\mathbf{r})] \equiv \int_\Lambda d\mathbf{r}\,\mathbf{W}_n[\rho(\mathbf{r})] \qquad \text{with} \qquad \mathbf{W}_n[\rho(\mathbf{r})] \equiv \frac{\mathbf{Q}^n_{\mathbf{E}}[\rho(\mathbf{r})]}{\sigma[\rho(\mathbf{r})]}\,. \tag{4.6}$$

Remarkably, the optimal profile $\rho_0(\mathbf{r};\mathbf{J})$ solution of Eq. (4.5) depends exclusively on $\mathbf{J}$ and $\mathbf{J}^2$. Such a simple quadratic dependence, inherited from the locally-Gaussian nature of fluctuations, has important consequences at the level of symmetries of the current distribution. In fact, it is clear from Eq. (4.5) that the condition

$$\frac{\delta\boldsymbol{\omega}_1[\rho(\mathbf{r})]}{\delta\rho(\mathbf{r}')} = 0\,, \tag{4.7}$$

implies that $\rho_0(\mathbf{r};\mathbf{J})$ will depend exclusively on the *magnitude* of the current vector, via $\mathbf{J}^2$, not on its *orientation*. In this way, all isometric current fluctuations characterized by a constant $|\mathbf{J}|$ will have the same associated optimal profile, $\rho_0(\mathbf{r};\mathbf{J}) = \rho_0(\mathbf{r};|\mathbf{J}|)$, independently of whether the current vector $\mathbf{J}$ points along the gradient direction, against it, or along any arbitrary direction. In other words, the optimal profile is invariant under current rotations if Eq. (4.7) holds.

It turns out that condition (4.7) follows from the time-reversibility of the dynamics, in the sense that the evolution operator in the Fokker-Planck formulation of Eq. (4.2) obeys a local detailed balance condition [12, 13]. In this case

$$\mathbf{W}_1[\rho(\mathbf{r})] = \frac{\mathbf{Q}_{\mathbf{E}}[\rho(\mathbf{r})]}{\sigma[\rho(\mathbf{r})]} = -\boldsymbol{\nabla}\frac{\delta\mathcal{H}[\rho]}{\delta\rho}\,, \tag{4.8}$$

where $\mathcal{H}[\rho(\mathbf{r})]$ is the system Hamiltonian. In this case, by using vector integration by parts, it is easy to show that

$$\frac{\delta}{\delta\rho(\mathbf{r}')}\int_\Lambda d\mathbf{r}\mathbf{W}_1[\rho(\mathbf{r})]\cdot\boldsymbol{\mathcal{A}}(\mathbf{r}) = -\frac{\delta}{\delta\rho(\mathbf{r}')}\int_{\partial\Lambda} d\Gamma\frac{\delta\mathcal{H}[\rho]}{\delta\rho}\boldsymbol{\mathcal{A}}(\mathbf{r})\cdot\hat{n} = 0\,, \tag{4.9}$$

for any divergence-free vector field $\boldsymbol{\mathcal{A}}(\mathbf{r})$. The second integral is taken over the boundary $\partial\Lambda$ of the domain Λ where the system is defined, and $\hat{n}$ is the

unit vector normal to the boundary at each point. In particular, by taking $\boldsymbol{\mathcal{A}}(\mathbf{r}) = \mathbf{J}$ constant, Eq. (4.9) implies that $\delta\boldsymbol{\omega}_1[\rho(\mathbf{r})]/\delta\rho(\mathbf{r}') = 0$. Hence for time-reversible systems the optimal profile $\rho_0(\mathbf{r};\mathbf{J})$ remains invariant under rotations of the current $\mathbf{J}$, see Eq. (4.5), and this allows us to prove the isometric fluctuation relation (IFR) given by Eq. (4.1). The invariance of the optimal profile can be now used in Eq. (4.4) to relate in a simple way the current LDF of any pair of isometric current fluctuations $\mathbf{J}$ and $\mathbf{J}'$, with $|\mathbf{J}| = |\mathbf{J}'|$,

$$G(\mathbf{J}) - G(\mathbf{J}') = |\boldsymbol{\epsilon}||\mathbf{J}|(\cos\theta - \cos\theta')\,, \tag{4.10}$$

where θ and θ' are the angles formed by vectors $\mathbf{J}$ and $\mathbf{J}'$, respectively, with a constant vector $\boldsymbol{\epsilon} = \boldsymbol{\varepsilon} + \mathbf{E}$, see below. Eq. (4.10) is just an alternative formulation of the isometric fluctuation relation (4.1). By letting $\mathbf{J}$ and $\mathbf{J}'$ differ by an infinitesimal angle, the IFR can be cast in a simple differential form, $\partial_\theta G(\mathbf{J}) = |\boldsymbol{\epsilon}||\mathbf{J}|\sin\theta$, which reflects the high level of symmetry imposed by time-reversibility on the current distribution.

The condition $\delta\boldsymbol{\omega}_1[\rho(\mathbf{r})]/\delta\rho(\mathbf{r}') = 0$ can be seen as a conservation law. It implies that the observable $\boldsymbol{\omega}_1[\rho(\mathbf{r})]$ is in fact a *constant of motion*, $\boldsymbol{\epsilon} \equiv \boldsymbol{\omega}_1[\rho(\mathbf{r})]$, independent of the profile $\rho(\mathbf{r})$, which can be related with the rate of entropy production via the Gallavotti-Cohen theorem [8, 12, 13]. In a way similar to Noether's theorem, the conservation law for $\boldsymbol{\epsilon}$ implies a symmetry for the optimal profiles under rotations of the current and a fluctuation relation for the current LDF. This constant can be easily computed under very general assumptions (see Sec. 4.4).

4.3 Implications and Generalizations

The isometric fluctuation relation, Eq. (4.1), has far-reaching and nontrivial consequences. As we shall see, the IFR implies remarkable hierarchies of equations for the current cumulants, see Eq. (4.14), and the nonlinear response coefficients, see eqs. (4.16)-(4.19), going far beyond Onsager's reciprocity relations and Green-Kubo formulas.

4.3.1 Hierarchies for the cumulants and response coefficients

The moment-generating function associated to $\mathrm{P}_\tau(\mathbf{J})$, defined as

$$\Pi_\tau(\boldsymbol{\lambda}) = \int \mathrm{P}_\tau(\mathbf{J}) \exp(\tau L^d \boldsymbol{\lambda}\cdot\mathbf{J}) d\mathbf{J}, \tag{4.11}$$

scales for long times as $\Pi_\tau(\boldsymbol{\lambda}) \sim \exp[+\tau L^d \mu(\boldsymbol{\lambda})]$, where $\mu(\boldsymbol{\lambda}) = \max_{\mathbf{J}}[G(\mathbf{J}) + \boldsymbol{\lambda}\cdot\mathbf{J}]$ is the cumulant generating function and corresponds to the Legendre transform of the current LDF. The cumulants of the current distribution can be obtained from the derivatives of $\mu(\boldsymbol{\lambda})$ evaluated at $\boldsymbol{\lambda} = 0$, i.e.

$$\mu^{(n)}_{(n_1\ldots n_d)} \equiv \left[\frac{\partial^n \mu(\boldsymbol{\lambda})}{\partial\lambda_1^{n_1}\ldots\lambda_d^{n_d}}\right]_{\lambda=0} = (\tau L^d)^{n-1}\langle \Delta J_1^{n_1}\ldots\Delta J_d^{n_d}\rangle_\epsilon \quad \text{for} \quad n \geq 1, \tag{4.12}$$

where $\Delta J_\alpha \equiv J_\alpha - (1-\delta_{n,1})\langle J_\alpha\rangle_\epsilon$ and $\delta_{n,m}$ is the Kronecker symbol. In virtue of the IFR, which states that $G(\mathbf{J}) - G(\mathcal{R}\mathbf{J}) = \boldsymbol{\epsilon}\cdot(\mathbf{J}-\mathcal{R}\mathbf{J})$, the Legendre transform of the current LDF fullfills

$$\mu(\boldsymbol{\lambda}) = \max_{\mathbf{J}}[G(\mathbf{J})+\boldsymbol{\lambda}\cdot\mathbf{J}] = \max_{\mathbf{J}'}[G(\mathbf{J}')+(\mathcal{R}(\boldsymbol{\lambda}+\boldsymbol{\epsilon})-\boldsymbol{\epsilon})\cdot\mathbf{J}'] = \mu[\mathcal{R}(\boldsymbol{\lambda}+\boldsymbol{\epsilon})-\boldsymbol{\epsilon})],$$

where we have used the change of variables $\mathbf{J}' = \mathcal{R}\mathbf{J}$. Hence, the IFR can be stated for $\mu(\boldsymbol{\lambda})$ as

$$\mu(\boldsymbol{\lambda}) = \mu[\mathcal{R}(\boldsymbol{\lambda}+\boldsymbol{\epsilon})-\boldsymbol{\epsilon}], \tag{4.13}$$

where $\mathcal{R}$ is any d-dimensional rotation. Using this relation in the definition of the n-th order cumulant in the limit of infinitesimal rotations, $\mathcal{R} = \mathbb{I} + \Delta\theta\mathcal{L}$, it is easy to show that

$$n_\alpha \mathcal{L}_{\beta\alpha}\mu^{(n)}_{(n_1\ldots n_\alpha-1\ldots n_\beta+1\ldots n_d)} + \epsilon_\nu \mathcal{L}_{\gamma\nu}\mu^{(n+1)}_{(n_1\ldots n_\gamma+1\ldots n_d)} = 0\,, \tag{4.14}$$

where $\mathcal{L}$ is any generator of d-dimensional rotations, and summation over repeated Greek indices ($\in[1,d]$) is assumed. The above hierarchy relates in a simple way cumulants of orders n and $n+1$ $\forall n \geq 1$, and is valid arbitrarily far from equilibrium. As an example, eqs. (4.20) and (4.21) below show the first two sets of relations ($n = 1, 2$) of the above hierarchy in two dimensions.

In a similar way, we can explore the consequences of the IFR on the linear and nonlinear response coefficients. For that, we now expand the cumulants of the current in powers of $\boldsymbol{\epsilon}$

$$\mu^{(n)}_{(n_1\ldots n_d)}(\boldsymbol{\epsilon}) = \sum_{k=0}^{\infty}\frac{1}{k!}\sum_{\substack{k_1\ldots k_d=0\\ \sum_i k_i=k}}^{k} {}^{(k)}_{(n)}\chi^{(k_1\ldots k_d)}_{(n_1\ldots n_d)}\,\epsilon_1^{k_1}\ldots\epsilon_d^{k_d} \tag{4.15}$$

Inserting expansion (4.15) into the cumulant hierarchy, Eq. (4.14), and matching order by order in k, we derive another interesting hierarchy for the response coefficients of the different cumulants. For $k = 0$ this reads

$$n_\alpha \mathcal{L}_{\beta\alpha}\,{}^{(0)}_{(n)}\chi^{(0\ldots0)}_{(n_1\ldots n_\alpha-1\ldots n_\beta+1\ldots n_d)} = 0\,, \tag{4.16}$$

which is a symmetry relation for the equilibrium ($\boldsymbol{\epsilon} = 0$) current cumulants. For $k \geq 1$ we obtain

$$\sum_{\substack{k_1\ldots k_d=0\\ \sum_i k_i=k\geq1}}^{k}\left[\frac{n_\alpha}{k}\mathcal{L}_{\beta\alpha}\,{}^{(k)}_{(n)}\chi^{(k_1\ldots k_d)}_{(n_1\ldots n_\alpha-1\ldots n_\beta+1\ldots n_d)} + \mathcal{L}_{\gamma\nu}\,{}^{(k-1)}_{(n+1)}\chi^{(k_1\ldots k_\nu-1\ldots k_d)}_{(n_1\ldots n_\gamma+1\ldots n_d)}\right] = 0\,, \tag{4.17}$$

which relates k-order response coefficients of n-order cumulants with $(k-1)$-order coefficients of $(n+1)$-order cumulants. Relations (4.16)-(4.17) for the response coefficients result from the IFR in the limit of infinitesimal rotations. For a finite rotation $\mathcal{R} = -\mathbb{I}$, which is equivalent to a current

inversion, we have $\mu(\boldsymbol{\lambda}) = \mu(-\boldsymbol{\lambda} - 2\boldsymbol{\epsilon})$ and we may use this in the definition of response coefficients,

$$ {}^{(k)}_{(n)}\chi^{(k_1\ldots k_d)}_{(n_1\ldots n_d)} \equiv k! \left[\frac{\partial^{n+k}\mu(\boldsymbol{\lambda})}{\partial\lambda_1^{n_1}\ldots\lambda_d^{n_d}\partial\epsilon_1^{k_1}\ldots\epsilon_d^{k_d}} \right]_{\lambda=0=\epsilon}, \tag{4.18} $$

see Eq. (4.15), to obtain a complementary relation for the response coefficients

$$ {}^{(k)}_{(n)}\chi^{(k_1\ldots k_d)}_{(n_1\ldots n_d)} = k! \sum_{p_1=0}^{k_1} \ldots \sum_{p_d=0}^{k_d} \frac{(-1)^{n+p}2^p}{(k-p)!} \, {}^{(k-p)}_{(n+p)}\chi^{(k_1-p_1\ldots k_d-p_d)}_{(n_1+p_1\ldots n_d+p_d)}, \tag{4.19} $$

where $p = \sum_i p_i$. A similar equation was derived in [51] from the standard fluctuation theorem, although the IFR adds further relations. All together, eqs. (4.16)-(4.19) imply deep relations between the response coefficients at arbitrary orders which go far beyond Onsager's reciprocity relations and Green-Kubo formulae.

As an example, the cumulant hierarchy in two dimensions implies the following relations

$$ \begin{aligned} \langle J_x\rangle_\epsilon &= \tau L^2 \left[\epsilon_x\langle\Delta J_y^2\rangle_\epsilon - \epsilon_y\langle\Delta J_x\Delta J_y\rangle_\epsilon\right] \\ \langle J_y\rangle_\epsilon &= \tau L^2 \left[\epsilon_y\langle\Delta J_x^2\rangle_\epsilon - \epsilon_x\langle\Delta J_x\Delta J_y\rangle_\epsilon\right] \end{aligned} \tag{4.20} $$

$$ \begin{aligned} 2\langle\Delta J_x\Delta J_y\rangle_\epsilon &= \tau L^2 \left[\epsilon_y\langle\Delta J_x^3\rangle_\epsilon - \epsilon_x\langle\Delta J_x^2\Delta J_y\rangle_\epsilon\right] \\ &= \tau L^2 \left[\epsilon_x\langle\Delta J_y^3\rangle_\epsilon - \epsilon_y\langle\Delta J_x\Delta J_y^2\rangle_\epsilon\right] \\ \langle\Delta J_x^2\rangle_\epsilon - \langle\Delta J_y^2\rangle_\epsilon &= \tau L^2 \left[\epsilon_x\langle\Delta J_x\Delta J_y^2\rangle_\epsilon - \epsilon_y\langle\Delta J_x^2\Delta J_y\rangle_\epsilon\right], \end{aligned} \tag{4.21} $$

for the first cumulants, with $\Delta J_\alpha \equiv J_\alpha - \langle J_\alpha\rangle_\epsilon$. It is worth stressing that the cumulant hierarchy is valid arbitrarily far from equilibrium.

In a similar way, the IFR implies a set of hierarchies for the nonlinear response coefficients, see eqs. (4.16)-(4.19) above. In our two-dimensional example, let ${}^{(k)}_{(n)}\chi^{(k_x,k_y)}_{(n_x,n_y)}$ be the response coefficient of the cumulant $\langle\Delta J_x^{n_x}\Delta J_y^{n_y}\rangle_\epsilon$ to order $\epsilon_x^{k_x}\epsilon_y^{k_y}$, with $n = n_x + n_y$ and $k = k_x + k_y$. To the lowest order these hierarchies imply Onsager's reciprocity symmetries and Green-Kubo relations for the linear response coefficients of the current. They further predict that in fact the linear response matrix is proportional to the identity, so

$$ {}^{(1)}_{(1)}\chi^{(1,0)}_{(1,0)} = {}^{(1)}_{(1)}\chi^{(0,1)}_{(0,1)} = {}^{(0)}_{(2)}\chi^{(0,0)}_{(2,0)} = {}^{(0)}_{(2)}\chi^{(0,0)}_{(0,2)}, $$

while

$$ {}^{(1)}_{(1)}\chi^{(0,1)}_{(1,0)} = 0 = {}^{(1)}_{(1)}\chi^{(1,0)}_{(0,1)}. $$

The first nonlinear coefficients of the current can be simply written in terms of the linear coefficients of the second cumulants as

$$ {}^{(2)}_{(1)}\chi^{(2,0)}_{(1,0)} = 2{}^{(1)}_{(2)}\chi^{(1,0)}_{(2,0)} \quad \text{and} \quad {}^{(2)}_{(1)}\chi^{(0,2)}_{(1,0)} = -2{}^{(1)}_{(2)}\chi^{(1,0)}_{(1,1)}, $$

while the cross-coefficient reads

$$\overset{(2)}{(1)}\chi^{(1,1)}_{(1,0)} = 2\left[\overset{(1)}{(2)}\chi^{(0,1)}_{(2,0)} + \overset{(1)}{(2)}\chi^{(0,1)}_{(1,1)}\right]$$

(symmetric results hold for $n_x = 0$, $n_y = 1$). Linear response coefficients for the second-order cumulants also obey simple relations, e.g.

$$\overset{(1)}{(2)}\chi^{(1,0)}_{(1,1)} = -\overset{(1)}{(2)}\chi^{(0,1)}_{(1,1)} \quad \text{and} \quad \overset{(1)}{(2)}\chi^{(1,0)}_{(2,0)} + \overset{(1)}{(2)}\chi^{(0,1)}_{(2,0)} = \overset{(1)}{(2)}\chi^{(1,0)}_{(0,2)} + \overset{(1)}{(2)}\chi^{(0,1)}_{(0,2)},$$

and the set of relations continues to arbitrary high orders. In this way hierarchies (4.16)-(4.19), which derive from microreversibility as reflected in the IFR, provide deep insights into nonlinear response theory for nonequilibrium systems [51].

4.3.2 Generalized IFR

The IFR and the above hierarchies all follow from the invariance of optimal profiles under certain transformations. This idea can be further exploited in more general settings. In fact, by writing explicitly the dependence on the external field $\mathbf{E}$ in Eq. (4.5) for the optimal profile, one realizes that if

$$\frac{\delta}{\delta\rho(\mathbf{r}')}\int_\Lambda \mathbf{Q}[\rho(\mathbf{r})]d\mathbf{r} = 0, \tag{4.22}$$

together with the time-reversibility condition, Eq. (4.7), the resulting optimal profiles are invariant under *independent* rotations of the current and the external field. It thus follows that the current LDFs for pairs $(\mathbf{J}, \mathbf{E})$ and $(\mathbf{J}' = \mathcal{R}\mathbf{J}, \mathbf{E}^* = \mathcal{S}\mathbf{E})$, with $\mathcal{R}$, $\mathcal{S}$ independent rotations, obey a generalized isometric fluctuation relation

$$G_{\mathbf{E}}(\mathbf{J}) - G_{\mathbf{E}^*}(\mathbf{J}') = \boldsymbol{\varepsilon}\cdot(\mathbf{J}-\mathbf{J}') - \boldsymbol{\nu}\cdot(\mathbf{E}-\mathbf{E}^*) + \mathbf{J}\cdot\mathbf{E} - \mathbf{J}'\cdot\mathbf{E}^*, \tag{4.23}$$

where we write explicitly the dependence of the current LDF on the external field. The vector $\boldsymbol{\nu} \equiv \int_\Lambda \mathbf{Q}[\rho(\mathbf{r})]d\mathbf{r}$ is now another constant of motion, independent of $\rho(\mathbf{r})$, which can be easily computed (see Sec. 4.4). For a fixed boundary gradient, the above equation relates any current fluctuation $\mathbf{J}$ in the presence of an external field $\mathbf{E}$ with any other isometric current fluctuation $\mathbf{J}'$ in the presence of an arbitrarily-rotated external field $\mathbf{E}^*$, and reduces to the standard IFR for $\mathbf{E} = \mathbf{E}^*$. Condition $\frac{\delta}{\delta\rho(\mathbf{r}')}\int_\Lambda \mathbf{Q}[\rho(\mathbf{r})]d\mathbf{r} = 0$ is rather general, as most time-reversible systems with a local mobility $\sigma[\rho]$ do fulfill this condition (e.g., diffusive systems).

The IFR can be further generalized to cases where the current profile is not constant, relaxing hypothesis (*ii*) above. Let $\mathrm{P}_\tau[\boldsymbol{\mathcal{J}}(\mathbf{r})]$ be the probability of observing a time-averaged current field $\boldsymbol{\mathcal{J}}(\mathbf{r}) = \tau^{-1}\int_0^\tau dt\,\mathbf{j}(\mathbf{r},t)$. Notice that this vector field must be divergence-free because it is coupled via the continuity equation to an optimal density profile which is assumed to be time-independent, see hypothesis (i) above. This probability also obeys a large deviation principle,

$$\mathrm{P}_\tau[\boldsymbol{\mathcal{J}}(\mathbf{r})] \sim \exp\left(+\tau L^d G[\boldsymbol{\mathcal{J}}(\mathbf{r})]\right), \tag{4.24}$$

with a current LDF equivalent to that in Eq. (4.4) but with a space-dependent current field $\boldsymbol{\mathcal{J}}(\mathbf{r})$. The optimal density profile $\rho_0[\mathbf{r};\boldsymbol{\mathcal{J}}(\mathbf{r})]$ is now solution of

$$\frac{\delta}{\delta\rho(\mathbf{r}')}\int_\Lambda d\mathbf{r}\left(W_2[\rho(\mathbf{r})]-2\boldsymbol{\mathcal{J}}(\mathbf{r})\cdot\mathbf{W}_1[\rho(\mathbf{r})]+\boldsymbol{\mathcal{J}}^2(\mathbf{r})W_0[\rho(\mathbf{r})]\right)=0\,, \quad (4.25)$$

which is the equivalent to Eq. (4.5) in this case. For time-reversible systems condition (4.9) holds and $\rho_0[\mathbf{r};\boldsymbol{\mathcal{J}}(\mathbf{r})]$ remains invariant under (local or global) rotations of $\boldsymbol{\mathcal{J}}(\mathbf{r})$. In this way we can simply relate $\mathrm{P}_\tau[\boldsymbol{\mathcal{J}}(\mathbf{r})]$ with the probability of any other divergence-free current field $\boldsymbol{\mathcal{J}}'(\mathbf{r})$ locally-isometric to $\boldsymbol{\mathcal{J}}(\mathbf{r})$, i.e. $\boldsymbol{\mathcal{J}}'(\mathbf{r})^2=\boldsymbol{\mathcal{J}}(\mathbf{r})^2\ \forall\mathbf{r}$, via a generalized isometric fluctuation relation,

$$\lim_{\tau\to\infty}\frac{1}{\tau}\ln\left[\frac{\mathrm{P}_\tau[\boldsymbol{\mathcal{J}}(\mathbf{r})]}{\mathrm{P}_\tau[\boldsymbol{\mathcal{J}}'(\mathbf{r})]}\right]=\int_{\partial\Lambda}d\Gamma\,\frac{\delta\mathcal{H}[\rho]}{\delta\rho}\hat{n}\cdot[\boldsymbol{\mathcal{J}}'(\mathbf{r})-\boldsymbol{\mathcal{J}}(\mathbf{r})]\,, \quad (4.26)$$

where the integral (whose result is independent of $\rho(\mathbf{r})$) is taken over the boundary $\partial\Lambda$ of the domain Λ where the system is defined, and $\hat{n}$ is the unit vector normal to the boundary at each point. Notice that in general an arbitrary local or global rotation of a divergence-free vector field does not conserve the zero-divergence property, so this constraints the current fields and/or local rotations for which this generalized IFR applies. Note that the probability of observing a time averaged integrated current, $\mathrm{P}_\tau(\mathbf{J})$, is given by

$$\mathrm{P}_\tau(\mathbf{J})=\int\mathcal{D}\boldsymbol{\mathcal{J}}\mathrm{P}_\tau[\boldsymbol{\mathcal{J}}(\mathbf{r})]\delta\left(\mathbf{J}-\int_\Lambda d\mathbf{r}\,\boldsymbol{\mathcal{J}}(\mathbf{r})\right). \quad (4.27)$$

Hence, taking into account the above equation and that for long times Eq. (4.24) holds and $\mathrm{P}_\tau(\mathbf{J})\sim\exp\left(+\tau L^d G(\mathbf{J})\right)$, we can relate the large deviation function for the space- and time-averaged current, $G(\mathbf{J})$, to $G[\boldsymbol{\mathcal{J}}(\mathbf{r})]$ via a contraction principle

$$G(\mathbf{J})=\max_{\substack{\boldsymbol{\mathcal{J}}(\mathbf{r}):\boldsymbol{\nabla}\cdot\boldsymbol{\mathcal{J}}(\mathbf{r})=0\\ \mathbf{J}=\int_\Lambda d\mathbf{r}\,\boldsymbol{\mathcal{J}}(\mathbf{r})}}G[\boldsymbol{\mathcal{J}}(\mathbf{r})]\,. \quad (4.28)$$

The optimal, divergence-free current field $\boldsymbol{\mathcal{J}}_0(\mathbf{r};\mathbf{J})$ solution of this variational problem may have spatial structure in general. Eq. (4.26) generalizes the IFR to situations where hypothesis (*ii*) is violated, opening the door to isometries based on local (in addition to global) rotations. However, numerical results and phenomenological arguments strongly suggest that the constant solution, $\boldsymbol{\mathcal{J}}_0(\mathbf{r};\mathbf{J})=\mathbf{J}$, is the optimizer at least for a wide interval of current fluctuations, showing that hypothesis (ii) above is not only plausible but also well justified on physical grounds. In any case, the range of validity of this hypothesis can be explored by studying the limit of local stability of the constant current solution using tools similar to those in Ref. [39].

Hypotheses (i) and (ii) are the straightforward generalization to d-dimensional systems of the Additivity Principle recently conjectured by Bodineau and Derrida for one-dimensional diffusive systems [34]. This conjecture, which has been recently confirmed for a broad current interval in extensive simulations of a general diffusion model [36, 37], is however known to break down

in some special cases for extreme current fluctuations, where time-dependent profiles in the form of traveling waves propagating along the current direction may emerge [15, 16, 17, 39, 40]. As in previous cases, we can now study the probability $\mathrm{P}\left(\{\mathbf{j}(\mathbf{r},t)\}_0^\tau\right)$ of observing a particular history for the current field, which can be written as the path integral of the probability in Eq. (1.11) over histories of the density field $\{\rho(\mathbf{r},t)\}_0^\tau$ coupled to the desired current field via the continuity Eq. (4.2) at every point in space and time. This probability obeys another large deviation principle, with an optimal history of the density field $\{\rho_0(\mathbf{r},t)\}_0^\tau$ which is solution of an equation similar to Eq. (4.25) but with time-dependent profiles. However, as opposed to the cases above, the current field $\mathbf{j}(\mathbf{r},t)$ is not necessarily divergence-free because of the time-dependence of the associated $\rho_0(\mathbf{r},t)$, resulting in a violation of condition (4.9). In this way the optimal $\rho_0(\mathbf{r},t)$ depends on both $\mathbf{j}(\mathbf{r},t)$ and $\mathbf{j}(\mathbf{r},t)^2$ so it does not remain invariant under (local or global) instantaneous rotations of the current field, resulting in a violation of the generalized isometric fluctuation relation in the time-dependent regime. Nevertheless, as we shall show in chapter 5, if we consider a d-dimensional periodic system, there is particular spatio-temporal structure for the optimal profiles that still fullfills the IFR. This structure which emerges for extreme current fluctuations consists in traveling profiles with a fixed shape moving at a constant velocity. We will show how in this case, due to the periodicity of the system, Eq. (4.9) still holds and consequently the IFR (4.1) is also vaild.

4.4 Constants of motion

A sufficient condition for the IFR to hold is that

$$\frac{\delta \boldsymbol{\omega}_1[\rho(\mathbf{r})]}{\delta \rho(\mathbf{r}')} = 0\,, \tag{4.29}$$

with the functional $\boldsymbol{\omega}_1[\rho(\mathbf{r})]$ defined in Eq. (4.6) above. We have shown that condition (4.29) follows from the time-reversibility of the dynamics, in the sense that the evolution operator in the Fokker-Planck formulation of Eq. (4.2) obeys a local detailed balance condition, see Eq. (4.9). Condition (4.29) implies that $\boldsymbol{\omega}_1[\rho(\mathbf{r})]$ is in fact a *constant of motion*, $\boldsymbol{\epsilon}$, independent of the profile $\rho(\mathbf{r})$. Therefore we can use an arbitrary profile $\rho(\mathbf{r})$, compatible with boundary conditions, to compute $\boldsymbol{\epsilon}$. We now choose boundary conditions to be gradient-like in the $\hat{x}$-direction, with densities ρ_L and ρ_R at the left and right reservoirs, respectively, and periodic boundary conditions in all other directions. Given these boundaries, we now select a linear profile

$$\rho(\mathbf{r}) = \rho_L + (\rho_R - \rho_L)x\,, \tag{4.30}$$

to compute $\boldsymbol{\epsilon}$, with $x \in [0,1]$, and assume very general forms for the current and mobility functionals

$$\begin{aligned}
\mathbf{Q}[\rho(\mathbf{r})] &\equiv D_{0,0}[\rho]\boldsymbol{\nabla}\rho + \sum_{n,m>0} D_{nm}[\rho](\boldsymbol{\nabla}^m\rho)^{2n}\boldsymbol{\nabla}\rho\,,\\
\sigma[\rho(\mathbf{r})] &\equiv \sigma_{0,0}[\rho] + \sum_{n,m>0} \sigma_{nm}[\rho](\boldsymbol{\nabla}^m\rho)^{2n}\,,
\end{aligned}$$

where as a convention we denote as $F[\rho]$ a generic functional of the profile but not of its derivatives. It is now easy to show that $\boldsymbol{\epsilon} = \varepsilon\hat{x} + \mathbf{E}$, with

$$\varepsilon = \int_{\rho_L}^{\rho_R} d\rho \frac{D_{0,0}(\rho) + \sum_{n>0} D_{n1}(\rho)(\rho_R - \rho_L)^{2n}}{\sigma_{0,0}(\rho) + \sum_{m>0} \sigma_{m1}(\rho)(\rho_R - \rho_L)^{2m}}\,, \tag{4.31}$$

and $\hat{x}$ the unit vector along the gradient direction. In a similar way, if the following condition holds

$$\frac{\delta}{\delta\rho(\mathbf{r}')} \int_\Lambda \mathbf{Q}[\rho(\mathbf{r})] d\mathbf{r} = 0\,, \tag{4.32}$$

together with time-reversibility, Eq. (4.29), the system can be shown to obey an extended isometric fluctuation relation which links any current fluctuation $\mathbf{J}$ in the presence of an external field $\mathbf{E}$ with any other isometric current fluctuation $\mathbf{J}'$ in the presence of an arbitrarily-rotated external field $\mathbf{E}^*$, and reduces to the standard IFR for $\mathbf{E} = \mathbf{E}^*$, see Eq. (11) in the chapter. Condition (4.32) implies that $\boldsymbol{\nu} \equiv \int \mathbf{Q}[\rho(\mathbf{r})] d\mathbf{r}$ is another constant of motion, which can be now written as $\boldsymbol{\nu} = \nu\hat{x}$, with

$$\nu = \int_{\rho_L}^{\rho_R} d\rho \left[D_{0,0}(\rho) + \sum_{n>0} D_{n1}(\rho)(\rho_R - \rho_L)^{2n} \right]\,, \tag{4.33}$$

As an example, for a diffusive system $\mathbf{Q}[\rho(\mathbf{r})] = -D[\rho]\boldsymbol{\nabla}\rho(\mathbf{r})$, with $D[\rho]$ the diffusivity functional, and the above equations yield the familiar results

$$\begin{aligned} \varepsilon &= \int_{\rho_R}^{\rho_L} \frac{D(\rho)}{\sigma(\rho)} d\rho\,, \\ \nu &= \int_{\rho_R}^{\rho_L} D(\rho) d\rho\,, \end{aligned}$$

for a standard local mobility $\sigma[\rho]$.

4.5 Checking the Isometric Fluctuation Relation

We have tested the validity of the IFR in extensive numerical simulations of two different nonequilibrium systems. The first one is the already described in chapter 3 two-dimensional KMP model [43, 36, 37, 35] coupled to boundary heat baths along the x-direction at temperatures ρ_L and ρ_R and periodic boundary conditions in the y-direction. Recall that this model is described at the macroscopic level by Eq. (4.2) with a diffusive current term $\mathbf{Q}[\rho(\mathbf{r},t)] = -D[\rho]\boldsymbol{\nabla}\rho$ with $D[\rho] = \frac{1}{2}$ and $\sigma[\rho] = \rho^2$, and it turns out to be an optimal candidate to test the IFR because: (1) the associated macroscopic fluctuation theory can be solved analytically (see Ref. [43] and chapter 3), and (2) its dynamics is simple enough to allow for a detailed numerical study of current fluctuations (see chapter 3).

In order to test the IFR in this model we performed a large number of steady-state simulations of long duration $\tau > L^2$ (the unit of time is the Monte Carlo step) for $L = 20$, $T_L = 2$ and $T_R = 1$, accumulating statistics for the space- and time-averaged current vector $\mathbf{J}$. The measured current distribution is shown in the bottom inset to figure 4.2, together with a fine polar binning which allows us to compare the probabilities of isometric current fluctuations along each polar corona, see Eq. (4.1). Taking $G(\mathbf{J}) = (\tau L^d)^{-1} \ln \mathrm{P}_\tau(\mathbf{J})$, figure 4.2 confirms the IFR prediction that $G(\mathbf{J}) - G(\mathbf{J}')$, once scaled by $|\mathbf{J}|^{-1}$, collapses onto a linear function of $\cos\theta - \cos\theta'$ for all values of $|\mathbf{J}|$, see Eq. (4.10). Here θ, θ' are the angles formed by the isometric current vectors $\mathbf{J}$, $\mathbf{J}'$ with the x-axis ($\mathbf{E} = 0$ in our case). We also measured the average energy profile associated to each current fluctuation, $\rho_0(\mathbf{r}; \mathbf{J})$, see top inset to figure 4.2. As predicted above, profiles for different but isometric current fluctuations all collapse onto a single curve, confirming the invariance of optimal profiles under current rotations. Standard simulations allow us

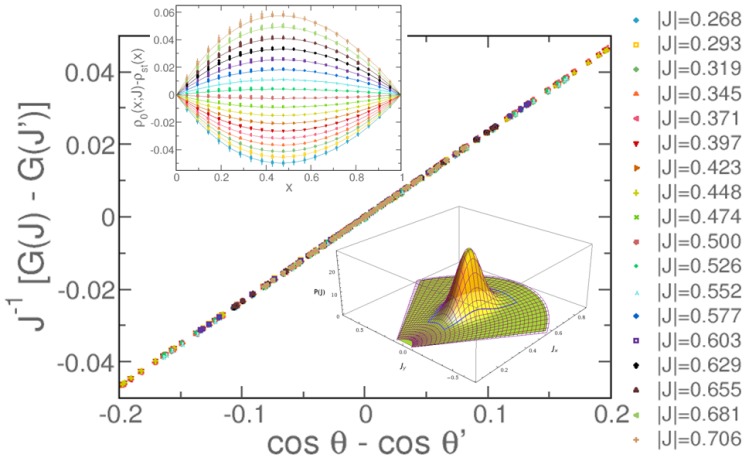

Figure 4.2: Confirmation of IFR in a diffusive system. The IFR predicts that $|\mathbf{J}|^{-1}[G(\mathbf{J}) - G(\mathbf{J}')]$ collapses onto a linear function of $\cos\theta - \cos\theta'$ for all values of $|\mathbf{J}|$. This collapse is confirmed here in the energy diffusion model for a wide range of values for $|\mathbf{J}|$. Bottom inset: Measured current distribution together with the polar binning used to test the IFR. Top inset: Average profiles for different but isometric current fluctuations all collapse onto single curves, confirming the invariance of optimal profiles under current rotations. Angle range is $|\theta| \leq 16.6°$, see marked region in the histogram.

to explore moderate fluctuations of the current around the average. In order to test the IFR in the far tails of the current distribution, corresponding to exponentially unlikely rare events, we implemented the method already introduced in chapter 3 to measure large deviation functions in many-particle systems [41]. Recall that this method, which yields the Legendre transform of

the current LDF, $\mu(\boldsymbol{\lambda})$, is based on a modification of the dynamics so that the rare events responsible of the large deviation are no longer rare [41], and has been recently used with success to confirm an additivity conjecture regarding large fluctuations in nonequilibrium systems [36, 37]. Using this method we measured $\mu(\boldsymbol{\lambda})$ in increasing manifolds of constant $|\boldsymbol{\lambda}+\boldsymbol{\epsilon}|$, see figure 4.3. The IFR implies that $\mu(\boldsymbol{\lambda})$ is constant along each of these manifolds, or equivalently $\mu(\boldsymbol{\lambda}) = \mu[\mathcal{R}_\phi(\boldsymbol{\lambda}+\boldsymbol{\epsilon})-\boldsymbol{\epsilon}]$, $\forall\phi \in [0, 2\pi]$, with $\mathcal{R}_\phi$ a rotation in 2D of angle ϕ. figure 4.3 shows the measured $\mu(\boldsymbol{\lambda})$ for different values of $|\boldsymbol{\lambda}+\boldsymbol{\epsilon}|$ corresponding to very large current fluctuations, different rotation angles ϕ and increasing system sizes, together with the theoretical predictions [43] already obtained in chapter 3. As a result of the finite, discrete character of the lattice system studied here, we observe weak violations of IFR in the far tails of the current distribution, specially for currents orthogonal to $\boldsymbol{\epsilon}$. These weak violations are expected since a prerequisite for the IFR to hold is the existence of a macroscopic limit, i.e. Eq. (4.2) should hold strictly, which is not the case for the relatively small values of L studied here. However, as L increases, a clear convergence toward the IFR prediction is observed as the effects associated to the underlying lattice fade away, strongly supporting the validity of IFR in the macroscopic limit. We also

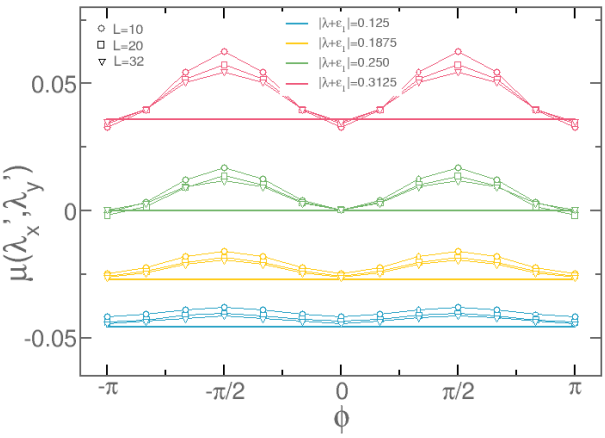

Figure 4.3: IFR for large current fluctuations. Legendre transform of the current LDF for the energy diffusion model, for different values of $|\boldsymbol{\lambda}+\boldsymbol{\epsilon}|$ corresponding to very large current fluctuations, different rotation angles ϕ such that $\boldsymbol{\lambda}' = \mathcal{R}_\phi(\boldsymbol{\lambda}+\boldsymbol{\epsilon})-\boldsymbol{\epsilon}$, and increasing system sizes. Lines are theoretical predictions. The IFR predicts that $\mu(\boldsymbol{\lambda}) = \mu[\mathcal{R}_\phi(\boldsymbol{\lambda}+\boldsymbol{\epsilon})-\boldsymbol{\epsilon}]$ $\forall\phi \in [0, 2\pi]$. The isometric fluctuation symmetry emerges in the macroscopic limit as the effects associated to the underlying lattice fade away.

measured current fluctuations in a Hamiltonian hard-disk fluid subject to a temperature gradient [50]. This model is a paradigm in liquid state theory, condensed matter and statistical physics, and has been widely studied during

last decades. The model consists in N hard disks of unit diameter interacting via instantaneous collisions and confined to a box of linear size L such that the particle density is fixed to $\Phi = N/L^2 = 0.58$. Here we choose $N = 320$. The box is divided in three parts: a central, bulk region of width $L - 2\alpha$ with periodic boundary conditions in the vertical direction, and two lateral stripes of width $\alpha = L/4$ which act as deterministic heat baths, see bottom inset to figure 4.4. This is achieved by keeping constant the total kinetic energy within each lateral band via a global, instantaneous rescaling of the velocity of bath particles after bath-bulk particle collisions. This heat bath mechanism has been shown to efficiently thermostat the fluid [50], and has the important advantage of being deterministic. As for the previous diffusive model, we performed a large number of steady state simulations of long duration ($\tau > 2N$ collisions per particle) for $T_L = 4$ and $T_R = 1$, accumulating statistics for the current $\mathbf{J}$ and measuring the average temperature profile associated to each $\mathbf{J}$. figure 4.4 shows the linear collapse of $|\mathbf{J}|^{-1}[G(\mathbf{J}) - G(\mathbf{J}')]$ as a function of $\cos\theta - \cos\theta'$ for different values of $|\mathbf{J}|$, confirming the validity of the IFR for this hard-disk fluid in the moderate range of current fluctuations that we could access. Moreover, the measured optimal profiles for different isometric current fluctuations all nicely collapse onto single curves, see top inset to figure 4.4, confirming their rotational invariance.

It is interesting to notice that the hard-disk fluid is a fully macroscopic system, with 4 different locally-conserved coupled fields possibly subject to memory effects, defining a far more complex situation than the one studied here, see Eq. (4.2). Therefore the validity of IFR in this context suggests that this fluctuation relation, based on the invariance of optimal profiles under symmetry transformations, is in fact a rather general result valid for arbitrary fluctuating macroscopic systems.

A few remarks are now in order. First, as a corollary to the IFR, it should be noted that for time-reversible systems with additive fluctuations, i.e. with a constant, profile-independent mobility σ, the optimal profile associated to a given current fluctuation is in fact independent of $\mathbf{J}$, see Eq. (4.5), and hence equal to the stationary profile. In this case it is easy to show that current fluctuations are Gaussian, with $G(\mathbf{J}) = \boldsymbol{\epsilon} \cdot (\mathbf{J} - \langle \mathbf{J} \rangle_\epsilon) + \sigma^{-1}(\mathbf{J}^2 - \langle \mathbf{J} \rangle_\epsilon^2)$. This is the case, for instance, of model B in the Hohenberg-Halperin classification [2] [1]. On the other hand, it should be noticed that the time-reversibility condition for the IFR to hold, Eq. (4.7) , is just a *sufficient* but not necessary condition. In fact, we cannot discard the possibility of time-irreversible systems such that, only for the optimal profiles, $\delta\boldsymbol{\omega}_1[\rho(\mathbf{r})]/\delta\rho(\mathbf{r}')|_{\rho_0} = 0$.

4.6 Conclusions

The IFR is a consequence of time-reversibility for systems in the hydrodynamic scaling limit, and reveals an unexpected high level of symmetry in the statistics of nonequilibrium fluctuations. It generalizes and comprises the

[1] Notice that ρ-dependent corrections to a constant mobility σ, which are typically irrelevant from a renormalization-group point of view [2], turn out to be essential for current fluctuations as they give rise to non-Gaussian tails in the current distribution.

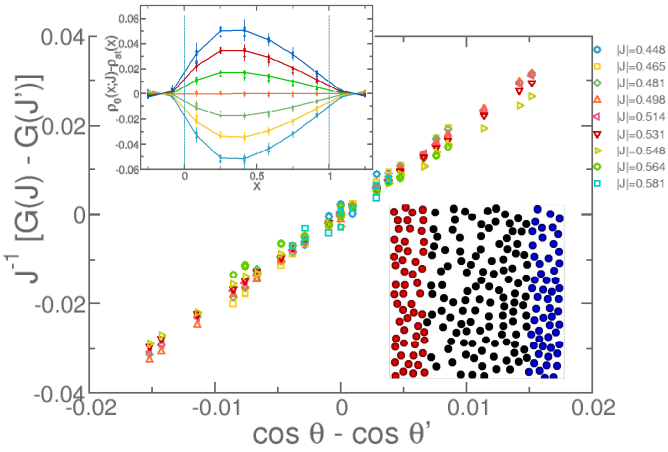

Figure 4.4: IFR in a macroscopic hard-disk fluid. Confirmation of IFR in a two dimensional hard-disk fluid under a temperature gradient after a polar binning of the measured current distribution. As predicted by IFR, the difference of current LDFs for different isometric current fluctuations, once scaled by the current norm, collapses in a line when plotted against $\cos\theta - \cos\theta'$. Top inset: Optimal temperature profiles associated to different current fluctuations. Profiles for a given $|\mathbf{J}|$ and different angles $\theta \in [-7.5°, +7.5°]$ all collapse onto a single curve, thus confirming the invariance of optimal profiles under current rotations. Notice that the profiles smoothly penetrate into the heat baths. Bottom inset: Snapshot of the 2D hard-disk fluid with Gaussian heat baths.

Gallavotti-Cohen fluctuation theorem for currents, relating the probabilities of an event not only with its time-reversal but with any other isometric fluctuation. This has important consequences in the form of hierarchies for the current cumulants and the linear and nonlinear response coefficients, which hold arbitrarily far from equilibrium and can be readily tested in experiments. A natural question thus concerns the level of generality of the isometric fluctuation relation. In this chapter we have demonstrated the IFR for a broad class of systems characterized at the macroscale by a single conserved field, using the tools of macroscopic fluctuation theory (MFT). This theoretical framework, summarized in the path large deviation functional, Eq. (1.11), has been rigorously proven for a number of interacting particle systems [14, 15, 16, 17], but it is believed to remain valid for a much larger class of systems. The key is that the Gaussian nature of local fluctuations, which lies at the heart of the approach, is expected to emerge for most situations in the appropriate macroscopic limit as a result of a central limit theorem: although microscopic interactions can be extremely complicated, the ensuing fluctuations of the slow macroscopic fields result from the sum of an enormous amount of random events at the microscale which give rise

to Gaussian statistics. There exist of course anomalous systems for which local fluctuations at the macroscale can be non-Gaussian. In these cases we cannot discard that a modified version of the IFR could remain valid, though the analysis would be certainly more complicated. Furthermore, our numerical results show that the IFR remains true even in cases where it is not clear whether the MFT applies, strongly supporting the validity of this symmetry for arbitrary fluctuating macroscopic systems.

A related question is the demonstration of the IFR starting from microscopic dynamics. Techniques similar to those in Refs. [13, 38], which derive the Gallavotti-Cohen fluctuation theorem from the spectral properties of the microscopic stochastic evolution operator, can prove useful for this task. However, in order to prove the IFR these techniques must be supplemented with additional insights on the asymptotic properties of the microscopic transition rates as the macroscopic limit is approached. In this way we expect finite-size corrections to the IFR which decay with the system size, as it is in fact observed in our simulations for the energy diffusion model, see figure 4.3. Also interesting is the possibility of an IFR for discrete isometries related with the underlying lattice in stochastic models. These open questions call for further study.

We have shown in this chapter how symmetry principles come forth in fluctuations far from equilibrium. By demanding invariance of the optimal path responsible of a given fluctuation under symmetry transformations, we unveiled a novel and very general isometric fluctuation relation for time-reversible systems which relates in a simple manner the probability of any pair of isometric current fluctuations. Invariance principles of this kind can be applied with great generality in diverse fields where fluctuations play a fundamental role, opening the door to further exact and general results valid arbitrarily far from equilibrium. This is particularly relevant in mesoscopic biophysical systems, where relations similar to the isometric fluctuation relation might be used to efficiently measure free-energy differences in terms of work distributions [52]. Other interesting issues concern the study of general fluctuation relations emerging from the invariance of optimal paths in full hydrodynamical systems with several conserved fields, or the quantum analog of the isometric fluctuation relation in full counting statistics.

Chapter 5

Spontaneous symmetry breaking at the fluctuating level

5.1 Introduction

As we have seen in chapter 1, the MFT offers predicitions for both the LDF and the optimal path in phase space responsible of a given fluctuation (see Eq. 1.14), which can be in general time-dependent [16]. However, we have shown in chapter 3 that this optimal path is in fact time-independent in a broad regime [34, 36, 43], supporting the validity of the additivity conjecture. As we shall see, this scenario eventually breaks down for large fluctuations via a dynamical phase transition *at the fluctuating level*, where the optimal fields become time-dependent. In this chapter we report compelling evidences of this phenomenon in a paradigmatic non-equilibrium model in one and two dimensions, namely the weakly assymetric exclusion process (WASEP, see chapter 2), where we study fluctuations of the time-averaged current. We find that small current fluctuations result indeed from the sum of weakly-correlated local random events in the density field, thus giving rise to Gaussian statistics as dictated by the central limit theorem, see left panels of figure 5.1. However, for large enough currents, the system self-organizes into a coherent traveling wave which facilitates this rare event by accumulating energy in a localized packet, thus breaking translational invariance [16, 39, 40], see right panels of figure 5.1), with a critical current $|J_c|$ separating both regimes. It is worth emphasizing that this phenomenon may also occur in an isolated equilibrium system in the absence of external field, as for instance in the KMP model. In this way, phase transitions not allowed in equilibrium steady states may happen however at the fluctuating level. In Ref. [40] Hurtado and Garrido observed for the first time this striking and general phenomenon measuring current fluctuations in the periodic 1D-KMP model.

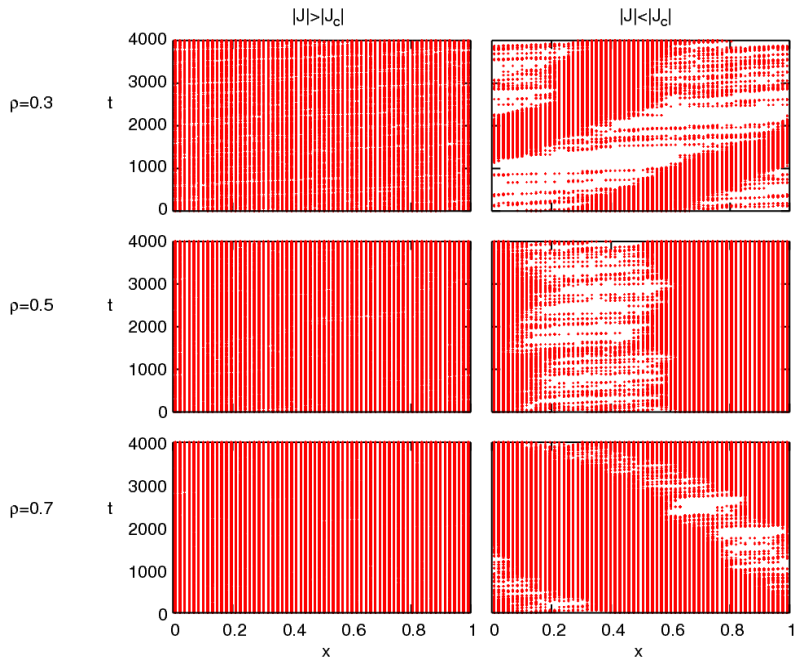

Figure 5.1: Typical evolution of the density profile for current fluctuations above and below the critical current for three different densities in the 1D-WASEP on a ring. Left panels correspond to currents above the critical one where there is no phase transition. Right panels correspond to subcritical current fluctuations where a travelling wave emerges. The velocity of the traveling wave of the top right panel ($\rho_0 = 0.3$) is positive. The *travelling* wave of the middle right panel does not move in average for corresponding to $\rho_0 = 1/2$ and the moving profile of the bottom left panel ($\rho_0 = 0.7$) moves with negative velocity

In the first part of this chapter we characterize this dynamical phase transition in the periodic one-dimensional weakly assymetric simple exclusion process (WASEP). In this case we measure using numerical simulations the time integrated current large deviation function as well as the traveling wave-like profiles associated to those configurations. We find very good agreement with the analytical results based on the prediction of T. Bodineau and B. Derrida in Ref. [39].

In the second part, we focus on the study of the dynamical phase transition in higher dimensional systems. In particular, we show that this phase transition does exist in the periodic 2D-WASEP, giving rise to a traveling profile moving at constant velocity for current fluctuations beyond a critical threshold. In addition, we show that the IFR (4.1) derived in chapter 4 still holds in this case, thus extending its validity to d-dimensional periodic systems which adopt time-dependent optimal profiles in order to sustain a given current fluctuation.

5.2 Periodic one-dimensional diffusive system

According to the MFT described in chapter 1, the LDF of the space- and time- integrated current, $J = \frac{1}{\tau}\int_0^\tau dt \int_0^1 j(x,t)dx$, is given by Eq. (1.14), which for a one-dimensional driven diffusive system reads

$$G(J) = \lim_{\tau\to\infty} \frac{1}{\tau} \max_{\rho(x,t),j(x,t)} \left\{ -\int_0^\tau dt \int_0^1 dx \frac{(j(x,t) + D[\rho]\partial_x\rho - E\sigma[\rho])^2}{2\sigma[\rho]} \right\}, \tag{5.1}$$

with the constraints $J = \frac{1}{\tau}\int_0^\tau dt \int_0^1 j(x,t)dx$ and $\partial_t\rho(x,t) + \partial_x j(x,t) = 0$. As we are considering a system with periodic boundary conditions, we have $\rho(0,t) = \rho(1,t)$ and $j(0,t) = j(1,t)$, where the total density is a conserved quantity $\int_0^1 \rho(x,t) = \rho_0$. The stationary profile is the flat one (uniformly equal to ρ_0) and the average current is $\langle J\rangle = \sigma[\rho_0]E$. Hence, for small current fluctuations away from the average resulting from weakly-correlated local fluctuations, the average density profile associated to these small fluctuations corresponds still to the flat, stationary one,

$$\rho_0(x;J) = \rho_0 \tag{5.2}$$

Thus, the large deviation function (5.1) for small current fluctuations is given by

$$G_{\text{flat}}(J) = -\frac{(J - E\sigma[\rho_0])^2}{2\sigma[\rho_0]}, \tag{5.3}$$

resulting in Gaussian current statistics. We are also interested not only in the LDF but also in its Legendre transform

$$\mu(\lambda) = -\frac{1}{L}\max_J[\lambda J + G(J)], \tag{5.4}$$

where λ is the parameter conjugated to the current.
Thus, for time-independent optimal density profiles we have

$$\mu_{\text{flat}}(\lambda) = \frac{\lambda(\lambda + 2E)\sigma[\rho_0]}{2L}. \tag{5.5}$$

One can now consider if there are optimal *time-dependent* density and current fields which increase the value of the probability of observing a given current fluctuation J, i.e, if $G(J) > G_{\rm flat}(J)$, with $G(J)$ is given by Eq. (5.1).

5.3 Stability criteria and time dependent optimal profile

Bodineau and Derrida [39] showed by adding a small space and time dependent perturbation to the constant profiles, that the value of $G(J)$ was increased for current fluctuations away from a critical value. They proved that the flat profile becomes unstable whenever

$$8\pi^2 D^2[\rho_0]\sigma[\rho_0] + (E^2\sigma^2[\rho_0] - J^2)\sigma''[\rho_0] < 0, \tag{5.6}$$

where σ'' denotes the second derivative. The above equation can be rewritten in terms of λ as

$$4\pi^2 D^2[\rho_0] < L\mu_{\rm flat}(\lambda)\sigma''[\rho_0]. \tag{5.7}$$

The inequality (5.6) defines a critical current for the instability to dominate,

$$|J_c| = \sqrt{\frac{8\pi^2 D^2[\rho_0]\sigma[\rho_0]}{\sigma''[\rho_0]} + E^2\sigma^2[\rho_0]}. \tag{5.8}$$

Recall that $\lambda = -\partial G(J)/\partial J|_{J=J^*}$, hence in the flat region one has $J^*(\lambda) = \sigma[\rho_0](\lambda+E)$. Therefore the time-dependent regime in terms of λ corresponds to

$$|\lambda + E| < \frac{|J_c|}{\sigma[\rho_0]} \tag{5.9}$$

with $|J_c|$ given by Eq. (5.8). Once the flat profile is unstable, the form of the associated perturbation suggests a traveling wave-like profile moving at a constant velocity v

$$\rho(x,t;J) = \omega(x - vt;J), \tag{5.10}$$

which implies via the continuity equation

$$j(x,t;J) = J - v\rho_0 + v\omega(x - vt;J). \tag{5.11}$$

In the sequel we drop the dependence of $\omega(x-vt;J)$ on J from the notation. With these profiles, the variational principle (5.1) reduces to

$$G(J) = -\min_{\omega(x),v} \int_0^1 \frac{dx}{2\sigma[\omega]}[J - v\rho_0 + v\omega(x) + D[\omega]\omega'(x) - \sigma[\omega]E]^2 \tag{5.12}$$

where we have dropped the time dependence because if $F(x)$ is an arbitrary periodic function with period 1 then $\int_0^\tau dt \int_0^1 F(x-vt)dx = \tau\int_0^1 F(x)dx$. Expanding the square the terms linear in $\omega'(x)$ give a null contribution, due again to the periodicity, and taking also into account that $\int_0^1 \omega(x)dx = \rho_0$ one gets

$$G(J) = -\min_{\omega(x),v}\left[\int_0^1 dx(X[\omega] + \omega'(x)^2 Y[\omega])\right] + JE, \tag{5.13}$$

where

$$X[\omega] = \frac{[J - v(\rho_0 - \omega)]^2}{2\sigma[\omega]} + \frac{E^2\sigma[\omega]}{2} \tag{5.14}$$

and

$$Y[\omega] = \frac{D[\omega]^2}{2\sigma[\omega]}. \tag{5.15}$$

By performing the variational problem around $\omega(x)$ and v, the resulting differential equation for the optimal profile, $\omega_0 \equiv \omega_0(x)$, is

$$X[\omega_0] - \omega_0'(x)^2 Y[\omega_0] = C_1 + C_2\omega_0 \tag{5.16}$$

where C_1 and C_2 are constants. For the optimal velocity, v_0, we get

$$v_0 = -J\frac{\displaystyle\int_0^1 dx \frac{(\omega_0 - \rho_0)}{\sigma[\omega_0]}}{\displaystyle\int_0^1 dx \frac{(\omega_0 - \rho_0)^2}{\sigma[\omega_0]}}. \tag{5.17}$$

It is worth to emphasize that the optimal velocity is proportional to J. This implies for the optimal profile solution of Eq. (5.16) to depend exclusively on J^2 and not on its sign, reflecting that the Gallavotti-Cohen symmetry holds. This invariance of the optimal profile under the sign of the integrated current can now be used in Eq. (5.13) to show explicitely the GC symmetry

$$G(J) - G(-J) = 2JE. \tag{5.18}$$

The GC symmetry in terms of the parameter conjugated to the current reads

$$\mu(\lambda) = \mu(-\lambda - 2E). \tag{5.19}$$

As we are interested in getting the optimal profile, we proceed to solve Eq. (5.16). The differential equation (5.16) generically yields a symmetric optimal profile with a single minimum $\omega_1 = \omega(x_1)$ and a single maximum $\omega_2 = \omega(x_2)$ such that $|x_2 - x_1| = 1/2$. The constants can be expressed in terms of the extrema ω_1 and ω_2

$$X[\omega_1] = C_1 + C_2\omega_1 \tag{5.20}$$

$$X[\omega_2] = C_1 + C_2\omega_2 \tag{5.21}$$

and the extrema are fixed by the constraints on the distance between them and the total density, ρ_0, of the system,

$$\frac{1}{2} = \int_{x_1}^{x_2} dx = \int_{\omega_1}^{\omega_2} \frac{d\omega_0}{\omega_0'} = \int_{\omega_1}^{\omega_2} \sqrt{\frac{Y[\omega_0]}{X[\omega_0] - C_1 - C_2[\omega_0]}}\, d\omega_0 \tag{5.22}$$

and

$$\frac{\rho_0}{2} = \int_{\omega_1}^{\omega_2} \sqrt{\frac{Y[\omega_0]}{X[\omega_0] - C_1 - C_2[\omega_0]}}\, d\omega_0. \tag{5.23}$$

In this way, given our input external constants J and ρ_0 we use Eqs. (5.20)-(5.23) and Eq. (5.17) in order to determine $\omega_1, \omega_2, C_1, C_2, v$ and get the whole optimal profile $\omega(x)$. Notice that in order to proceed we need to know the macroscopic parameters $D[\sigma]$ and σ, specific of each considered model. Once we have the optimal shape of the time-dependent optimal density profile, $\omega(x)$, and the constant velocity at which it moves, we are able to compute using Eq. (5.13) the large deviation function $G(J)$.

5.4 Analytical solution for the 1D-WASEP

We study now the analytical solution of the time-dependent optimal profile in the weakly asymmetric exclusion process (WASEP). First of all, it is worth comparing it with the KMP model [35]. Notice that for both models $D[\rho_0] = 1/2$. However, for the WASEP $\sigma[\rho_0] = \rho_0(1-\rho_0)$ whereas for the KMP model $\sigma[\rho_0] = \rho_0^2$. This has important consequences on the way the dynamical phase transition emerges in each model. In the WASEP case, the time-dependent regime occurs for a magnitude of current fluctuations *below* the critical value (5.8)

$$|J| < \sqrt{\rho_0(1-\rho_0)(E^2\rho_0(1-\rho_0) - \pi^2)}, \tag{5.24}$$

and by using Eqs. (5.7) and (5.9) it can be rewritten in terms of λ,

$$L\mu_{\text{flat}}(\lambda) < -\frac{\pi^2}{2} \iff |\lambda + E| < \sqrt{E^2 - \frac{\pi^2}{\rho_0(1-\rho_0)}}. \tag{5.25}$$

This means that in order to have a dynamical phase transition we need the magnitude of the external field to satisfy $|E| > \pi/\sqrt{\rho_0(1-\rho_0)}$. Hence, in the absence of external field we do not have any time dependent regime for any current fluctuation. Nevertheless, for the KMP model the time-dependent regime takes place for a magnitude of the current fluctuations *above* the critical value (5.8)

$$|J| > \sqrt{\rho_0^2(\pi^2 + E^2\rho_0^2)} \tag{5.26}$$

or

$$L\mu_{\text{flat}}(\lambda) > \frac{\pi^2}{2\rho_0} \iff |\lambda + E| > \sqrt{E^2 + \frac{\pi^2}{\rho_0^2}}, \tag{5.27}$$

meaning that for any value of the external field, even in the absence of it, we can have a time-dependent regime whenever the associated current fluctuation is large enough ($|J| > |J_c|$). As we have mentioned in the introduction of this chapter, Hurtado and Garrido [40] observed this phenomenon for the KMP model in the absence of external field, confirming the theoretical predictions of the MFT with numerical simulations. In what follows we extend the analytical results captured by the MFT for the WASEP. We have done the calculations for a external field $E = 10$ and for three different values of the density $\rho_0 = 0.3, \rho_0 = 1/2$ and $\rho_0 = 0.7$. It is worth noting that due to the particle-hole symmetry present in the WASEP, the optimal density profile $\omega_0(x)$ associated to a current fluctuation J given a density ρ_0, is the

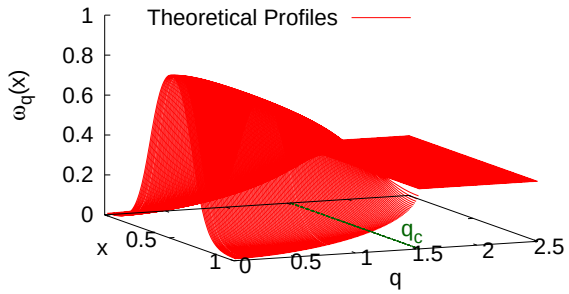

Figure 5.2: ($q \equiv J$) Theoretical density profiles associated to different current fluctuations for $\rho_0 = 0.3$. Below the dashed green line corresponding to the critical current $|J_c| = 1.52885$ the profiles stop being flat and the traveling wave profiles emerge

correponding complementary optimal profile associated to the same value of J for a density $1 - \rho_0$, i.e.

$$\omega_0(x; \rho_0) = 1 - \omega_0(x; 1 - \rho_0). \tag{5.28}$$

The above relation implies via Eq. (5.17) that an optimal profile travels with the same velocity of its complementary profile but in opposite direction

$$v_0[\omega_0(x; \rho_0)] = -v_0[\omega_0(x; 1 - \rho_0)]. \tag{5.29}$$

In the particular case of $\rho_0 = 1/2$, any profile and its complementary are the same. Thus, due to Eq. (5.29) the average velocity for the optimal profiles with $\rho_0 = 1/2$ is null. For this particular density, the configurations in the time-dependent regime have a well defined structure given by Eq. (5.16) which does not move in average. This can be observed in figure 5.1 where the evolution of a typical configuration above and below the critical current is displayed for $\rho_0 = 0.3, 1/2, 0.7$. Notice that for $|J| < |J_c|$ there is a well defined structure which travels in opposite velocities for $\rho_0 = 0.3$ and 0.7 and which does not move when $\rho_0 = 1/2$. Furthermore, by replacing ρ_0 by $1 - \rho_0$, $\omega_0(x)$ by $1 - \omega_0(x)$ in Eq. (5.13) and using Eqs. (5.28)-(5.29), we get that the LDF, $G(J)$, is the same for a density ρ_0 and $1 - \rho_0$,

$$G(J; \rho_0) = G(J; 1 - \rho_0). \tag{5.30}$$

Hence, given a external field it is enough to compute the LDF for $\rho_0 \in [0, 1/2]$.

To determine the time-dependent optimal profile we proceed as indicated at the end of Sec. 5.3. The profiles obtained for $\rho_0 = 0.3$ versus J are shown in figure 5.2. We can see how for $|J| < |J_c| = 1.52885$ the profile stops

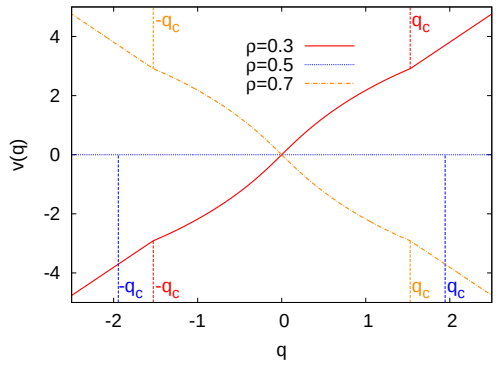

Figure 5.3: ($q \equiv J$) Theoretical velocities for $\rho_0 = 0.3$ (solid red line), $\rho_0 = 1/2$ (blue dotted line) and $\rho_0 = 0.7$ (orange dot-dashed line). A non-linear dependence yields for $|J| < |J_c|$

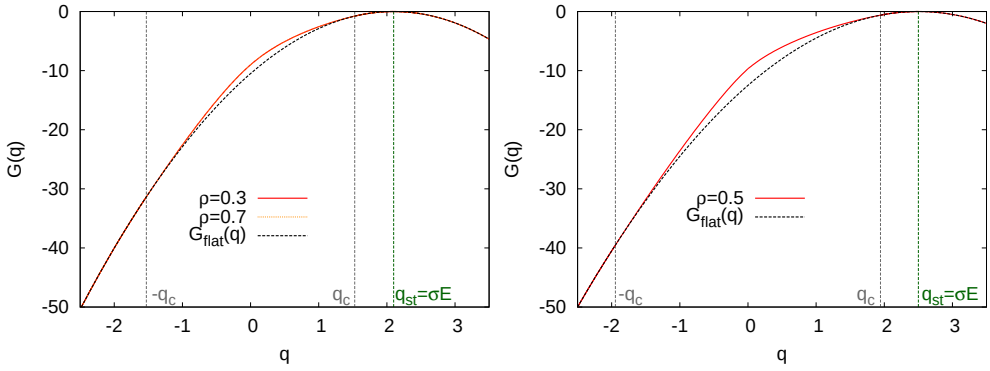

Figure 5.4: ($q \equiv J$) Left: Large Deviation Function for $\rho_0 = 0.3$ and $\rho_0 = 0.7$. They are the same in virtue of Eq. (5.30). Right: LDF for $\rho_0 = 1/2$. For the three densities the traveling profiles enhance the probability for $|J| < |J_c|$ (solid red line) with respect to the flat profiles (dashed black line)

being flat and becomes a travelling wave. One obtains the same profiles for $J < 0$ due to the invariance of them under the current sign. In figure 5.3 we show the velocities at which the travelling profiles cheking how they are opposite for $\rho_0 = 0.3$ and 0.7 and null for $\rho = 1/2$ (Eq. (5.29)). Once we have calculated the profile and the constant velocity at wich it moves, we use it in Eq. (5.13) to get $G(q)$, see figure 5.4. We see how the LDF is the same for $\rho_0 = 0.3$ and 0.7 (Eq. (5.30)) and how the GC symmetry (5.18) holds. As expected, $G(q)$ is maximum (null) for the stationary value of the current $\langle q \rangle = \sigma[\rho_0]E$.

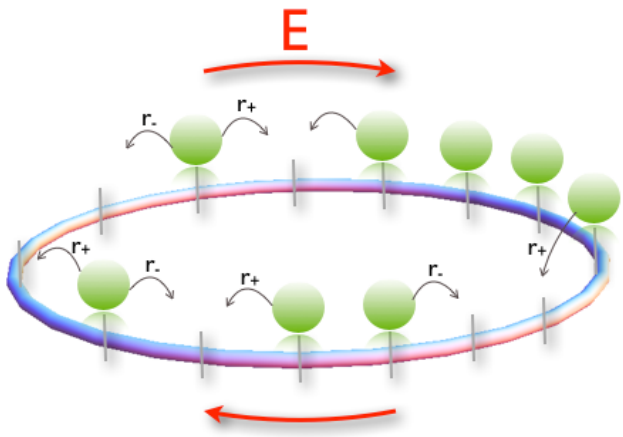

Figure 5.5: Top: Skecth of the weakly assymetric exclusion process with a weak external field, E, to the right

5.5 Numerical results for the 1D-WASEP

We have tested the theoretical predictions of the previous section with numerical simulations on a ring with L sites with $P = L\rho$ particles for an external field $E = 10$ to the right, see figure 5.5. Unlike the simple symmetric exclusion process (SSEP), where each particle attempts to jump to an empty site to its right or to its left at rate $1/2$, in the WASEP (e.g. with a external field, E, to the right) the rates become $r_+ = 1/2 + E/2L$ to the right and $r_- = 1/2 - E/2L$ to the left. Standard simulations allow

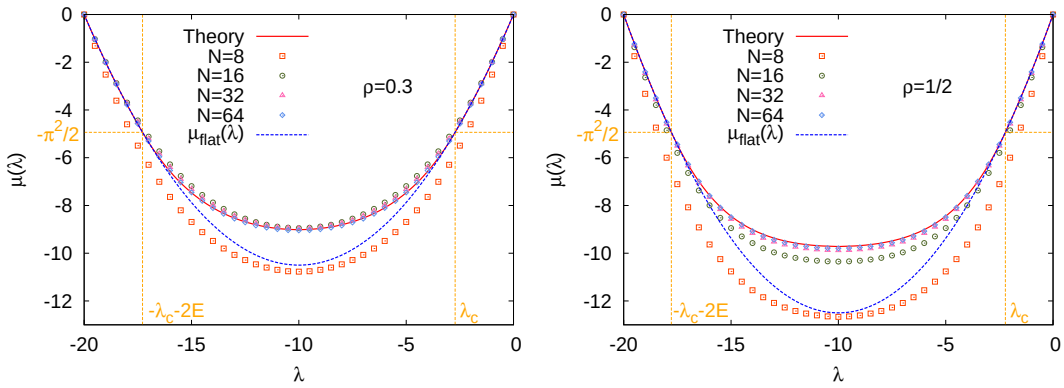

Figure 5.6: ($N \equiv L$) Legendre transform of the LDF, $\mu(\lambda)$. Left: Measured $\mu(\lambda)$ for $\rho_0 = 0.3$ and increasing L, together with the MFT result (solid red line) and the Gaussian approximation (dashed blue line). Right: Same results for $\rho_0 = 1/2$

us to explore very moderate current fluctuations around the average. For

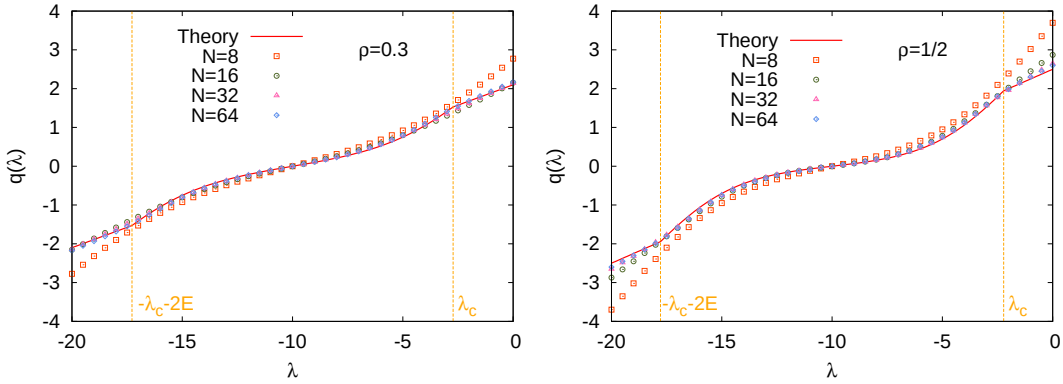

Figure 5.7: ($N \equiv L$) Left: Measured time integrated current q as a function of λ for $\rho_0 = 0.3$ and increasing L, together with the analytical prediction base on the MFT. Right: Same results for $\rho_0 = 1/2$

that reason, we implemented a direct continuous-time algorithm to measure large deviations in many particle systems [42]. This method (see appendix B), which is an extension of the already mentioned discrete-time algorithm [41], is based on a modified dynamics so that the rare events responsible of the large deviation are no longer rare, and requires the simulation of multiple *clones* of the system. Using this method, we measured the Legendre transform of the current LDF, $\mu(\lambda)$, for $L = 8, 16, 32$ and 64 for $\rho_0 = 0.3$ and 0.5. In the same way as in Ref. [39], we replaced in our program the rates $1/2 \pm E/2L$ by $\exp[\pm E/L]/2$ in order to avoid negative rates for small sizes. As λ is our input parameter in our simulations, we are going to work from now on in $\lambda -$ space instead of $J -$ space. The results for $\mu(\lambda)$ are shown in figure 5.6. We observe the convergence to the theoretical prediction with the system size. For $L = 64$, there is a perfect agreement with the theory. Moreover, the GC symmetry (5.19) holds in the whole current range. To get these results we performed a large number of stead-state simulations of long duration $\tau > L^2$. As well as the LDF, we also meausured the time integrated current J versus its conjugated parameter λ, see figure 5.7. It is remarkable to see how the dependence of J respect to λ becomes non-linear for the time-dependent regime. We see again a good agreement as the size of the system increases. We also measured the average velocity corresponding to a given current fluctuation by fitting the motion center of mass during small time intervals Δt to a ballistic law, $x_{CM}(t + \Delta t) - x_{CM}(t) = vt$. The resulting velocities for $\Delta t = 200$ are displayed in figure 5.8, where once again the concordance with the theory becomes very good for $L = 64$. Notice again how the non-linear dependence of the velocity with the current emerges for the time-dependent regime for $\rho_0 = 0.3$ and how is null for the whole current interval when $\rho_0 = 1/2$.

To conclude our numerical analysis, we measured the profiles associated to a given current fluctuation. Because of the periodicity of the system, if we average the resulting configurations without taking into account their move-

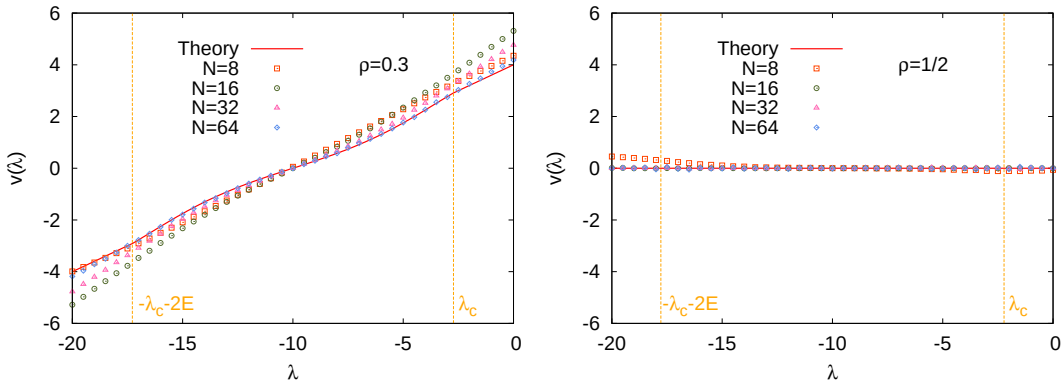

Figure 5.8: ($N \equiv L$) Left: Measured velocity as a function of λ for $\rho_0 = 0.3$ and increasing L, together with the MFT result. Right: Same results for $\rho_0 = 1/2$

ment, we do not observe any structure but the flat one. For that reason, it is necessary to average the configurations around their instantaneous center of mass above mentioned. To do that, we consider the system as a 1D ring embeded in two-dimensional space, and compute the angular position of the center of mass, shifting it to the origin before averaging. One has to be aware that this way of averaging yields for the time-independent regime a spurious structure equivalent to averaging random profiles around their (random) center of mass. This spurious structure is independent of J and can be subtracted in the subcritical region ($J > |J_c|$). On the other hand, for the time-dependent regime, the resulting structure is much more pronounced due to the appearance of the traveling wave. In the left panel of figure 5.9 we show for $\rho_0 = 0.3$ the profiles associated to supercritical current fluctuations ($|\lambda + 10| < 7.2802$). For $L = 64$ the simulated profile fits very well with the theoretical one. In the right panel we display the measured profiles for different values of λ appreciating the appearance of the traveling wave for currents below the critical one. In figure 5.10 we show the same as the previous figure but for $\rho_0 = 1/2$. We find again a very good agreement for the travelling profiles for $L = 64$ (left panel). In the right panel the emergence of this travelling wave for supercritical currents ($|\lambda + 10| < 7.7796$) is displayed.

It is worth showing how the optimal time-dependent profiles are invariant under the current fluctuation sign, i.e. $\omega_0(x; J) = \omega_0(x; -J)$, or equivalently, $\omega_0(x; \lambda) = \omega_0(x; -\lambda - 2E)$ (see figure 5.11) reflecting the GC symmetry. In the left panel of figure 5.11 this invariance is shown for $\rho_0 = 0.3$, where the profile of a given current fluctuation $\omega_0(x; \lambda)$ overlap the profile associated to the opposite current $\omega_0(x; -\lambda - 2E)$. This invariance is also shown for different current fluctuations for $\rho_0 = 1/2$, see right panel of figure 5.11.

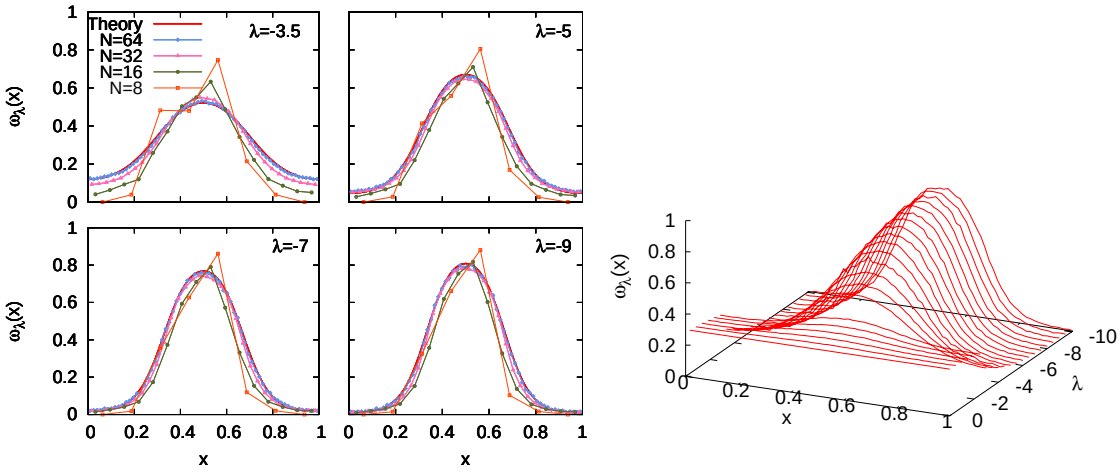

Figure 5.9: $(, N \equiv L)$ Left: Time-dependent profiles for $\rho_0 = 0.3$ and different λ and increasing L, and MFT predictions. Right: Measured profiles as a function of λ for $L = 64$. Profiles are flat up to a critical current where a travelling wave emerges

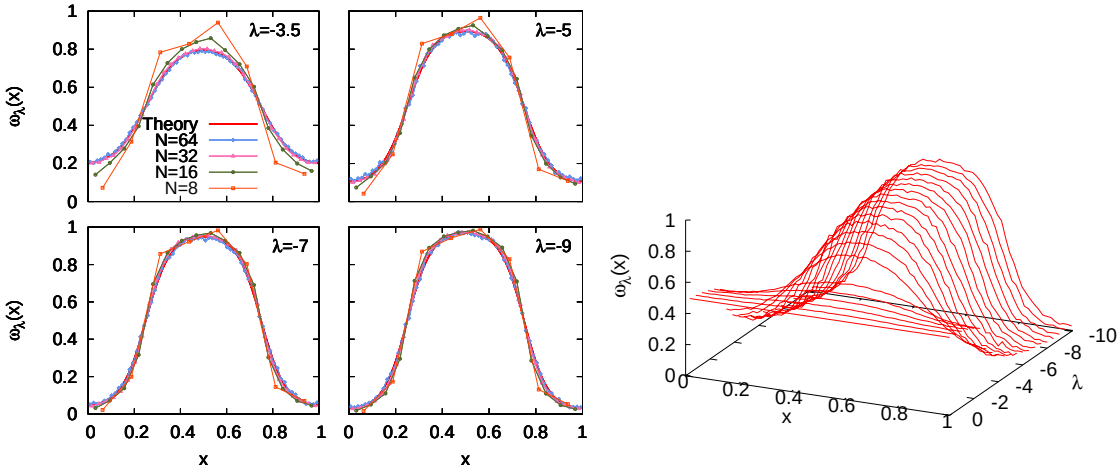

Figure 5.10: $(N \equiv L)$Left: Time-dependent profiles for $\rho_0 = 1/2$ and different λ and increasing L, together with the MFT predictions. Right: Measured profiles as a function of λ for $L = 64$. Profiles are flat up to a critical current where a travelling wave emerges

5.6 Periodic two-dimensional diffusive system

It is also insteresting to study whether higher dimensional systems also exhibit a dynamical phase transition for large enough current fluctuations. If that is the case, another interesting issue is to see whether there is an

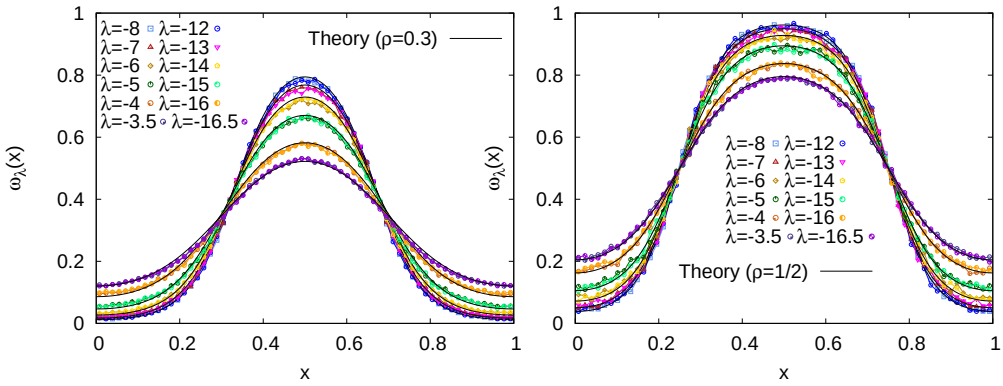

Figure 5.11: ($N \equiv L$) Left: Measured profiles associated to different current fluctuations $\omega_0(x;\lambda)$ and their opposite fluctuation $\omega_0(x;-\lambda-2E)$ for $L = 64$ and $\rho_0 = 0.3$. Right: Same results for $\rho_0 = 1/2$

extension of the Isometric Fluctuation Relation (IFR), already derived in chapter 4 for time-independent optimal profiles. Therefore, we now proceed to study the probability of the time-averaged integrated in a two dimesional diffusive system with periodic boundary conditions. Here, the total density is a conserved quantity

$$\int_\Lambda \rho(\mathbf{r},t)d\mathbf{r} = \rho_0 \tag{5.31}$$

where $\Lambda \in [0,1]\times[0,1]$. According to the MFT described in chapter 1, the LDF of the space- and time- integrated current, $\mathbf{J} = \frac{1}{\tau}\int_0^\tau dt \int_\Lambda \mathbf{j}(\mathbf{r},t)dx$, is given by Eq. (1.14), which for a two-dimensional driven diffusive system (where $\mathbf{Q}[\rho] = -D[\rho]\boldsymbol{\nabla}\rho$) reads

$$G(\mathbf{J}) = \lim_{\tau\to\infty}\frac{1}{\tau}\max_{\rho(\mathbf{r},t),\mathbf{j}(\mathbf{r},t)}\left\{-\int_0^\tau dt\int_\Lambda d\mathbf{r}\frac{(\mathbf{j}(\mathbf{r},t)+D[\rho]\boldsymbol{\nabla}\rho-\mathbf{E}\sigma[\rho])^2}{2\sigma[\rho]}\right\}, \tag{5.32}$$

Again, the optimal density profile associated to small current fluctuations away from the stationary current, $\langle\mathbf{J}\rangle = \sigma[\rho]\mathbf{E}$, is still the stationary flat one $\rho_0(\mathbf{r},t;\mathbf{J}) = \rho_0$. Hence, we have that Eq. (5.32) turns into

$$G_{\text{flat}}(\mathbf{J}) = -\frac{(\mathbf{J}-\mathbf{E}\sigma[\rho_0])^2}{2\sigma[\rho_0]}. \tag{5.33}$$

We now may ask if one could increase the probability of observing a given $\mathbf{J}$ considering time-dependent profiles. Applying again, in a similar way as in 1D, a spatio temporal periodic perturbation to the stationary solution and studying the local stability of it, we get that the flat profile becomes unstable if the following inequality is satisfied

$$8\pi^2 D^2[\rho_0]\sigma[\rho_0] + (|\mathbf{E}|^2\sigma^2[\rho_0] - |\mathbf{J}|^2)\sigma''[\rho_0] < 0, \tag{5.34}$$

where σ'' denotes the second derivative. The inequality (5.34) defines a critical current for the instability to dominate,

$$|\mathbf{J}_c| = \sqrt{\frac{8\pi^2 D^2[\rho_0]\sigma[\rho_0]}{\sigma''[\rho_0]} + |\mathbf{E}|^2\sigma^2[\rho_0]}. \tag{5.35}$$

Thus, getting into the time-dependent regime only depends on the magnitude of the current fluctuations and the magnitude of the external fields and not on their respective orientations. The form of the perturbation beyond the critical value suggests a fixed non-flat profile moving at constant velocity,

$$\rho(\mathbf{r}, t; \mathbf{J}) = \omega(\mathbf{r} - \mathbf{v}t; \mathbf{J}). \tag{5.36}$$

Due to the continuity equation, $\partial_t \rho(\mathbf{r}, t) = \boldsymbol{\nabla} \cdot \mathbf{j}(\mathbf{r}, t)$, the current field then is

$$\mathbf{j}(\mathbf{r}, t; \mathbf{J}) = \mathbf{v}\omega(\mathbf{r} - \mathbf{v}t) + \boldsymbol{\varphi}(\mathbf{r} - \mathbf{v}t), \tag{5.37}$$

being $\boldsymbol{\varphi}(\mathbf{r} - \mathbf{v}t)$ a free divergence vector field.

5.7 IFR for periodic time-dependent optimal profiles

In this section we show how for time-dependent density and current fields with a travelling structure given by Eqs. (5.36) and (5.37), the IFR still holds. This means an extension of its validity to time-dependent optimal profiles. To do that, we have to make another hypothesis which is to assume that the free divergence vector field $\boldsymbol{\varphi}(\mathbf{r} - \mathbf{v}t)$ of Eq. (5.37) is constant. Hence, in virtue of the continuity equation, the current field (5.37) then reads

$$\mathbf{j}(\mathbf{r}, t; \mathbf{J}) = \mathbf{J} - \mathbf{v}\rho_0 + \mathbf{v}\omega(\mathbf{r} - \mathbf{v}t; \mathbf{J}). \tag{5.38}$$

In the sequel we drop the dependence of $\omega(\mathbf{r} - \mathbf{v}t; \mathbf{J})$ and $\mathbf{j}(\mathbf{r}, t; \mathbf{J})$ on $\mathbf{J}$ from the notation. With these fields (Eqs. (5.36) and (5.38)), the LDF (5.32) takes the form

$$G(\mathbf{J}) = -\min_{\omega(\mathbf{r}),\mathbf{v}} \int_\Lambda \frac{d\mathbf{r}}{2\sigma[\omega]} [\mathbf{J} - v\rho_0 + v\omega(\mathbf{r}) + D[\omega]\boldsymbol{\nabla}\omega(\mathbf{r}) - \sigma[\omega]\mathbf{E}]^2, \tag{5.39}$$

where we have dropped the time dependence ($\mathbf{r} - vt \to \mathbf{r}$) because if $F(\mathbf{r})$ is an arbitrary periodic function with period 1 in all directions, it then holds that $\int_0^\tau dt \int_\Lambda F(\mathbf{r} - \mathbf{v}t)dx = \tau \int_\Lambda F(\mathbf{r})d\mathbf{r}$. Expanding the square we have a null contribution of the linear terms in $\boldsymbol{\nabla}\omega$ due again to the periodicity. Taking finally into account that $\int_\Lambda \omega(\mathbf{r})d\mathbf{r} = \rho_0$, Eq. (5.39) reads

$$G(\mathbf{J}) = -\min_{\omega(\mathbf{r}),\mathbf{v}} \left[\int_\Lambda d\mathbf{r}(X[\omega] + (\boldsymbol{\nabla}\omega)^2 Y[\omega]) \right] + \mathbf{J} \cdot \mathbf{E}, \tag{5.40}$$

where

$$Y[\omega] = \frac{D[\omega]^2}{2\sigma[\omega]} \tag{5.41}$$

and

$$X[\omega] = \frac{[\mathbf{J} - \mathbf{v}(\rho_0 - \omega)]^2}{2\sigma[\omega]} + \frac{|\mathbf{E}|^2 \sigma[\omega]}{2}. \tag{5.42}$$

By performing the variational problem around $\omega(\mathbf{r})$ and $\mathbf{v}$, the resulting differential equation for the optimal profile $\omega_0(\mathbf{r})$ is

$$(\boldsymbol{\nabla}\omega_0)^2 = \left(\frac{\partial \omega_0}{\partial x}\right)^2 + \left(\frac{\partial \omega_0}{\partial y}\right)^2 = F[\omega_0] \tag{5.43}$$

where

$$F[\omega_0] \equiv (X[\omega_0] - C_1 - C_2\omega_0)/Y[\omega_0], \tag{5.44}$$

being C_1 and C_2 constants of integration. The optimal velocity is given implicitely by

$$\mathbf{v}_0 = -\mathbf{J}\frac{\displaystyle\int_\Lambda d\mathbf{r}\frac{(\omega_0 - \rho_0)}{\sigma[\omega_0]}}{\displaystyle\int_\Lambda d\mathbf{r}\frac{(\omega_0 - \rho_0)^2}{\sigma[\omega_0]}}. \tag{5.45}$$

Remarkably, as the optimal velocity is proportional to $\mathbf{J}$, the optimal profile solution of Eq. (5.45) depends exclusively on the magnitude of $\mathbf{J}$ via $|\mathbf{J}|^2$, and not on its orientation respect to the external field $\mathbf{E}$. Consequently, all the isometric current fluctuations characterized by a constant $|\mathbf{J}|$ will have the same associated optimal profile $\omega_0(\mathbf{r};\mathbf{J}) = \omega_0(\mathbf{r};|\mathbf{J}|)$, independently of weather the current vector $\mathbf{J}$ points along the external field, against it, or along any arbitrary direction. This invariance of the optimal profile under current rotations has important consequences at the level of symmetries of the current distribution, because it can be used in Eq. (5.13) to relate in a simple way the LDF of any pair of isometric current fluctuations $\mathbf{J}$ and $\mathbf{J}'$, with $|\mathbf{J}| = |\mathbf{J}'|$

$$G(\mathbf{J}) - G(\mathbf{J}') = |\mathbf{E}||\mathbf{J}|(\cos\theta - \cos\theta'), \tag{5.46}$$

where θ and θ' are the angles formed by vectors $\mathbf{J}$ and $\mathbf{J}'$, respectively, with the constant external field vector $\mathbf{E}$. In this way, we extend the previously (see chapter 4) introduced IFR [10] to time-dependent density profiles. The IFR (5.46) can be rewritten in terms of the probability $P_\tau(\mathbf{J})$ of observing a current $\mathbf{J}$ averaged over a long time τ as

$$\lim_{\tau\to\infty}\frac{1}{\tau}\ln\left[\frac{P_\tau(\mathbf{J})}{P_\tau(\mathbf{J}')}\right] = \mathbf{E}\cdot(\mathbf{J} - \mathbf{J}'). \tag{5.47}$$

Notice that the IFR is also present in a trivial way for the time-independent regime via Eq. (5.33), $G_{\text{flat}}(\mathbf{J}) - G_{\text{flat}}(\mathbf{J}') = |\mathbf{E}||\mathbf{J}|(\cos\theta - \cos\theta')$, where the optimal profiles associated to any current fluctuation are flat.

5.8 Possible solutions for the optimal density profile

In order to get $G(\mathbf{J})$ for the time dependent-regime, we have to solve for a given value of $\mathbf{J}$, $\mathbf{E}$ and ρ_0, Eq. (5.43) together with Eq. (5.45). However,

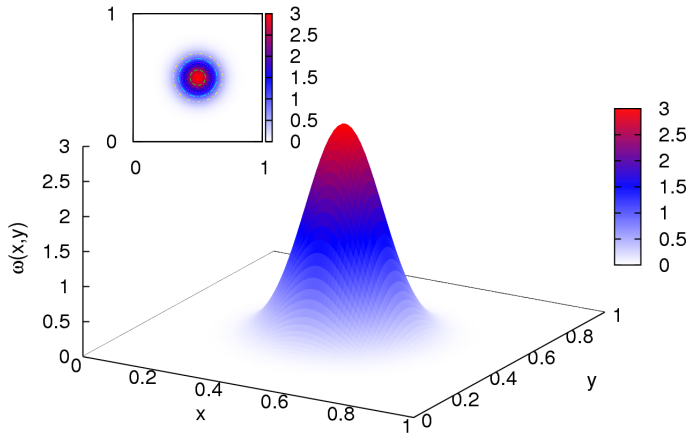

Figure 5.12: Skecth of the first possible solution (5.48) to Eq. (5.43). Inset: Top view where we can appreciate the radial symmetry around $(1/2, 1/2)$

Eq. (5.43) is a non linear partial differential equation and may have several solutions. We could find three possibles solutions to analyze.

1. To explore the first possible solution we have to do the change of variables $(x, y) \to (r, \theta)$ where $r = \sqrt{(x-\frac{1}{2})^2 + (y-\frac{1}{2})^2}$, with $(r, \theta) \in [0, 1/2] \times [0, 2\pi]$. This possible solution of Eq. (5.43) has the following form

$$\begin{aligned} \int \frac{d\omega}{\sqrt{F(\omega)}} &= r; \quad \text{for} \quad r < R_c, \forall\theta \\ \omega(r,\theta) &= K; \quad \text{for} \quad r \geq R_c, \forall\theta \end{aligned} \tag{5.48}$$

   where R_c is a given radius and K is a constant such that $\omega(R_c) = K$. It is easy to check that this kind of solution fullfills Eq. (5.43). This solution (5.48) has radial symmetry, i.e., $\omega(r, \theta) = \omega(r)$. Figure 5.12 shows a sketch of it.

2. The second possible solution takes the form

$$\begin{aligned} \omega(x,y) &= \omega(x); \quad \text{if} \quad |x-\tfrac{1}{2}| > |y-\tfrac{1}{2}| \\ \omega(x,y) &= \omega(y); \quad \text{if} \quad |x-\tfrac{1}{2}| \leq |y-\tfrac{1}{2}| \end{aligned} \tag{5.49}$$

   with $(x, y) \in [0, 1] \times [0, 1]$. It is easy to prove that Eq.(5.43) holds and can be rewritten as

$$\begin{aligned} \omega'(x)^2 &= F[\omega(x)]; \quad \text{if} \quad |x-\tfrac{1}{2}| > |y-\tfrac{1}{2}| \\ \omega'(y)^2 &= F[\omega(y)]; \quad \text{if} \quad |x-\tfrac{1}{2}| \leq |y-\tfrac{1}{2}| \end{aligned} \tag{5.50}$$

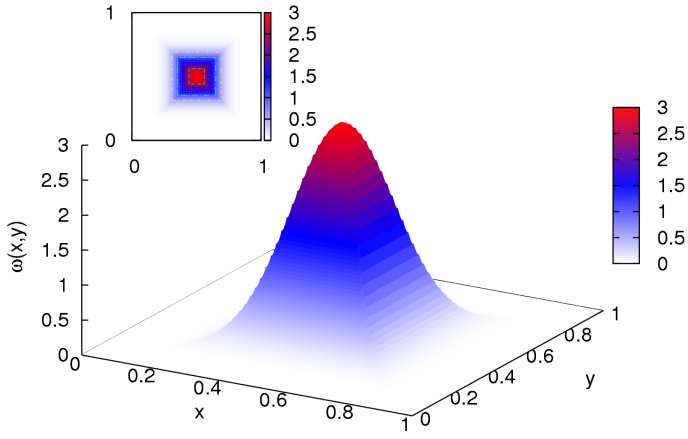

Figure 5.13: Skecth of the second possible solution (5.50) to Eq. (5.43). Inset: Top view.

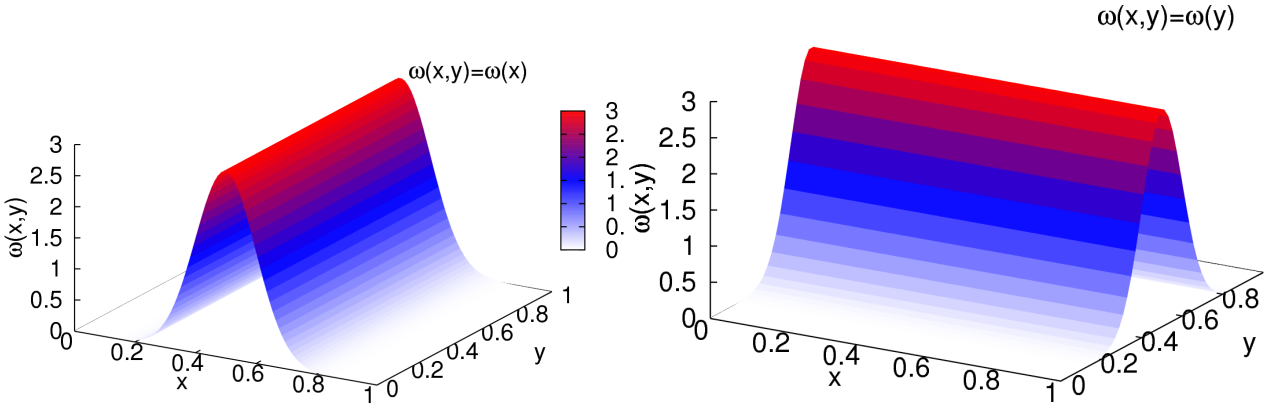

Figure 5.14: Skecth of the second possible solution (5.51) to Eq. (5.43). Left panel: $\omega(x,y) = \omega(x)$. Right panel: $\omega(x,y) = \omega(y)$

In figure 5.13 a sketch of this kind of solution is displayed.

3. The third possible solution is the wave, i.e., $\omega(x,y) = \omega(x)$ or $\omega(x,y) = \omega(y)$, with $(x,y) \in [0,1] \times [0,1]$. In this case Eq.(5.43) reads

$$\omega'(x)^2 = F[\omega(x)] \quad \forall y, \qquad \text{or} \qquad \omega'(y)^2 = F[\omega(y)] \quad \forall x, \tag{5.51}$$

which is equivalent to solve the 1D problem. In figure 5.14 we show a sketch of this possible solution.

As we have three possible solutions, we will be guided by the measured profiles using numerical simulations in order to study analytically the right solution.

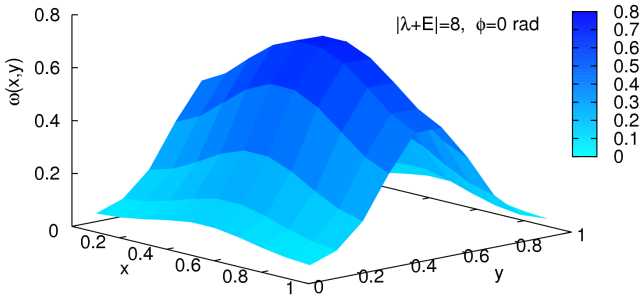

Figure 5.15: Measured optimal profile for $L = 10$ averaging configurations during a long time interval around (x_{CM}, y_{CM}).

5.9 Results for the 2D-WASEP

In order to check the theoretical predicitions for two-dimensional systems above derived, we focused on a paradigmatic diffusive system: the 2D weakly assymetric exclusion process (2D-WASEP) with periodic boundary conditions, where $D[\rho_0] = 1/2$ and $\sigma[\rho_0] = \rho_0(1-\rho_0)$. In this case the time-dependent regime yields for (see Eq. (5.8))

$$|\mathbf{J}| < \sqrt{\rho_0(1-\rho_0)(|\mathbf{E}|^2\rho_0(1-\rho_0) - \pi^2)},$$

meaning that to have a phase transition we need a external field $|\mathbf{E}| > \pi/\sqrt{\rho_0(1-\rho_0)}$. As Eq. (5.43) has several possible solutions for the optimal profile, we performed numerical simulations to see how the shape of $\omega_0(\mathbf{r};\mathbf{J})$ was. The simulations were carried out in a 2D torus of $N = L \times L$ sites with $P = N\rho_0$ particles. Considering a external field to the right ($\mathbf{E} = (E_x, 0)$), each particle attempts to jump to an empty site to its right at rate $1/2 + E_x/2L$ or to its left at rate $1/2 - E_x/2L$, whereas in the y-direction the particles jump up or down at rate $1/2$ whenever there is an empty site. In the same way as in Ref. [39], we replaced in our program the rates $1/2 \pm E_x/2L$ by $\exp[\pm E_x/L]/2$ in order to avoid negative rates for small sizes. To measure the profiles associated to a given current fluctuation we implemented a direct continuous-time algorithm to measure large deviations in many particle systems [42] (see appendix B). This method, which yields the Legendre transform of the current LDF, $\mu(\boldsymbol{\lambda}) = \max_{\mathbf{J}}[G(\mathbf{J}) + \boldsymbol{\lambda}\cdot\mathbf{J}]$, being $\boldsymbol{\lambda}$ the paramter conjugated to $\mathbf{J}$, is based on a modified dynamics so that the rare events responsible of the large deviation are no longer rare, and requires the simulation of multiple *clones* of the system. As $\boldsymbol{\lambda}$ is the input parameter in our simulations, we work from now on in $\boldsymbol{\lambda}$-space where the time-dependent regime occurs for

$$|\boldsymbol{\lambda} + \mathbf{E}| < |\mathbf{J}_c|/\sigma[\rho_0], \tag{5.52}$$

with $|\mathbf{J}_c|$ given by Eq. (5.8).

In order to correctly measure the shape of $\omega_{\boldsymbol{\lambda}}(\mathbf{r})$ in the supercritical regime

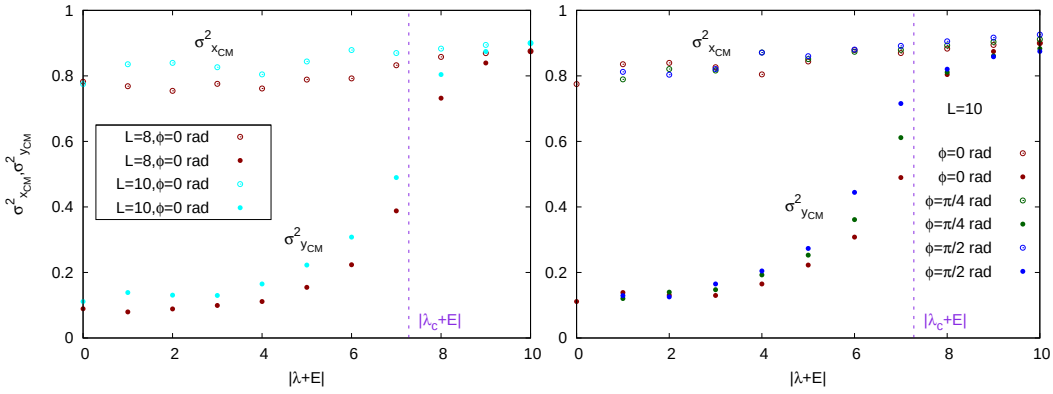

Figure 5.16: Measured variance in each direction, $\sigma^2_{x_{CM}}$ and $\sigma^2_{y_{CM}}$, as a function of $|\boldsymbol{\lambda}+\mathbf{E}|$ for a field pointing in the x-direction, i.e., $\mathbf{E}=(10,0)$. Left panel: Results for increasing L and $\phi=0$ rad. Right panel: Results for $L=10$ and different orientations, ϕ, of the current fluctuations with respect to the field.

($|\mathbf{J}|<|\mathbf{J}_c|$), we averaged the configurations associated to a large fluctuation $|\boldsymbol{\lambda}+\mathbf{E}|$ during a long time interval $\tau>L^2$ taking into account their movement. Therefore we averaged them around their instantaneous center of mass (x_{CM},y_{CM}). If we do not consider this, the structure blurs away due to the periodicity of the system and we get the flat profile. As occured in the 1D case, one has to be aware that this way of averaging yields for the time-independent regime a spurious structure equivalent to averaging random profiles around their (random) center of mass. This spurious structure is independent of $\mathbf{J}$ and can be subtracted in the subcritical region ($\mathbf{J}>|\mathbf{J}_c|$). On the other hand, for the time-dependent regime, the resulting structure is much more pronounced due to the appearance of the traveling profile. In figure 5.15 we show for $\rho_0=0.3$, $L=10$ and $\mathbf{E}=(10,0)$ the profile associated to a supercritical current fluctuation with $|\boldsymbol{\lambda}+\mathbf{E}|=2$ pointing along the field direction, i.e., $\boldsymbol{\lambda}=(-8,0)$. Nevertheless, this way of measuring may be misleading because we actually have to average the profiles, for an external field pointing along the x-direction, around $(1/2,y_{CM})$ since the structure we get taking into account x_{CM} is spurius. This can be shown by measuring the variance of the center of mass in each direction over many configurations for a given fluctuation, i.e.,

$$\sigma^2_{y_{CM}}=\langle y^2_{CM}\rangle-\langle y_{CM}\rangle^2=\langle(\sum_i^L y_{CM_i}/L)^2\rangle-\langle\sum_i^L y_{CM_i}/L\rangle^2, \qquad (5.53)$$

where y_{CM_i} is the center of mass of the i-th column (recall $N=L$-rows $\times$ L-columns), and

$$\sigma^2_{x_{CM}}=\langle x^2_{CM}\rangle-\langle x_{CM}\rangle^2=\langle(\sum_i^L x_{CM_i}/L)^2\rangle-\langle\sum_i^L x_{CM_i}/L\rangle^2, \qquad (5.54)$$

where x_{CM_i} is the center of mass of the i-th row. Using the method above described, with $\mathbf{E} = (10, 0)$, $\rho_0 = 0.3$ and 2×10^5 clones, we measured this variance for different system sizes ($N = 8 \times 8, 10 \times 10$), and different orientations of the current respect to the field ($\phi = 0, \pi/4, \pi/2$ rad) for $L = 10$, see figure 5.16. We can observe how $\sigma^2_{y_{CM}}$ decreases as $|\boldsymbol{\lambda} + \mathbf{E}|$ diminishes and how this change is more pronounced for increasing L, see left panel of figure 5.16, meaning that a well defined structure in the y-direction is formed below the critical current ($|\boldsymbol{\lambda}_c + \mathbf{E}| = |\mathbf{J}_c|/\sigma[\rho_0]$). However, $\sigma^2_{x_{CM}}$ remains constant for the whole current interval, which means that no structure is formed in that direction. The behaviour is the same independently of ϕ, see right panel of figure 5.16, so the travelling profile has only structure in the perpendicular direction to the field (y-direction) no matter the orientation of the current with respect to the field is. Hence, the right way of averaging the configurations is around $(1/2, y_{CM})$, namely around the center of mass of the coordinate perpendiacular to the field.

The exclusive dependence of the optimal demsity profile on the magnitude of the current, $|\mathbf{J}|$, and on the perpendicular coordinate to the field, i.e., $\omega_0(x, y; \mathbf{J}) = \omega_0(y; |\mathbf{J}|)$, allow us to simplify Eqs. (5.43) and (5.45) into the 1D-WASEP problem (see Sec. 5.4)

$$X[\omega_0] - \omega_0'(y)^2 Y[\omega_0] = C_1 + C_2\omega_0. \tag{5.55}$$

In $\boldsymbol{\lambda}$-space, the exclusive dependence of the optimal profile on $|\mathbf{J}|$ and on the y-coordinate (if $\mathbf{E}$ points along the x-direction), turns into

$$\omega_0(x, y; \boldsymbol{\lambda}) = \omega_0(y; \boldsymbol{\lambda}) = \omega_0(y; |\boldsymbol{\lambda} + \mathbf{E}|).$$

In figure 5.17 we show the measured profiles for $\rho_0 = 0.3$, $\mathbf{E} = (10, 0)$ and $N = 10 \times 10$ with 2×10^5 clones for a current fluctuation $|\boldsymbol{\lambda} + \mathbf{E}| = 2$ and different rotation angles ϕ with respect to the external field $\mathbf{E}$. This current fluctuation belongs to the time-dependent regime because $|\boldsymbol{\lambda} + \mathbf{E}| = 2 < |\boldsymbol{\lambda}_c + \mathbf{E}| = 7.2802$. Therefore we observe that the profiles, which were correctly averaged, i.e. around $(1/2, y_{CM})$, have a travelling-wave form. We can appreciate how they remain invariant independently of ϕ how they only have structure in the y-direction.

We now focus on the Legendre transform of the current LDF. One the one hand, the IFR (5.46) implies for $\mu(\boldsymbol{\lambda})$ to satisfy $\mu(\boldsymbol{\lambda}) = \mu[\mathcal{R}_\phi(\boldsymbol{\lambda} + \mathbf{E}) - \mathbf{E}]$, $\forall \phi \in [0, 2\pi]$, being $\mathcal{R}_\phi$ a rotation in 2D of angle ϕ. Notice that for $\phi = \pi$ we recover the GC symmetry, $\mu(\boldsymbol{\lambda}) = \mu(-\boldsymbol{\lambda} - 2\mathbf{E})$. Thus the $\mu(\boldsymbol{\lambda})$ fullfills

$$\mu(\boldsymbol{\lambda}) = \mu(|\boldsymbol{\lambda} + \mathbf{E}|)$$

On the other hand, as the 2D optimal density profiles are the same as in one dimension (taking $|\mathbf{J}| = |J|$), the 2D $\mu(\boldsymbol{\lambda})$ reads

$$\mu(\boldsymbol{\lambda}) = \mu(|\boldsymbol{\lambda} + \mathbf{E}|) = \mu_{1D}(|\boldsymbol{\lambda} + \mathbf{E}|)$$

Hence, the IFR implies for $\mu(\boldsymbol{\lambda})$ and $\omega_{\boldsymbol{\lambda}}(\mathbf{r})$ to be constant along the manifold $|\boldsymbol{\lambda} + \mathbf{E}|$. The invariance of the profile along this manifold has been already

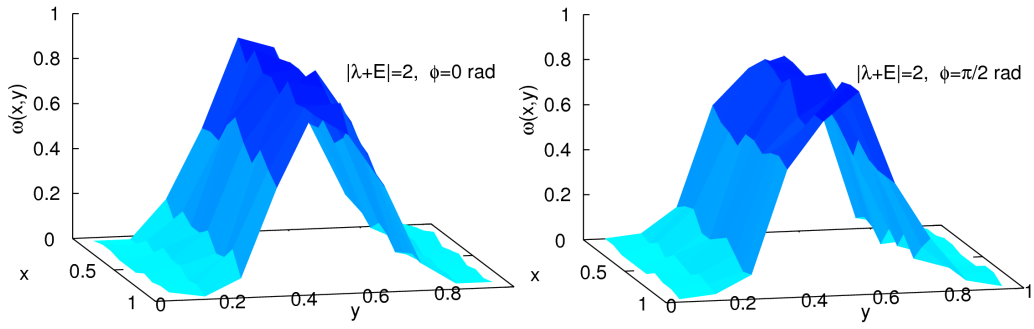

Figure 5.17: Measured optimal profiles during a long time interval averaging configurations around $(1/2, y_{CM})$. Left panel: Measured optimal profile for $|\boldsymbol{\lambda}+\mathbf{E}| = 2$ and $\phi = 0$ rad, corresponding to a current fluctuation parallel to the field. Right panel: Measured optimal profile for $|\boldsymbol{\lambda}+\mathbf{E}| = 2$ and $\phi = \pi/2$ rad, corresponding to a current fluctuation perpendicular to the field.

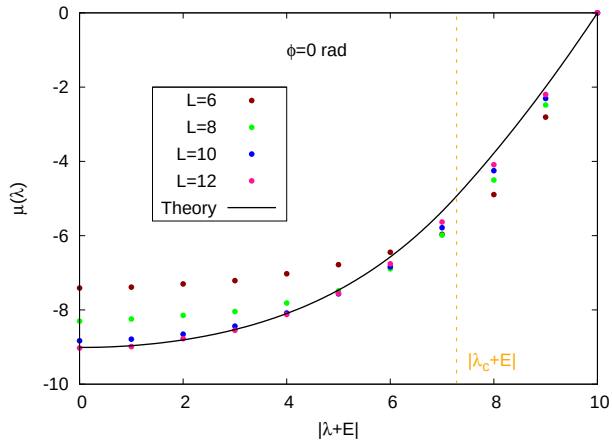

Figure 5.18: Legendre transform of the current LDF as a function $|\boldsymbol{\lambda} + \mathbf{E}|$ for different system sizes, together with the MFT prediction. We observe how for increasing L the data accumulate to the value predicted.

shown in figure 5.17. Hence, we proceed to check numerically the IFR by measuring $\mu(\boldsymbol{\lambda})$ as a fuction of $|\boldsymbol{\lambda} + \mathbf{E}|$ for different angles. Firstly, we measured $\mu(\boldsymbol{\lambda})$ for $\phi = 0$ rad. The numerical results, together with the theoretical predicition, are displayed in figure 5.18. We observe how for increasing L, the data accumulate to the value predicted. Then, we measured $\mu(\boldsymbol{\lambda})$ as a fuction of $|\boldsymbol{\lambda} + \mathbf{E}|$ for different angles for the maximum size we could reach ($L = 12$ and 5.12×10^5 clones). We show these results in figure 5.19, where we can observe that $\mu(\boldsymbol{\lambda})$ remains constant for a given current fluctuation, $|\boldsymbol{\lambda} + \mathbf{E}|$, independently of the angle ϕ with respect to the external field. These results show that the IFR holds even in the time-dependent regime. We can observe weak violations of the IFR for large

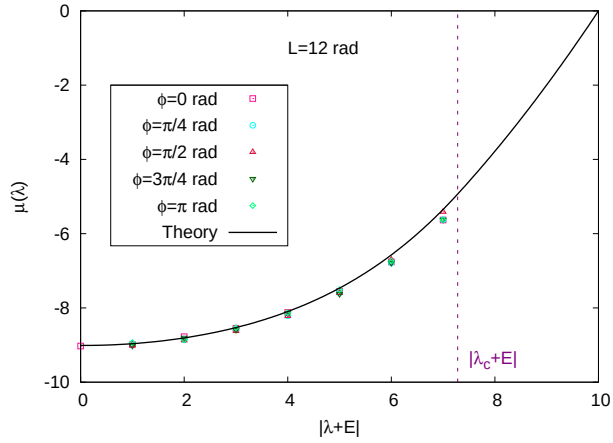

Figure 5.19: Legendre transform of the current LDF as a function $|\boldsymbol{\lambda}+\mathbf{E}|$ for $L = 12$, 5.12×10^5 clones and different angles

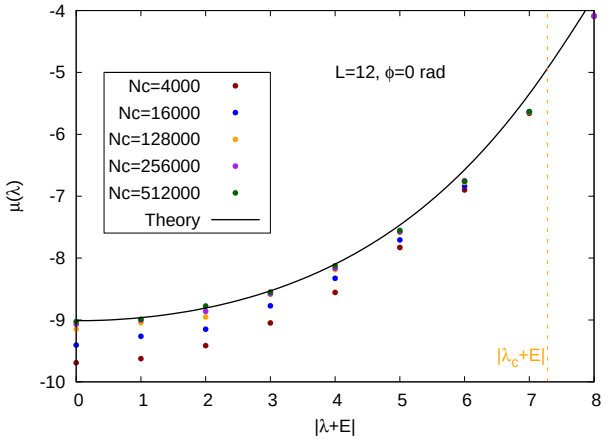

Figure 5.20: Legendre transform of the current LDF as a function $|\boldsymbol{\lambda}+\mathbf{E}|$ for $L = 12$, $\phi = 0$ rad and different number of clones. The solid line corresponds to the MFT prediction.

currents orthogonal to the field ($\phi = \pi/2$ rad). These weak violations are again expected due to the small value of L. Recall that a prerequisite for the IFR to hold is the existence of a macroscopic limit. This is also confirms that the time-dependent optimal density profiles adopt a traveling wave form in order to sustain a large current fluctuation. It is remarkable that, in order the simulations to converge for large sizes in the time-dependent regime, we need to use a huge number of clones in the algorithm (see appendix B). In figure 5.20 the measured $\mu(\boldsymbol{\lambda})$ as a function of $|\boldsymbol{\lambda}+\mathbf{E}|$ for $L = 12$ and different number of clones is displayed. We can appreciate that 5.12×10^5 clones are necessary in order to converge to the *clone-free* regime. This can be also seen in figure 5.21, where the measured value of $\mu(\boldsymbol{\lambda})$ for several $|\boldsymbol{\lambda}+\mathbf{E}|$ as a

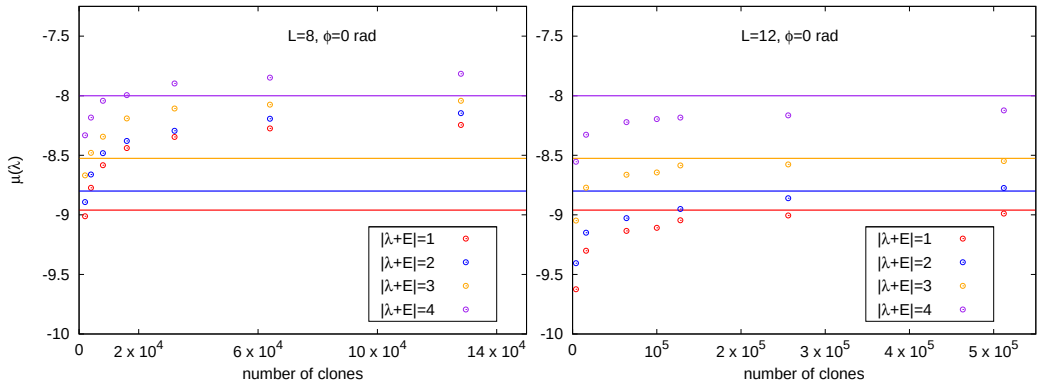

Figure 5.21: Left panel: Legendre transform of the current LDF as a function of the number of clones for $L = 8$, $\phi = 0$ rad and several $|\boldsymbol{\lambda} + \mathbf{E}|$. The solid lines correspond to the MFT prediction. Right panel: Same results for $L = 12$.

function of the number of clones and different system sizes is displayed. We observe that the larger the system is, the more number of clones we need. For that reason, we could simulate a maximum size of $N = 12 \times 12$ with 5.12×10^5 clones.

5.10 Conclusions

In this chapter we have studied how time-dependent profiles enhance the probability of observing a large current fluctuation. This gives rise to a dynamical phase transition between a time-independent and a time-dependent regime. We have analyzed it for both one and two dimensional systems. In the former case, we have measured the optimal density profiles for the periodic one-dimensional weakly assymetric exlusions process (WASEP). In this case, for a large enough value of the field, there is a critical current $|J_c|$ below which a traveling wave emerges. This time-dependent profile moves at constant velocity which we could also measure following the movement of the center of mass of the system. We found a very good agreement with the theoretical predictions based on the previous calculations done in Ref [39]. It is worth noting that these profiles are invariant under the current sign as predicted by the Gallavotti-Cohen symmetry. We have also measured the Legendre transform of the LDF, and again our numerical results fit very well with theory obtained from the MFT. These results suggest that a traveling wave is in fact the most favorable time-dependent profile in the supercritical regime. This observation may greatly simplify general time-dependent calculations, but the question remains to whether this is the whole story or other, more complex solutions may play a dominant role for even larger fluctuations. In any case, it seems clear that rare events call in general for coherent, self-organized patterns in order to be sustained

In the two dimensional case, particularly, in the periodic 2D-WASEP, we have observed that there is again a dynamical phase transition below a critical current fluctuation $|\mathbf{J}_c|$. It is surprising that the time-dependent regime emerges for magnitudes of the current fluctuation such that $|\mathbf{J}| < |\mathbf{J}_c|$, and is independent of its orientation with respect to the external field $\mathbf{E}$. According to the theory, the optimal time-dependent density profiles could in principle have several possible shapes. Nevertheless, the numerical results show that they are travelling waves with structure only along the perpendicular direction to the field. These profiles are invariant under current rotations and depend only on the magnitude of the current fluctuation, proving that the IFR holds even in the time-dependent regime. Actually, we have also theoretically derived the IFR (see Eq. (5.47)) for a periodic d-dimensional system assuming periodic time-dependent optimal current and density fields of the form given by Eqs. (5.36) and (5.38). Our numerical results strongly support that the system adopt these kind of time-dependent profiles in order to sustain a large current fluctuation.

Chapter 6

Infinite family of second-law-like inequalities

6.1 Introduction

As we have so far discussed, the probability distribution function for an out of equilibrium system is very hard to compute. However, as we shall see in this chapter, it may sometimes be approximated by a physically motivated 'trial' distribution [29]. A particularly interesting case is when a driven system (e.g. active matter) is approximated by a thermodynamic one. We show here that every set of trial distributions yields an inequality playing the role of a generalization of the Second Law. The better the approximation, the more constraining the inequality becomes: this suggests a criterion for its accuracy, as well as an optimization procedure that may be implemented numerically and even experimentally. The fluctuation relation behind this inequality –a natural and practical extension of the Hatano-Sasa theorem– does not rely on the a priori knowledge of the stationary probability distribution.

A recurring strategy applied to out of equilibrium systems is to represent the complex energy and dissipation sources by a bath with 'good' equilibrium thermal properties. Two examples are the Edwards 'thermodynamic' approach to granular matter [57], and recent developments for active matter (see Ref. [58, 59, 60] for a recent examples), in which the combination of rapid energy bursts and friction is mimicked by a thermal bath. The aim of such pursuits is not necessarily to make the problem more easily solvable, but rather to cast it in a form that provides thermodynamic intuition and constraints. In this chapter we derive some simple relations that help make this mapping more systematic and controlled. The method is based on the use of inequalities of the form of the Second-Law, associated to each guess for the distribution function.

In these last two decades there has been a development of a family of relations valid for out of equilibrium systems [61], starting from the Fluctuation Theorem in its various forms [8, 9, 12, 10], the Jarzynski [25] and Crooks [26] relations. A later and extremely simple result is the Hatano-

Sasa equality [27][1], which applies to systems that are continuously driven by time-dependent potentials inducing currents, so that even the stationary regimes are out of equilibrium. Their result is essentially a version of Jarzynski equality and the Second Principle, but with the energy replaced by the logarithm of the stationary distribution.

In this chapter we derive an extension of the Hatano-Sasa theorem for Markovian systems, which has the practical advantage that it *does not rely on the a priori knowledge of the stationary probability distribution*. Instead, arbitrary 'trial' smooth distributions can be used, thus allowing one to treat systems whose stationary distribution is either (i) too difficult to calculate, as generically occurs in out of equilibrium systems with many degrees of freedom, or (ii) unwieldy, as for instance in the deterministic limit, where the non-equilibrium steady-state distributions are nonzero only over a fractal support. Our approach leads in particular to an inequality that can be used as a variational principle for improving, in a controlled way, physically motivated approximations to non-equilibrium steady-state distributions. The optimization procedure might be implemented numerically or even experimentally. As an illustration, we numerically approximate the stationary distribution of a paradigmatic non-equilibrium driven system with many degrees of freedom, the Simple Symmetric Exclusion Process in one dimension.

Just as in the case of the Hatano-Sasa equality [27, 69, 70, 71], there is a 'dual' (or adjoint) 'backward' process that yields, when compared to the forward process of the original dynamics, a trajectory-dependent quantity playing the role of an entropy production, that satisfies a form of Fluctuation Theorem. For systems described by a Langevin / Fokker-Planck dynamics, the dual 'backward' process is obtained easily, since it is given by a Langevin dynamics involving only additional *a priori known* external forces derived from the trial function itself. This remarkable property offers the possibility to explore numerically or even experimentally the interesting consequences of the associated detailed fluctuation relations, valid for systems which spontaneously relax to non-equilibrium steady-states.

The organization of the chapter is as follows. In Sec. 6.2 we review the derivation of the Hatano-Sasa fluctuation theorem [27]. After motivating a more general approach we provide in Sec. 6.3.1 a first derivation of the integral version of our fluctuation relation along the same lines of the original Hatano-Sasa derivation. In Sec. 6.3.2 we give a second, more general derivation, which yields the detailed version of the theorem (containing the integral version as a particular case), and in Sec. 6.3.3 we discuss the physical interpretation of the dual dynamics behind it. In Sec. 6.3.4 we discuss a family of inequalities that play the role of the Second-Law. In Sec. 6.4 we propose an optimization procedure for approximating steady-state distributions. As an example, we apply it to the paradigmatic symmetric exclusion process in one dimension. In Sec. 6.5 we give conclusion and perspectives.

[1] see also Y. Oono, and M. Paniconi, Prog. Theor. Phys. Suppl. **130**, 29 (1998) and S. Sasa and H. Tasaki, J. of Stat. Phys. **125**, 125 (2006).

6.2 The Hatano-Sasa relation

Consider a driven system with dynamic variables $\mathbf{x}$ with time-dependent external fields $\alpha(t)$ (e.g. shear rate, temperature gradient, etc), with distribution $\rho(\mathbf{x},t)$ evolving through a generator H_α:

$$\dot{\rho}(\mathbf{x},t) = -H_{\alpha(t)}\,\rho(\mathbf{x},t). \tag{6.1}$$

Let us assume the dynamics admit, for every fixed value of the parameter α, a non-equilibrium steady state with distribution

$$\rho_{ss}(\mathbf{x};\alpha) = e^{-\phi(\mathbf{x};\alpha)} \qquad ; \qquad H_\alpha \rho_{ss}(\mathbf{x};\alpha) = 0. \tag{6.2}$$

The Hatano-Sasa [27] result may be written

$$\left\langle e^{-\int_0^\tau dt\ \frac{\partial\phi(\mathbf{x};\alpha)}{\partial\alpha}\dot{\alpha}} \right\rangle_{\rho_{ss}(\mathbf{x};\alpha_1)} = 1 \tag{6.3}$$

which implies, by virtue of Jensen's inequality:

$$\left\langle \int_{\alpha_1}^{\alpha(\tau)} \frac{\partial\phi(\mathbf{x};\alpha)}{\partial\alpha} d\alpha \right\rangle_{\rho_{ss}(\mathbf{x};\alpha_1)} \geq 0. \tag{6.4}$$

The average $\langle\bullet\rangle$ is over all trajectories $\mathbf{x}(t)$ of duration τ, starting with an initial configuration chosen with the distribution $\rho_{ss}(\mathbf{x};\alpha_1)$ with $\alpha_1 \equiv \alpha(0)$. We shall refer to (6.3) and (6.4) as the Hatano-Sasa equality and inequality, respectively. In the particular case in which the stationary states $\rho_{ss}(\mathbf{x};\alpha)$ are Gibbs states we have:

$$\rho_{ss}(\mathbf{x};\alpha) = \frac{e^{-\beta E(\mathbf{x},\alpha)}}{e^{-\beta F(\alpha)}}; \phi(\mathbf{x};\alpha) = \beta[E(\mathbf{x},\alpha) - F(\alpha)] \tag{6.5}$$

and the Hatano-Sasa equality and inequality become the Jarzynski equality and the Second Law, respectively.

The proof is extremely simple. We start by decomposing the evolution in a large number M of time steps and compute, in operator (bra-ket) formalism, the quantity:

$$\begin{aligned} \langle \quad & -|e^{-\frac{\tau}{M}H(\alpha_M)} \frac{\hat{\rho}_{ss}(\alpha_M)}{\hat{\rho}_{ss}(\alpha_{M-1})} \ldots \frac{\hat{\rho}_{ss}(\alpha_3)}{\hat{\rho}_{ss}(\alpha_2)} e^{-\frac{\tau}{M}H(\alpha_2)} \\ & \frac{\hat{\rho}_{ss}(\alpha_2)}{\hat{\rho}_{ss}(\alpha_1)} e^{-\frac{\tau}{M}H(\alpha_1)} |\rho_{ss}(\alpha_1)\rangle = \langle -|\rho_{ss}(\alpha_M)\rangle = 1 \end{aligned} \tag{6.6}$$

We denote $\hat{\rho}(\alpha)$ the operator such that $\langle\mathbf{x}|\hat{\rho}(\alpha)|\mathbf{x}'\rangle = \delta(\mathbf{x}-\mathbf{x}')\,\rho(\mathbf{x};\alpha)$, and $|\rho(\alpha)\rangle$ the state such that $\rho(\mathbf{x};\alpha) \equiv \langle\mathbf{x}|\rho(\alpha)\rangle$. The state $|-\rangle$ corresponds to the flat distribution $\langle\mathbf{x}|-\rangle = 1$; i.e. the left eigenvector of H_α having zero eigenvalue.

Now, using that the time step τ/M is small, we can write

$$\frac{\rho_{ss}(\mathbf{x};\alpha_{k+1})}{\rho_{ss}(\mathbf{x};\alpha_k)} \approx \quad e^{-\frac{\tau}{M}\ \frac{\partial\phi(\mathbf{x};\alpha_k)}{\partial\alpha}\ \dot{\alpha}}. \tag{6.7}$$

Therefore (6.6) may be written as Eq. (6.3), and the result is proven. The exponential of the term $\left[-\int dt\ \frac{\partial\phi(\mathbf{x};\alpha)}{\partial\alpha}\ \dot{\alpha}\right]$, a functional of the trajectory, is thus weighted in (6.3) with the probability of each dynamical trajectory $\mathbf{x}(t)$ such that $\mathbf{x}(0)$ is sampled from $\rho_{ss}(\mathbf{x},\alpha_1)$.

In the Hatano-Sasa inequality (6.4), the equality holds in the quasi-stationary limit, when the probability distribution may be assumed to be, at each time t, the stationary one $\rho_{ss}(\mathbf{x};\alpha)$ corresponding to the value of α at that time:

$$\left\langle \int \frac{\partial\phi(\mathbf{x};\alpha)}{\partial\alpha} d\alpha \right\rangle = \int d\mathbf{x}\ d\alpha\ e^{-\phi(\mathbf{x};\alpha)} \frac{\partial\phi(\mathbf{x};\alpha)}{\partial\alpha}$$

$$= \int d\mathbf{x}[\rho_{ss}(\mathbf{x};\alpha_M) - \rho_{ss}(\mathbf{x};\alpha_1)] = 0. \tag{6.8}$$

This result is the generalization of the entropy change $S(\alpha_M) - S(\alpha_1) = \langle\int_0^\tau dt\ \dot{\mathbf{x}}\cdot\nabla\phi\rangle$, under reversible transformations, with $S(\alpha) \equiv -\int d\mathbf{x}\rho_{ss}(\mathbf{x};\alpha)\ln\rho_{ss}(\mathbf{x};\alpha)$ the generalized Shannon entropy [27].

6.3 A more general approach

The quantity $\phi(\mathbf{x};\alpha) = -\ln\rho_{ss}(\mathbf{x};\alpha)$ plays a role similar to the one of the energy function in a system with detailed balance, but it may become intractable as soon as we consider a driven system. A first difficulty is that it is in general impossible to obtain analytically. This is aggravated by the fact that in order to use (6.3) and (6.4), we need to know ρ_{ss} also where it is exponentially small. Another, more serious problem, arises from the fact that the function $\phi(\mathbf{x};\alpha)$ may only be small in a limited domain, and very large everywhere else. An extreme form of this situation arises in the deterministic limit. Consider a noisy dynamics with a (Hoover [63]) thermostat:

$$\begin{cases} \dot{q}_i &= p_i \\ \dot{p}_i &= -\frac{\partial\mathcal{H}}{\partial q_i} + \underbrace{\gamma(t)p_i}_{thermostat} - \underbrace{f_i(\mathbf{q})}_{forcing} - \underbrace{\eta_{\mathbf{i}}(\mathbf{t})}_{noise} \end{cases} \tag{6.9}$$

where $\eta(\mathbf{t})$ is a Gaussian white noise of variance ϵ. Energy is conserved provided $\gamma(t) = \frac{(\mathbf{f}+\boldsymbol{\eta})\cdot\mathbf{p}}{\mathbf{p^2}}$. When there is forcing $\mathbf{f} \neq 0$, the stationary distribution is not flat. Indeed, in the limit of zero noise $\epsilon \to 0$, ρ_{ss} has in fact fractal support, and $\phi(\mathbf{x};\alpha)$ is infinity almost everywhere on the energy surface! If we attempt to apply the Hatano-Sasa inequality for a small noise amplitude in a process with varying α, because the region on the energy shell where $\phi(\mathbf{x};\alpha)$ is small is sparse and strongly dependent on α, almost all of the process takes place in regions in which $\phi(\mathbf{x};\alpha)$ is large: the trajectories are very far from quasi-stationary and the Hatano-Sasa inequality, though true, becomes useless.

A similar situation arises when the potential is rapidly oscillating, as in vibrated granular matter – which we may think of as subjected to an oscillating gravity field. Here again, the system is always very far from the

stationary situation corresponding to any instantaneous value of the field, because it does not have the time to catch up with the oscillating stationary measure. And yet, we still observe that rapidly vibrated granular matter behaves in a manner that resembles motion in contact with a heat bath, and would expect some form of Second Law to apply in that case.

With the above motivations, we look for a more flexible approach. Instead of working with the true stationary distributions $\rho_{ss}(\mathbf{x};\alpha)$, we choose an arbitrary family of smooth functions as reference states, $\rho_{\mathtt{ref}}(\mathbf{x};\alpha)$, and the corresponding $\phi_{\mathtt{ref}}(\mathbf{x};\alpha) \equiv -\ln \rho_{\mathtt{ref}}(\mathbf{x};\alpha)$. In the following we derive an extension of the Hatano-Sasa integral and detailed fluctuation relations, using only these smooth functions.

6.3.1 Integral fluctuation theorem

In order to obtain a relation, we go through the same steps as in Sec. 6.2. Starting from the initial distribution $\phi_{\mathtt{ref}}(\mathbf{x};\alpha_1)$, we compute, just as in (6.6):

$$\begin{aligned} \langle \quad - \quad & |e^{-\frac{\tau}{M}H(\alpha_M)} \frac{\hat{\rho}_{\mathtt{ref}}(\alpha_M)}{\tilde{\rho}_{\mathtt{ref}}(\alpha_{M-1})} \cdots \frac{\hat{\rho}_{\mathtt{ref}}(\alpha_2)}{\tilde{\rho}_{\mathtt{ref}}(\alpha_1)} e^{-\frac{\tau}{M}H(\alpha_1)} |\rho_{\mathtt{ref}}(\alpha_1)\rangle \\ = \quad & \langle -|\rho_{\mathtt{ref}}(\alpha_M)\rangle = 1, \end{aligned} \tag{6.10}$$

but with $\tilde{\rho}(\alpha)$ the operator associated with the state evolved by one time-step $e^{-\frac{\tau}{M}H_\alpha}|\rho(\alpha)\rangle$. We can thus write, for large M:

$$\frac{\tilde{\rho}_{\mathtt{ref}}(\mathbf{x};\alpha)}{\rho_{\mathtt{ref}}(\mathbf{x};\alpha)} \approx e^{\frac{\tau}{M}\varphi(\mathbf{x};\alpha)} \tag{6.11}$$

with

$$\varphi(\mathbf{x};\alpha) \equiv -\frac{1}{\rho_{\mathtt{ref}}(\mathbf{x};\alpha)} \{H_\alpha \, \rho_{\mathtt{ref}}(\mathbf{x};\alpha)\} \tag{6.12}$$

Here H_α acts over the function $\rho_{\mathtt{ref}}(\mathbf{x};\alpha)$, so that it is in fact $\varphi(\mathbf{x};\alpha) = -\langle \mathbf{x}|\frac{1}{\hat{\rho}_{\mathtt{ref}}(\alpha)} H_\alpha |\rho_{\mathtt{ref}}(\alpha)\rangle$. We hence have:

$$\frac{\rho_{\mathtt{ref}}(\mathbf{x};\alpha_{k+1})}{\tilde{\rho}_{\mathtt{ref}}(\mathbf{x};\alpha_k)} \approx e^{-\frac{\tau}{M} \; \frac{\partial \phi_{\mathtt{ref}}(\mathbf{x};\alpha_k)}{\partial \alpha} \, \dot{\alpha} - \frac{\tau}{M} \, \varphi(\mathbf{x},\alpha)} \tag{6.13}$$

and we obtain a new equality, valid for all sets $\phi_{\mathtt{ref}}(\mathbf{x};\alpha)$

$$\left\langle e^{-\int dt \; \frac{\partial \phi_{\mathtt{ref}}(\mathbf{x};\alpha)}{\partial \alpha} \, \dot{\alpha} \; - \int dt \; \varphi(\mathbf{x};\alpha)} \right\rangle_{\rho_{\mathtt{ref}}(\mathbf{x};\alpha_1)} = 1. \tag{6.14}$$

which is the first main result of this chapter. Defining

$$\mathcal{Y} \equiv \int dt \; \frac{\partial \phi_{\mathtt{ref}}(\mathbf{x};\alpha)}{\partial \alpha} \, \dot{\alpha} \; + \int dt \; \varphi(\mathbf{x};\alpha) \tag{6.15}$$

it can be simply written as $\langle e^{-\mathcal{Y}} \rangle = 1$. This integral fluctuation theorem is valid for any protocol $\alpha(t)$ and arbitrary times τ, as the Hatano-Sasa equality — to which it reduces if the reference state is chosen as $\rho_{\mathtt{ref}}(\mathbf{x};\alpha) = \rho_{ss}(\mathbf{x};\alpha)$ — but it holds for arbitrary smooth functions $\rho_{\mathtt{ref}}$ [81].

As we shall see, this immediately implies an inequality $\langle \mathcal{Y} \rangle \geq 0$ of the form of the Second Law.

6.3.2 Detailed fluctuation theorem

Just as in the case of the Hatano-Sasa relation, the result of Eq. (6.14) can be alternatively derived as a particular case of a detailed Fluctuation Theorem. We will use here a procedure that generalizes the one used for obtaining the detailed fluctuation theorem associated to the Hatano-Sasa theorem [27, 80, 69, 70, 71, 74].

We are looking for a time-reversed form of the dynamics. Let us start by a rewriting of (6.10):

$$\begin{aligned}
\langle \quad - \quad & |e^{-\frac{\tau}{M}H(\alpha_M)}\frac{\hat{\rho}_{\mathtt{ref}}(\alpha_M)}{\tilde{\rho}_{\mathtt{ref}}(\alpha_{M-1})}...\frac{\hat{\rho}_{\mathtt{ref}}(\alpha_2)}{\tilde{\rho}_{\mathtt{ref}}(\alpha_1)}e^{-\frac{\tau}{M}H(\alpha_1)}|\rho_{\mathtt{ref}}(\alpha_1)\rangle \\
= \quad & \langle\rho_{\mathtt{ref}}(\alpha_M)|\frac{1}{\tilde{\rho}_{\mathtt{ref}}(\alpha_{M-1})}...\frac{\hat{\rho}_{\mathtt{ref}}(\alpha_2)}{\tilde{\rho}_{\mathtt{ref}}(\alpha_1)}e^{-\frac{\tau}{M}H(\alpha_1)}\hat{\rho}_{\mathtt{ref}}(\alpha_1)|-\rangle \\
= \quad & \langle\rho_{\mathtt{ref}}(\alpha_M)|\Pi_{k=1}^{M-1}\left[\frac{1}{\tilde{\rho}_{\mathtt{ref}}(\alpha_k)}e^{-\frac{\tau}{M}H(\alpha_k)}\hat{\rho}_{\mathtt{ref}}(\alpha_k)\right]|-\rangle
\end{aligned}$$

We may now take the adjoint, in order to reverse time:

$$\begin{aligned}
\langle \quad & -|\Pi_{k=M-1}^{1}\left[\frac{1}{\tilde{\rho}_{\mathtt{ref}}(\alpha_k)}e^{-\frac{\tau}{M}H(\alpha_k)}\hat{\rho}_{\mathtt{ref}}(\alpha_k)\right]^{\dagger}|\rho_{\mathtt{ref}}(\alpha_M)\rangle = \\
\langle - \quad | \quad & \Pi_{k=M-1}^{1}\left[\frac{1}{\hat{\rho}_{\mathtt{ref}}(\alpha_k)}e^{-\frac{\tau}{M}\{H(\alpha_k)+\varphi(\alpha_k)\}}\hat{\rho}_{\mathtt{ref}}(\alpha_k)\right]^{\dagger}|\rho_{\mathtt{ref}}(\alpha_M)\rangle \\
= \quad & \langle -|\Pi_{k=M-1}^{1}\left[e^{-\frac{\tau}{M}H^{adj}(\alpha_k)}\right]|\rho_{\mathtt{ref}}(\alpha_M)\rangle
\end{aligned}$$

This is a time-reversed dynamics with generator:

$$[H^{adj}(\alpha)]^{\dagger} \equiv \frac{1}{\hat{\rho}_{\mathtt{ref}}(\alpha)}\left\{H(\alpha)+\varphi(\alpha)\right\}\hat{\rho}_{\mathtt{ref}}(\alpha) \tag{6.16}$$

We shall see below that it corresponds in fact to a Langevin process, with a modified force field (Cfr. Eq. (6.27)).

In terms of the original and the adjoint dynamics, the evolution in a time-step τ/M is:

$$P(\mathbf{x}'|\mathbf{x};\alpha) \equiv \langle\mathbf{x}'|e^{-\frac{\tau}{M}H_\alpha}|\mathbf{x}\rangle, \tag{6.17}$$

$$P^{adj}(\mathbf{x}'|\mathbf{x};\alpha) \equiv \langle\mathbf{x}'|e^{-\frac{\tau}{M}H_\alpha^{adj}}|\mathbf{x}\rangle \tag{6.18}$$

The construction (6.16) tells us that , for each trajectory $\mathcal{T} \equiv \{\mathbf{x}_1, \mathbf{x}_2, ..., \mathbf{x}_M\}$ with initial condition chosen with probability $\rho_{\mathtt{ref}}(\mathbf{x}_1;\alpha_1)$, there is a time-reversed (R) trajectory, with initial condition chosen with probability $\rho_{\mathtt{ref}}(\mathbf{x}_M;\alpha_M)$, and their respective weights are:

$$\mathcal{P}[\mathcal{T};\alpha] \quad = \quad \prod_{n=1}^{M-1} P(\mathbf{x}_{n+1}|\mathbf{x}_n;\alpha_n)\rho_{\mathtt{ref}}(\mathbf{x}_1;\alpha_1),$$

and

$$\left[\mathcal{P}^{adj}[\mathcal{T};\alpha]\right]^R \quad = \quad \prod_{n=1}^{M-1} P^{adj}(\mathbf{x}_n|\mathbf{x}_{n+1};\alpha_n)\rho_{\mathtt{ref}}(\mathbf{x}_M;\alpha_M).$$

We thus may define a quantity $\Xi[\mathcal{T};\alpha]$ associated to each path, having an interpretation analogous to the *entropy production*

$$\Xi[\mathcal{T};\alpha] \equiv \ln \frac{\mathcal{P}[\mathcal{T},\alpha]}{\left[\mathcal{P}^{adj}[\mathcal{T},\alpha]\right]^R}. \tag{6.19}$$

In the large M-limit, it becomes

$$\Xi[\mathcal{T};\alpha] \approx \int_0^\tau dt\ \left[\varphi(\mathbf{x};\alpha) + \dot{\alpha}\partial_\alpha \phi_{\mathtt{ref}}(\mathbf{x},\alpha)\right], \tag{6.20}$$

It is clear from Eq. (6.19) that in terms of Ξ, there is a detailed fluctuation theorem:

$$\begin{aligned} \langle \mathcal{O}[\mathcal{T}] e^{-\Xi[\mathcal{T},\alpha]} \rangle &= \langle \mathcal{O}[\mathcal{T}] e^{-\int_0^\tau dt\ [\varphi(\mathbf{x};\alpha)+\dot{\alpha}\partial_\alpha \phi_{\mathtt{ref}}(\mathbf{x},\alpha)]} \rangle \\ &= \left[\langle \mathcal{O}[\mathcal{T}] \rangle^{adj}\right]^R \end{aligned} \tag{6.21}$$

valid for an arbitrary fuctional $\mathcal{O}[\mathcal{T}]$ of the trajectory. The averages in (6.21) are performed with the real forward dynamics in the first term, and with the time-reversed (R) adjoint dynamics of Eq. (6.18) in the second term.

Equation (6.21) is a very general result. It represents a broad family of fluctuation theorems with a trajectory dependent 'entropy production' of the form of Eq. (6.20), completely determined by the distributions $\rho_{\mathtt{ref}}(\mathbf{x};\alpha)$.

Clearly, choosing $\mathcal{O} = 1$ in this equation we get the integral fluctuation relation of Eq (6.14). This detailed fluctuation theorem, which can be used to derive a variety of Crooks-like relations, is the second main result of this chapter.

6.3.3 Generalized dual (adjoint) dynamics

In order to give a simple physical interpretation of the dual dynamics let us now assume that our system is governed by a Langevin equation

$$\dot{\mathbf{x}} = \mathbf{f}(\mathbf{x};\alpha) + \boldsymbol{\xi}(t) \tag{6.22}$$

with $\mathbf{f}(\mathbf{x};\alpha)$ an arbitrary force (conservative or non-conservative), and $\boldsymbol{\xi}(t)$ a Gaussian uncorrelated noise at temperature T, such that $\langle \boldsymbol{\xi}(t) \rangle = 0$ and $\langle \xi_n(t)\xi_m(t') \rangle = 2T\delta(t-t')\delta_{nm}$. To this is associated the Fokker-Planck process:

$$\frac{d\rho}{dt} = \nabla \cdot \left[\left[T\nabla - \mathbf{f}(\mathbf{x};\alpha)\right]\rho\right] = -H_\alpha \rho \tag{6.23}$$

Using Eq. (6.12) φ is given in this case by

$$\varphi = -\nabla\cdot\mathbf{f} - T\nabla^2\phi_{\mathtt{ref}} + T\left|\nabla\phi_{\mathtt{ref}}\right|^2 + \mathbf{f}\cdot\nabla\phi_{\mathtt{ref}} \tag{6.24}$$

The expression for a path probability is:

$$\mathcal{P}[\mathcal{T};\alpha] \sim e^{-\frac{1}{4T}\int_0^\tau dt\ [(\dot{\mathbf{x}}-\mathbf{f}(\mathbf{x};\alpha))^2 + 4T\frac{\nabla\cdot\mathbf{f}}{2}]}, \tag{6.25}$$

The last term in the argument of the integral comes from the Stratonovich discretization scheme. Then, using equations (6.19) and (6.15), and time-reversing in order to obtain the dynamical weight (that is $[\mathcal{P}e^{-\mathcal{Y}}]^R = \left[[\mathcal{P}^{adj}]^R\right]^R = \mathcal{P}^{adj}$), we have,

$$\begin{aligned}&\mathcal{P}^{adj}[\mathbf{x};\alpha] \sim \\ &e^{-\frac{1}{4T}\int_0^\tau dt\,\left[(\dot{\mathbf{x}}+\mathbf{f}(\mathbf{x};\alpha))^2+4T(\varphi(\mathbf{x},\alpha)-\dot{\alpha}\partial_\alpha\phi_{\mathtt{ref}}(\mathbf{x},\alpha)+\frac{\nabla\cdot\mathbf{f}}{2})\right]} \sim \\ &e^{-\frac{1}{4T}\int_0^\tau dt\,\left[(\dot{\mathbf{x}}+\mathbf{f}(\mathbf{x};\alpha))^2+4T\varphi(\mathbf{x},\alpha)+4T\dot{\mathbf{x}}\cdot\nabla\phi_{\mathtt{ref}}(\mathbf{x},\alpha)+2T\nabla\cdot\mathbf{f}\right]}\end{aligned} \tag{6.26}$$

where in the last step we have dropped all reference to the boundary term, irrelevant for our present purposes.

Is there a Langevin equation associated with the weight of Eq. (6.26)?. In order to answer such a question, we follow a procedure analogous to the one used recently in Ref. [74] for the standard dual dynamic weight. Plugging expression (6.24) into Eq. (6.26) leads to a simple expression

$$\mathcal{P}^{adj}[\mathcal{T};\alpha] \sim e^{-\frac{1}{4T}\int_0^\tau dt\,\left[(\dot{\mathbf{x}}+\mathbf{f}+2T\nabla\phi_{\mathtt{ref}})^2-2T\nabla\cdot[\mathbf{f}+2T\nabla\phi_{\mathtt{ref}}]\right]}.$$

where we can clearly identify the action of the following Langevin equation (in Stratonovich scheme):

$$\dot{\mathbf{x}} = -\mathbf{f}(\mathbf{x};\alpha) - 2T\nabla\phi_{\mathtt{ref}}(\mathbf{x};\alpha) + \boldsymbol{\xi}(t) \tag{6.27}$$

The dual (adjoint) dynamics corresponds to a Langevin process with opposite force, and an additional external potential $\phi_{\mathtt{ref}}(\mathbf{x};\alpha)$ which depends on the choice of $\rho_{\mathtt{ref}}$.

All the results obtained so far reduce to the Hatano-Sasa results if we choose $\rho_{\mathtt{ref}} = \rho_{ss}$, in which case, $\varphi = 0$, Ξ becomes the Hatano-Sasa functional $\mathcal{Y}_{HS} = \int_0^\tau dt\ \dot{\alpha}\partial_\alpha\phi(\mathbf{x},\alpha)$, and the extended dual dynamics becomes the well known (†) standard dual dynamics [15, 27, 69, 70, 71, 80], which in terms of transition probabilities reads $P^\dagger(\mathbf{x}|\mathbf{x}';\alpha) \equiv P(\mathbf{x}'|\mathbf{x};\alpha)\frac{\rho_{ss}(\mathbf{x},\alpha)}{\rho_{ss}(\mathbf{x}';\alpha)}$, as can easily be obtained from Eq. (6.18). The Langevin equation for the usual Hatano-Sasa dual dynamics (see for instance its derivation in Ref.[74]) coincides with Eq. (6.27) replacing $\phi_{\mathtt{ref}}$ by $\phi = -\ln\rho_{ss}$.

Finally it is worth noting that the extended dual dynamics derived above has the advantage over the standard dual dynamics that all the forces are known, so that it might be implemented in practice, numerically or even experimentally, by applying appropriate external fields. It should thus be possible to verify, numerically or experimentally, the detailed fluctuation theorem of Eq. (6.19), as well as other *extended* Crooks-like [26] relations that easily follow from Eq.(6.19) and concern systems with non-equilibrium steady-states. It would also be interesting to explore further the implications of the extended dual dynamics, generalizing the results based on dual dynamics approaches in Refs. [15, 27, 69, 70, 71, 80]).

6.3.4 Generalizations of the Second Law

As we did in Section 6.2 we use the Jensen's inequality in Eq. (6.14) to obtain:

$$\left\langle \int \frac{\partial\phi_{\mathtt{ref}}(\mathbf{x};\alpha)}{\partial\alpha}d\alpha\ + \int dt\ \varphi(\mathbf{x};\alpha)\right\rangle_{\rho_{\mathtt{ref}}(\mathbf{x};\alpha_1)} \geq 0. \tag{6.28}$$

The relation is true for arbitrary $\rho_{\mathtt{ref}}(\mathbf{x};\alpha)$, a bad choice only makes the inequality less constraining. This is the third main result of this chapter and central formula we will exploit for applications. The function $\varphi(\mathbf{x};\alpha)$ is a known, well-behaved extensive function of the dynamic variables, which vanishes if $\rho_{\mathtt{ref}}(\mathbf{x};\alpha) = \rho_{ss}(\mathbf{x};\alpha)$. For example, for a Langevin / Fokker-Planck process (6.22) it is given by Eq (6.24).

If at constant α the system is able to converge to a stationary non-equilibrium regime, the inequality has to hold for large times such that the initial condition is forgotten. We thus get the stationary-state expectation:

$$\langle\varphi\rangle_{ss} = -\left\langle \frac{1}{\rho_{\mathtt{ref}}} H\ \rho_{\mathtt{ref}} \right\rangle_{ss} \geq 0 \quad \forall \rho_{\mathtt{ref}}. \tag{6.29}$$

This inequality is already implicit in the work of Lebowitz and Bergmann [64]. If we define $\dot{w}_{\mathtt{ref}} = -H w_{\mathtt{ref}}$ with $w_{\mathtt{ref}}(t=0) = \rho_{\mathtt{ref}}$, we can rewrite (6.29) as:

$$\begin{aligned} \langle\varphi\rangle_{ss} &= -\left[\frac{d}{dt}\int d\mathbf{x}\ \rho_{ss} \ln\left(\frac{\rho_{ss}}{w_{\mathtt{ref}}(t)}\right)\right]_{t=0} \\ &= -\left[\frac{d}{dt} D_{KL}(\rho_{ss} \parallel w_{\mathtt{ref}}(t))\right]_{t=0} \geq 0 \end{aligned} \tag{6.30}$$

by virtue of the general result $\dot{D}_{KL}(w_1(t) \parallel w_2(t)) \leq 0$ valid for all times $t \geq 0$ with $w_1(t)$ and $w_2(t)$ any two distributions evolving through H [64]. The positively defined Kullback-Leibler distance D_{KL} used above is often an actor in these problems, see [65, 66, 69, 70, 71, 72, 73].

For a purely Hamiltonian system $\dot{D}_{KL}(w_1(t) \parallel w_2(t)) = 0$ independently of w_1 and w_2: irreversibility in this case inescapably requires some form of coarse graining, which this method does not provide. Instead, in the case of a Langevin process (6.23), a short computation [75] gives:

$$\langle\varphi\rangle_{ss} = T\langle|\nabla(\phi_{\mathtt{ref}} - \phi)|^2\rangle_{ss} \geq 0, \tag{6.31}$$

where $\phi = -\ln \rho_{ss}$. We have easy access to the l.h.s. of the above equation numerically *or even experimentally* , because we know $\phi_{\mathtt{ref}}$ and the dynamics, but not to the r.h.s.

Let us consider now a system that is perturbed periodically, such as the granular system described above. Assume further that the system reaches after a long time a periodic state. We then have:

$$\left\langle \oint \frac{\partial \phi_{\mathtt{ref}}(\mathbf{x};\alpha)}{\partial \alpha} d\alpha\ + \oint dt\ \varphi(\mathbf{x};\alpha) \right\rangle \geq 0 \tag{6.32}$$

where the time integral is over one cycle, in the regime in which the distribution becomes periodic in time. If we make the further simplification that $\rho_{\mathtt{ref}}$ is constant in time, we get:

$$\left\langle \oint dt\ \varphi(\mathbf{x};\alpha) \right\rangle \geq 0 \tag{6.33}$$

where the dependence of φ on α comes from H_α.

6.4 A variational scheme

The preceding section suggests an iterative variational procedure to optimize $\rho_{\mathtt{ref}}$ at fixed α:

- Propose a change to $\rho_{\mathtt{ref}}(\mathbf{x})$.
- Compute the new $\varphi = -{\rho_{\mathtt{ref}}}^{-1} H \rho_{\mathtt{ref}}$ (immediate).
- Run $\langle \varphi(\mathbf{x}) \rangle_{stationary}$ and accept the change if the result is smaller.

The resulting φ yields directly a second-law like constraint, which is optimized. The optimization procedure we propose might be indeed implemented numerically or even experimentally to calculate, for instance, optimal effective interactions from steady-state measurements [76].

6.4.1 An application

As an illustrative and non-trivial example, we consider the simple symmetric exclusion process (SSEP), a one dimensional lattice of L sites which are either occupied by a single particle or empty. A configuration at time t is defined by the vector of occupation numbers $\mathbf{n}(t) = (n_1(t), ..., n_L(t))$ ($n_i(t)$=0,1). Each particle in the bulk independently attempts to jump to an empty site to its right or to its left site. At the left boundary each particle is injected at site 1 at rate α and removed from site 1 at rate γ, whereas at the right boundary particles are injected at site L at rate δ and removed from site L at rate β.

The choice of the rates α, γ, δ and β corresponds to the system being in contact with infinite left and right reservoirs at densities $\rho_0 = \alpha/(\alpha+\gamma)$ and $\rho_1 = \delta/(\delta+\beta)$ respectively [32]. If $\rho_0 = \rho_1 = \rho$ the system is in equilibrium and the distribution is of product form: $\rho_{eq}(\mathbf{n}) = \prod_{i=1}^{L} \rho^{n_i}(1-\rho)^{1-n_i} = e^{\sum_{i=1}^{L} \mu n_i}/(1+e^{\mu})^L$, where $\mu = \log(\rho/(1-\rho))$ is the chemical potential. As soon as $\rho_0 \neq \rho_1$, a current is established, and the problem becomes non trivial, with long range correlations. The evolution of the probability $\rho(\mathbf{n})$ of observing a configuration $\mathbf{n}$, is given by the master equation ($n_k^+ = n_k + 1$ and $n_k^- = n_k - 1$)

$$\begin{aligned}
\frac{\partial \rho(\mathbf{n})}{\partial t} = & \sum_{k=1}^{L-1} [\delta_{n_k,1}\delta_{n_{k+1},0}\rho(..., n_k^-, n_{k+1}^+, ...) \\
& + \delta_{n_k,0}\delta_{n_{k+1},1}\rho(..., n_k^+, n_{k+1}^-, ...) \\
& - (\delta_{n_k,1}\delta_{n_{k+1},0} + \delta_{n_k,0}\delta_{n_{k+1},1})\rho(..., n_k, n_{k+1}, ...)] \\
& + \alpha\delta_{n_1,1}\rho(n_1^-, ...) + \gamma\delta_{n_1,0}\rho(n_1^+, ...) \\
& + \delta\delta_{n_L,1}\rho(..., n_L^-) + \beta\delta_{n_L,0}\rho(..., n_L^+) \\
& - (\gamma\delta_{n_1,1} + \alpha\delta_{n_1,0} + \beta\delta_{n_L,1} + \delta\delta_{n_L,0})\rho(n_1, ..., n_L).
\end{aligned} \tag{6.34}$$

The full measure on the microscopic configurations in the steady state, $\rho_{ss}(\mathbf{n})$, may be computed analytically through the so-called matrix method [6]. Here we propose an approximate form $\phi_{\mathtt{ref}}(\mathbf{n}) = \sum_i h_i n_i + \sum_{i \neq j} J_{ij} n_i n_j$. Using the master equation, we evaluate $\varphi = \frac{1}{\rho_{\mathtt{ref}}(\mathbf{n})} \frac{\partial \rho_{\mathtt{ref}}(\mathbf{n})}{\partial t}$ (Eq. (6.12)) as:

$$\begin{aligned}
\varphi &= \sum_{k=1}^{L-1}[\delta_{n_k,1}\delta_{n_{k+1},0}e^{h_k-h_{k+1}+\sum_{j\neq k,k+1}2(J_{kj}-J_{k+1,j})n_j} \\
&+ \delta_{n_k,0}\delta_{n_{k+1},1}e^{h_{k+1}-h_k-\sum_{j\neq k,k+1}2(J_{kj}-J_{k+1,j})n_j} \\
&- (\delta_{n_k,1}\delta_{n_{k+1},0}+\delta_{n_k,0}\delta_{n_{k+1},1})] \\
&+ \alpha\delta_{n_1,1}e^{h_1+\sum_{j\neq 1}2J_{1j}n_j}+\gamma\delta_{n_1,0}e^{-h_1-\sum_{j\neq 1}2J_{1j}n_j} \\
&+ \delta\delta_{n_L,1}e^{h_L+\sum_{j\neq L}2J_{Lj}n_j}+\beta\delta_{n_L,0}e^{-h_L-\sum_{j\neq L}2J_{Lj}n_j} \\
&- (\gamma\delta_{n_1,1}+\alpha\delta_{n_1,0}+\beta\delta_{n_L,1}+\delta\delta_{n_L,0}) \qquad (6.35)
\end{aligned}$$

We compute the expectation value of this φ with the true SSEP dynamics, and minimize with respect to the $[h_i, J_{ij}]$ using a suitable algorithm [77]. Clearly, for $\rho_0 = \rho_1 = \rho$ the system is in equilibrium and we have for each site $h_i = h = -\mu = \log((1-\rho)/\rho)$ and $J_{ij} = 0$ (see $\rho_{eq}(\mathbf{n})$ above). Unlike the equilibrium case, as soon as $\rho_0 \neq \rho_1$ we obtain nonzero J_{ij} corresponding to the long-range correlations characteristic of the stationary non-equilibrium state, see Figure 6.1. These correlations extend over macroscopic distances and reflect the intrinsic non-additivity of non-equilibrium systems [32]. The optimized measure $\rho_{opt}(\mathbf{n}) = e^{-\phi_{opt}(\mathbf{n})}$ obtained with the $[h_i, J_{ij}]$ which minimize the expectation value of φ is not the exact solution of [6], but we have checked the quality of the approximation by computing expectation values with this measure: this is most easily done with a Monte Carlo procedure with 'energy' $\phi_{opt}(\mathbf{n})$. To do that one starts from a random initial configuration $\mathbf{n}(t=0)$ and evolves it with a Metropolis algorithm where the probability to go from a configuration $\mathbf{n}$ to a configuration $\mathbf{n}'$ in a single jump is $W(\mathbf{n}\to\mathbf{n}') = \min\left[\dfrac{\rho_{opt}(\mathbf{n}')}{\rho_{opt}(\mathbf{n})}, 1\right]$ (note that there are no reservois in this calculation). The configuration $\mathbf{n}'$ is the same as the configuration $\mathbf{n}$ except for the randomly chosen node k which changes its value to $n'_k = 1-n_k$. We then have

$$\frac{\rho_{opt}(\mathbf{n}')}{\rho_{opt}(\mathbf{n})} = \exp\left[(2n_k-1)\left(h_k + 2\sum_{j\neq k}J_{kj}n_j\right)\right]. \qquad (6.36)$$

Applying this dynamics we measured the steady state density profile $\rho_i \equiv \langle n_i\rangle$ shown in figure 6.2, and compared it with the analytical result obtained using the exact stationary state measure $\rho_{ss}(\mathbf{n})$, which is (see [32]):

$$\langle n_i\rangle = \frac{\rho_0(L+\frac{1}{\beta+\delta}-i)+\rho_1(i-1+\frac{1}{\alpha+\gamma})}{L+\frac{1}{\alpha+\gamma}+\frac{1}{\beta+\delta}-1}. \qquad (6.37)$$

We also compared with the result obtained assuming local equilibrium considering no reservoirs at the boundaries and a spatially varying chemical potential, which is adjusted to maintain the same steady state density profile (6.37). We then have that the local equilibrium measure is $\rho_{LE}(\mathbf{n}) = \prod_{i=1}^{L} e^{-h_i n_i}/(1+e^{-h_i})$, where $h_i = -\mu_i = \log((1-\langle n_i\rangle)/\langle n_i\rangle)$, with $\langle n_i\rangle$ given by (6.37). Notice that this local equilibrium measure for $\rho_0 \neq \rho_1$ turns

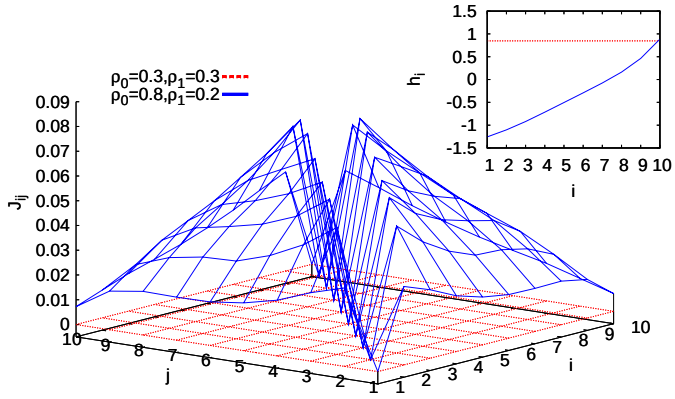

Figure 6.1: Optimized J_{ij} for the SSEP model with open boundaries for $\rho_0 = \rho_1$ (red) and for $\rho_0 \neq \rho_1$ (blue). Inset: Similar results for the optimized h_i

into the equilibrium measure by doing $\rho_0 = \rho_1$. In figure 6.2 we can see that there is a perfect agreement with the exact analytical results for both $\rho_0 = \rho_1$ and $\rho_0 \neq \rho_1$, and in this latter case, for the optimized measure and, very surprisingly, for the local equilibrium measure. We also measured the two-point correlation function $\langle n_i n_j \rangle_c \equiv \langle n_i n_j \rangle - \langle n_i \rangle \langle n_j \rangle$ obtaining the results shown in Figure 6.3. Using again the exact measure $\rho_{ss}(\mathbf{n})$,one finds that the analytical prediction in the steady state for $1 \leq i < j \leq L$ is [32]

$$\langle n_i n_j \rangle_c = \frac{-(\rho_0 - \rho_1)^2 (\frac{1}{\alpha+\gamma} + i - 1)(\frac{1}{\beta+\delta} + L - j)}{(\frac{1}{\alpha+\gamma} + \frac{1}{\beta+\delta} + L - 1)^2 (\frac{1}{\alpha+\gamma} + \frac{1}{\beta+\delta} + L - 2)}. \tag{6.38}$$

For large L, introducing macroscopic coordinates $i = Lx$ and $j = Ly$, this becomes for $x < y$, $\langle n_{Lx} n_{Ly} \rangle_c = -x(1-y)(\rho_0 - \rho_1)^2/L$. As stated in [32], one may think that these weak, but long range, correlations play no role in the macroscopic limit. However, they are responsible for a leading contribution in the variance of a macroscopic quantity such as the number of particles.
As expected, figure 6.3 shows how the Monte Carlo procedure fits exactly with the analytical results for $\rho_0 = \rho_1$ ($\langle n_i n_j \rangle_c = 0$) because we are using the equilibrium measure in which no spatial correlations are present. Besides, for $\rho_0 \neq \rho_1$ we see how the results obtained with the optimized measure are much closer to the exact analytical ones than those obtained with the local equilibrium assumption. This reflects the fact that with the optimized measure we are taking into account at least the two-site long range correlations which are not considered in the local equilibrium case. This shows that the physically motivated optimized trial is very good, at least regarding one and two point static spatial correlation functions. In this sense the out of equilibrium state of the SSEP can be thus fairly approximated by simple and intuitive quantities such as the local effective fields and two-site long-

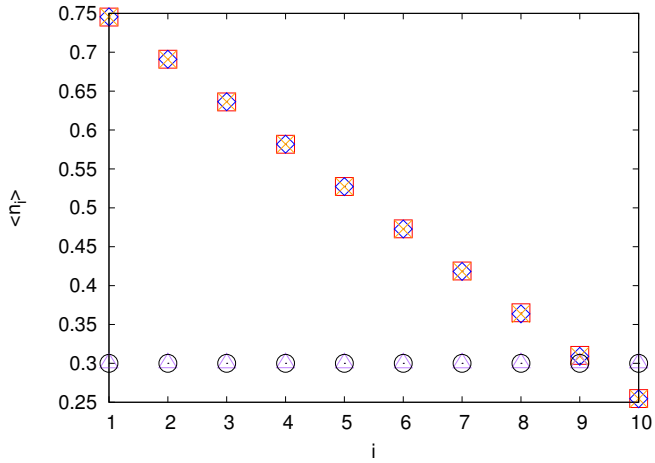

Figure 6.2: Analytical and simulation results for the steady state density profile $\langle n_i \rangle$. Red squares $\square$ and orange crosses $\times$ correspond to the Monte Carlo procedure for densities $\rho_0 = 0.8$, $\rho_1 = 0.2$ using the optimized trial $\rho_{opt}(\mathbf{n})$ and the local equilibrium measure $\rho_{LE}(\mathbf{n})$ respectively, whereas blue diamonds $\diamond$ are the analytical results, see Eq. (6.37). Purple triangles $\triangle$ correspond to the Monte Carlo procedure for densities $\rho_0 = \rho_1 = 0.3$ using the equilibrium measure $\rho_{eq}(\mathbf{n})$, whereas black circles $\bigcirc$ are the analytical results.

range interactions. Although more difficult to guess, one might of course add other terms to the trial function to improve the present agreement, for instance, higher order interaction terms, but the difficulty of the numerical minimization problem increases very rapidly.

6.5 Conclusions

We have derived an exact relation for Markovian systems which generalizes the Hatano-Sasa relation but does not rely on the a priori knowledge of the stationary probability distribution, but rather on arbitrary 'trial' functions for the stationary distribution. More generally, we have derived the detailed version of the fluctuation relation by identifying a generalized form of dual (adjoint) dynamics, generating the backward process that yields a trajectory-dependent 'entropy production' . For systems described by Langevin dynamics, we have showed that the dual dynamics is also governed by a simple Langevin dynamics, which may be expressed directly in terms of the 'trial' functions. One may also obtain in this context a version of the three extended 'detailed' fluctuation theorems of Refs. [69]-[71].

Our approach leads to an infinite family of inequalities that generalize the Second Law, and suggests a variational principle for optimizing trial measures, in a quantitative and controlled way, to approximate non-equilibrium probability distributions. The optimization procedure we propose might

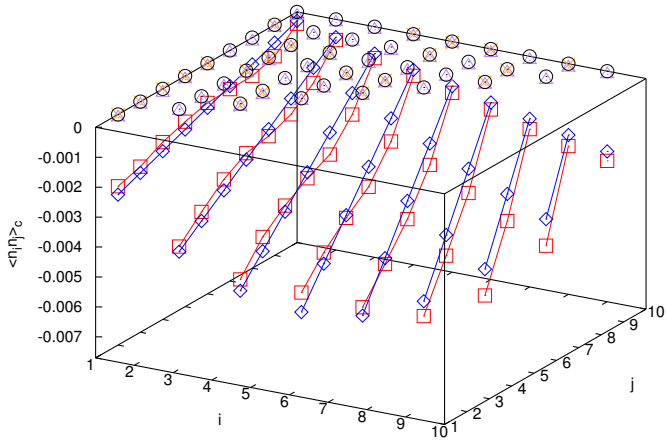

Figure 6.3: Analytical and simulation results for the two-point correlation function $\langle n_i n_j \rangle_c$ in the steady state. Red squares □ and orange crosses × correspond to the Monte Carlo procedure for densities $\rho_0 = 0.8$, $\rho_1 = 0.2$ using the optimized trial $\rho_{opt}(\mathbf{n})$ and the local equilibrium measure $\rho_{LE}(\mathbf{n})$ respectively, whereas blue diamonds ◇ are the analytical results, see Eq. (6.38). Purple triangles △ correspond to the Monte Carlo procedure for densities $\rho_0 = \rho_1 = 0.3$ using the equilibrium measure $\rho_{eq}(\mathbf{n})$, whereas black circles ◯ are the analytical results.

be implemented numerically or even experimentally in order to infer non-equilibrium steady-state distributions in terms of intuitive physical quantities. To illustrate this, we have implemented this approximating scheme for the Simple Symmetric Exclusion Process in one dimension.

A particularly interesting case for applying this variational approach is to Active Matter [78], where it has been proposed recently to represent the complex energy exchanges in the system by a bath with equilibrium-like properties Refs. [58, 59, 60]. Another interesting and somewhat related system is that of current-driven vortices in superconductors with pinning. In this case the complex interplay of driving, quenched disorder and vortex-vortex interactions yields a variety of non-equilibrium dynamical regimes and transitions that may sometimes be successfully described by effective temperatures [79]. At any rate, the important property of these approximations is that there is a Second Law-type inequality associated with them.

Conclusions

In this thesis we have deeply studied the role of macroscopic fluctuations to understand the behavior of nonequilibrium systems. This consists in estimating the probability that the evolution of a macroscopic observable, e.g. the current or density field, deviates from the solution of hydrodynamics. Key to this analysis, is to express this probability in a large deviation principle form (see Eq. 7 and Ref. [24]). By doing this, one can naturally identify the large deviation function (LDF) with a nonequilibrium thermodynamic potential, from which all macroscopic properties of the system can be obtained. This identification is inspired by the fact that in equilibrium systems the LDF is univocally related to the free energy. Unlike the equilibrium case, where the LDF depends locally on the density field and is convex, the nonequilibrium LDF may be non-local and non-convex. The non-locality is indicative of one of the most prominent features of nonequilibrium systems which are the ubiquitous long range correlations [21, 22]. It is also remarkable that in equilibrium systems we known (by Landau argument), with short range-range interactions, there is no phase transition if the dimension of space is one dimensional. However, in non-equilibrium systems nothing prevents the existence of phase transitions in one dimension [39, 40], as we have shown in chapter 5.

Another example that reinforces the importance of fluctuations and particularly the role of the LDF, is the Gallavotti-Cohen fluctuation theorem [8, 9, 12] which express the subtle but enduring consequences of microscopic time reversibility at the macroscopic level. The list continues however, with further breakthroughs ranging from the Jarzynski equality [25] or the Crooks fluctuation theorem [26] to the Hatano-Sasa relation [27] or the recent extension of Clausius inequality to nonequilibrium steady states [28], to mention just a few.

For all these reasons we have focused on the study of macroscopic fluctuations in out of equilibrium diffusive systems. The chosen macroscopic observable has been the time-averaged current. It can be considered as the most characteristic observable, together with the density, in nonequilibrium diffusive system characterized by a locally conserved magnitude (e.g. energy, particle density, momemtum, etc). The theoretical framework in which we have worked, has been the macroscopic fluctuation theory (MFT) of Bertini and coworkers [15]-[18]. This theory briefly introduced in chapter 1 has been developed to understand the fluctuating behavior of diffusive systems far from equilibrium and offers predictions for the LDF of certain observables,

e.g. the time-averaged current, from the knowledge of two transport coefficients $(D[\rho], \sigma[\rho])$ which can be readily obtained from experiments. Some of the models in which we have applied this theory have been described in chapter 2. They are all diffusive models in which local equilibrium has been proved and hydrodynamic evolution equations have been derived. However, the MFT leads to a difficult variational problem whose solution, in the particular case of the time-averaged current, remains challenging in most cases. Therefore, some symplifying hypotheses are necessary in order to get manageable equations. These hypotheses constitute the additivity conjecture, which is introduced in chapter 3. Hence, the main objective of this chapter has been to obtain by assuming the additivity conjecture, explicit predictions for the current LDF in a paradigmatic diffusive model as is the Kipnis-Marchioro-Presutti (KMP) model. Recall that the additivity conjecture consists in assuming the following hypotheses

1. The optimal profiles responsible of a given current fluctuation are time-independent.

2. The resulting divergence-free optimal current profile is in fact constant across space.

Provided this two hypotheses, we have been able to compute analytically the time-averaged current LDF in the two-dimensional KMP model with open boundaries at different energy densities in one direction and periodic boundary conditions in the other direction. For the 1D-KMP model this has been already done by Hurtado and Garrido [36, 37]. Our aim in this chapter was to see what happens in higher dimensions. Hence, once we predicted the current ditribution for the 2D-KMP model we tested the validity of the additivity conjecture by performing extended numerical simulations. It is worth remarking the role of numerical simulations here because they can be considered as the *experimental* laboratory to confirm if the hypotheses one makes are correct. As we were interested in large current fluctuations in the long time limit, standard simulations were not useful because they just allow us to explore moderate fluctuations around the average. Recall that the probability of observing a large current fluctuation decays exponentially in time. Hence, we had to implement an elegant method recently introduced to measure large deviation functions in many particle systems [41]. This method is based on a modification of the dynamics so that the rare events responsible of the large-deviation are no longer rare (see appendix B). Thus, we performed a large number of steady-state simulations of long duration to measure the LDF. From the analysis of our numerical results we concluded that the additivity conjecture for the 2D-KMP model was valid for a wide current interval. Remarkably the current distribution exhibits non-Gaussian tails for large current fluctuations away from the average. Furthermore, we also measured the optimal density profiles associated to a given current fluctuation. They happened to be either monotone for small current fluctuations, or non-monotone with a single maximum for large enough deviations. It is remarkable that these measured optimal profiles actually correspond to the theoretical profiles obtained by minimizing the functional resulting from the additivity conjecture. This confirms the idea that the system indeed

modifies its density profile to facilitate the deviation of the current, validating the power of the additivity conjecture to compute both the current LDF and the associated optimal profiles. In addition, they are invariant under current rotations with respect to the gradient direction because they only depend on the magnitude of $|\mathbf{J}|$ and not on its orientation. The origin of this invariance was studied in chapter 4 where we derived the Isometric Fluctuation Relation (IFR). A possible continuation of the research developed in chapter 3 could be the following:

- Analyze and test the additivity conjecture in low dimensional systems with anomalous, non-diffusive transport models [46], or to systems with several conserved fields.

In chapter 4 we have shown how symmetry principles come forth in fluctuations far from equilibrium. By demanding invariance of the optimal path responsible of a given fluctuation under symmetry transformations, we unveiled a novel and very general isometric fluctuation relation for time-reversible systems which relates in a simple manner the probability of any pair of isometric current fluctuations. Invariance principles of this kind can be applied with great generality in diverse fields where fluctuations play a fundamental role, opening the door to further exact and general results valid arbitrarily far from equilibrium. We proved that the IFR is a consequence of time-reversibility for systems in the hydrodynamic scaling limit, and reveals an unexpected high level of symmetry in the statistics of nonequilibrium fluctuations. It generalizes and comprises the Gallavotti-Cohen fluctuation theorem for currents, relating the probabilities of an event not only with its time-reversal but with any other isometric fluctuation. The new symmetry implies remarkable hierarchies of equations for the current cumulants and the nonlinear response coefficients, going far beyond Onsager's reciprocity relations and Green-Kubo formulas. The following open questions derived from chapter 4 call for further study

- It would be interesting to test in experiments the new hierarchies for the current cumulants and the nonlinear response coefficients which hold arbitrarily far from equilibrium.

- A natural question concerns the level of generality of the isometric fluctuation relation. In this chapter we have demonstrated the IFR for a broad class of systems characterized at the macroscale by a single conserved field, using the tools of macroscopic fluctuation theory (MFT). This theoretical framework, summarized in the path large deviation functional, Eq. (1.11), has been rigorously proven for a number of interacting particle systems [14, 15, 16, 17], but it is believed to remain valid for a much larger class of systems. The key is that the Gaussian nature of local fluctuations, which lies at the heart of the approach, is expected to emerge for most situations in the appropriate macroscopic limit as a result of a central limit theorem: although microscopic interactions can be extremely complicated, the ensuing fluctuations of the slow macroscopic fields result from the sum of an enormous amount of random events at the microscale which give rise to Gaussian statistics.

There exist of course anomalous systems for which local fluctuations at the macroscale can be non-Gaussian. In these cases we cannot discard that a modified version of the IFR could remain valid, though the analysis would be certainly more complicated. Furthermore, our numerical results have shown that the IFR remains true even in cases where it is not clear whether the MFT applies, strongly supporting the validity of this symmetry for arbitrary fluctuating macroscopic systems.

- A related question is the demonstration of the IFR starting from microscopic dynamics. Techniques similar to those in Refs. [13, 38], which derive the Gallavotti-Cohen fluctuation theorem from the spectral properties of the microscopic stochastic evolution operator, can prove useful for this task. However, in order to prove the IFR these techniques must be supplemented with additional insights on the asymptotic properties of the microscopic transition rates as the macroscopic limit is approached. In this way we expect finite-size corrections to the IFR which decay with the system size, as it is in fact observed in our simulations for the energy diffusion model, see Fig. 4.3. Also interesting is the possibility of an IFR for discrete isometries related with the underlying lattice in stochastic models.

- Demanding also invariance of the optimal path under symmetry transformations could be particularly relevant in mesoscopic biophysical systems, where relations similar to the isometric fluctuation relation might be used to efficiently measure free-energy differences in terms of work distributions [52].

- Other interesting issues concern the study of general fluctuation relations emerging from the invariance of optimal paths in full hydrodynamical systems with several conserved fields, or the quantum analog of the isometric fluctuation relation in full counting statistics.

In chapter 5 we have studied how optimal time-dependent profiles enhance the probability of observing a large current fluctuation. This gives rise to a dynamical phase transition between a time-independent and a time-dependent regime. We have analyzed it for both one and two dimensional systems. In one dimension, we have measured the optimal density profiles for the periodic one-dimensional weakly assymetric exlusions process (WASEP). In this case, for a large enough value of the field, there is a critical current below which a traveling wave emerges. This time-dependent profile moves at constant velocity which we could also measure following the movement of the center of mass of the system. We found a very good agreement with the theoretical predictions based on the previous calculations done in Ref [39]. It is worth noting that these profiles are invariant under the current sign as predicted by the Gallavotti-Cohen symmetry. We have also measured the Legendre transform of the LDF, and again our numerical results fit very well with theory obtained from the MFT. These results suggest that a traveling wave is in fact the most favorable time-dependent profile in the supercritical regime. This observation may greatly simplify general time-dependent calculations, but the question remains to whether this is the whole story

or other, more complex solutions may play a dominant role for even larger fluctuations. In any case, it seems clear that rare events call in general for coherent, self-organized patterns in order to be sustained In the two dimensional case, particularly, in the periodic 2D-WASEP, we have observed that there is again a dynamical phase transition below a critical current fluctuation.The numerical results have shown that the optimal profiles are travelling waves with structure only along the perpendicular direction to the field. These profiles are invariant under current rotations and depend only on the magnitude of the current fluctuation, proving that the IFR holds even in the time-dependent regime. Actually, we have also theoretically derived the IFR for a periodic d-dimensional system assuming periodic time-dependent optimal current and density fields with a travelling wave form. Our numerical results strongly support that the system adopt these kind of time-dependent profiles in order to sustain a large current fluctuation. As future lines of research we propose the following

- It would be interesting to extend this study to open boundaries geometries and test numerically if any time-dependent profile emerges in those situations for extreme current deviations. Nevertheless in a recent work [53] for the 1D-WASEP with open boundaries, no numerical evidence for dynamical phase transition has been found.

As we have mentioned above, the Jarzinsky equality [25] is a very important result which has been experimentally verified using small thermodynamic systems such as biomolecules or colloidal particles [54, 55]. This equality which holds for transitions between isothermal equilibrium states, was extended by Hatano and Sasa [27], thus establishing a generalization of the second law holding for transitions between steady states. The Hatano-Sasa theorem which has also been experimentally verfied [56], relies on the a priori knowdlege of the stationary probability distribution. Instead, arbitrary 'trial' smooth distributions can be used, thus allowing one to treat systems whose stationary distribution is too difficult to calculate, as generically occurs in out of equilibrium systems with many degrees of freedom. That is what we have done in chapter 6. We show that every set of trial distributions yields an inequality playing the role of a generalization of the Second Law. This suggests a variational principle for optimizing trial measures, in a quantitative and controlled way, to approximate non-equilibrium probability distributions. The optimization procedure we propose might be implemented numerically or even experimentally in order to infer non-equilibrium steady-state distributions in terms of intuitive physical quantities. To illustrate this, we have implemented this approximating scheme for the Simple Symmetric Exclusion Process in one dimension. as future work we propose the following research lines

- A particularly interesting case for applying this variational approach is to Active Matter [78], where it has been proposed recently to represent the complex energy exchanges in the system by a bath with equilibrium-like properties Refs. [58, 59, 60].

- Another interesting and somewhat related system is that of current-driven vortices in superconductors with pinning. In this case the

complex interplay of driving, quenched disorder and vortex-vortex interactions yields a variety of non-equilibrium dynamical regimes and transitions that may sometimes be successfully described by effective temperatures [79]. At any rate, the important property of these approximations is that there is a Second Law-type inequality associated with them.

Conclusiones

En esta tesis hemos estudiado en profundidad el papel fundamental que desempeñan las fluctuaciones de observables macroscópicos en los sistemas fuera del equilibrio. El marco teórico en el que nos hemos basado, es la llamada teoría macroscópica fluctante (MFT, por sus siglas en inglés), desarrollada por Bertini y colaboradores en los últimos diez años [15]-[18]. Esta teoría, descrita en el capítulo 1, describe en detalle las fluctuaciones dinámicas en sistemas difusivos, ofreciendo predicciones para la LDF a partir del conocimiento de la ecuación de evolución macróscopica (o hidrodinmica) del sistema y sólo dos coeficientes de transporte. La MFT es un marco teórico muy general y de amplia aplicación que normalmente desemboca en un problema variacional complicado cuya solución exacta es difícil en la mayoría de los casos. Como consecuencia, en el capítulo 3 de esta tesis, se suponen dos hipótesis simplificadoras que nos permiten resolver el problema variacional. Con estas dos hipótesis, que constituyen la conjetura de aditividad, hemos sido capaces de calcular explícitamente la función de grandes desviaciones de la corriente integrada en el tiempo, obteniendo así la probabilidad de observar dicha corriente transcurrido un tiempo largo pero finito. En particular, hemos calculado de manera teórica la LDF de la corriente integrada en un modelo paradigmático de transporte difusivo. Este es el modelo de Kipnis-Marchioro-Presutti (KMP), descrito en detalle en el capítulo 2. Una vez obtenida la predicción teórica de la LDF de la corriente suponiendo la conjetura de aditividad, hemos comprobado la validez de la misma realizando sofisticadas simulaciones numéricas para un rango amplio de fluctuaciones de la corriente. También hemos medido el perfil de densidad (independiente del tiempo) asociado a una fluctuación de la corriente dada, y hemos comprobado que se corresponde con el perfil teórico que minimiza el funcional para dicha fluctuación. Esto es indicativo de que el sistema adopta precisamente ese perfil para producir tal fluctuación.

En el capítulo 4 se muestra el papel que juegan los principios de simetría en las fluctuaciones lejos del equilibrio. Para producir una fluctuación, un sistema con muchos grados de libertad transita por un camino óptimo en el espacio de las fases mesoscópico. Tal y como ha quedado demostrado en los tests de la conjetura de aditividad realizados en el capítulo 3, este camino óptimo es un observable físico bien definido. En el capítulo 4 se ha demostrado, usando las herramientas de la MFT, que bajo condiciones muy generales y en dimensión arbitraria, este camino óptimo permanece in-

variante bajo ciertas transformaciones de simetría sobre el vector corriente. Usando esta invarianza se ha derivado una nueva relación de fluctuación isómetrica (IFR, por sus siglas en inglés) [10] para fluctuaciones de la corriente en sistemas d-dimensionales reversibles temporalmente y descritos por un único campo localmente conservado. Cabe destacar, que la IFR se ha demostrado en el marco de la MFT suplementado con el conjetura de aditividad. A su vez, se demuestra que la IFR no es más que una consecuencia de la reversibilidad temporal de la dinámica. También se comprueba que la IFR tiene implicaciones profundas en las propiedades de no-equilibrio de un sistema. En particular, la IFR implica una familia sorprendente de jerarquías en los cumulantes de la distribución de corriente y los coeficientes de respuesta no-lineal del sistema, válidas arbitrariamente lejos del equilibrio, y que van mucho más allá que las relaciones de reciprocidad de Onsager y las fórmulas de Green-Kubo.

Como hemos visto en el capítulo 3, de acuerdo con el conjetura de aditividad, el camino óptimo resulta ser independiente del tiempo para un rango amplio de fluctuaciones. Sin embargo, este camino óptimo, según la MFT, es en general un objeto dinámico que puede depender del tiempo. En el capítulo 5 hemos demostrado que en sistemas periódicos los caminos óptimos pasa a ser dependientes del tiempo para valores de las fluctuaciones muy desviados del valor estacionario. Esto se interpreta como una transición de fase dinámica. Además hemos observado dicha transición de fase en otro modelo difusivo paradigmático: el proceso de exclusión simple débilmente asimétrico (WASEP). En particular hemos corroborado que los perfiles adoptan una estructura de tipo onda viajera que se mueve a velocidad constante. También se ha demostrado que en el régimen dependiente del tiempo, la IFR se sigue cumpliendo, haciendo así extensiva su validez para perfiles dependientes del tiempo con estructura tipo onda viajera.

Por último, en el capítulo 6, nos hemos salido del marco de la MFT y hemos explotado la relación de Hatano-Sasa [27]. Dicha relación supone el conocimiento *a priori* de la distribución estacionaria de probabilidad. En lugar de esto, hemos propuesto usar distribuciones de probabilidad arbitrarias "de referencia" que sean suaves. De esta forma podemos tratar sistemas cuya distribución estacionaria es demasiado difícil de calcular, como generalmente ocurre en los sistemas fuera del equilibrio con muchos grados de libertad. Haciendo esto, hemos demostrado [29] que cada conjunto de distribuciones de referencia da lugar a una desigualdad que juega el papel de una generalización de la segunda ley. Cuanto mejor es la aproximación de la distribución de referncia a la estacionaria, más restringida es la desigualdad. Esto da lugar a un procedimiento de optimización de la distribución de referencia que puede ser implementado numérica o experimentalmente. Como ejemplo, hemos aproximado numéricamente la distribución de probabilidad estacionaria en otro modelo prototípico de no-equilibro: el proceso de exclusión simétrico simple (SSEP).

Futuras líneas de investigación

Los resultados obtenidos hasta la fecha nos hacen ser optimistas sobre el futuro de la teoría macroscópica fluctuante (MFT) como marco teórico general para entender la física de los fenómenos de no-equilibrio. De manera parecida a la teoría de colectividades en equilibrio, donde dado el hamiltoniano microscópico del sistema podemos definir una función de partición con conexión directa con la termodinámica, el programa teórico propuesto en esta tesis consiste en derivar, a partir de la dinámica microscópica y con métodos de coarse-graining, las ecuaciones de evolución mesoscpicas del sistema y unos pocos coeficientes de transporte. Partiendo de esta información, la MFT nos ofrece predicciones explícitas para las funciones de grandes desviaciones que caracterizan al sistema en cuestión. Estas LDFs juegan fuera del equilibrio un papel equivalente al de la energía libre (o la entropía) en equilibrio, y contienen información esencial para entender la física del sistema de interés.

A continuación se exponen algunas de las muchas líneas de invesigación que aún quedan por explorar.

- Los resultados de los capítulos 3, 4 y 5 han demostrado el potencial de la MFT para describir la física de diferentes sistemas fuera del equilibrio. Sin embargo, tal y como está formulada a día de hoy, la MFT aplica a sistemas caracterizados por un único campo conservado localmente. Una de las prioridades actuales consiste por tanto en generalizar la HFT a casos más realistas, de tipo hidrodinámico, donde la presencia de varios campos localmente conservados y acoplados entre sí determina la física del sistema

- La generalización anterior nos permitirá a su vez escribir una relación de fluctuación isométrica en el caso hidrodinámico. Esta extensión de la IFR resulta muy interesante ya que esta simetría constriñe fuertemente la forma de las distribuciones de corriente, ligando de manera jerárquica los coeficientes de respuesta no-lineales asociados a los diferentes observables que caracterizan el sistema. Esperamos por tanto que la generalización del IFR al caso hidrodinámico arroje relaciones cruzadas, inesperadas y sorprendentes, entre diferentes coeficientes de respuesta.

- La idea de aplicar principios de simetría para los perfiles óptimos en el estudio del comportamiento fluctuante macroscpico de diferentes sistemas fuera del equilibrio es muy general. Queremos usar esta idea en sistema biofísicos mesoscpicos, donde las fluctuaciones juegan un papel esencial. Un ejemplo prototípico es el plegado de proteínas y otras macromoléculas, donde las fluctuaciones intrínsecas del sistema provocan el plegado o lo inhiben. Aplicando principios de invariancia a los caminos óptimos responsables de las fluctuaciones raras en este caso, esperamos diseñar protocolos eficientes para medir diferencias de energía libre entre los diferentes estados de la macromolécula usando una generalización apropiada de la IFR en este contexto. Los métodos actuales, que se basan en observar sucesos conjugados por reversibilidad temporal, sufren graves problemas de muestreo ya que unos de los

dos sucesos es siempre altamente improbable. Sin embargo, la IFR y sus generalizaciones son simetrías diferenciables, lo que garantiza un muestreo experimental adecuado [10].

- La relación de fluctuación isométrica ha sido demostrada en el marco de la teoría macroscópica fluctuante. Su validez ha quedado claramente demostrada en diferentes tests numéricos, que sugieren además que esta relación sigue siendo válido incluso en regímenes para los cuales la MFT no rige en principio. Una pregunta fundamental es por tanto la demostración de esta relación desde un punto de vista puramente microscópico, partiendo de la dinámica microscpica del sistema. Técnicas similares a las usadas en las Refs. [12, 13], en las que se deriva el teorema de fluctuación de Gallavotti y Cohen a partir de las propiedades espectrales del operador de evolución estocástico, pueden resultar de utilidad en esta tarea.

Appendix A

Additivity Principle of current fluctuations in one-dimensional diffusive system

In this appendix, we present the original formulation of the *additivity principle* conjectured by Bodineau and Derrida [34] and we show its equivalence to the assumption of assuming time-independent optimal profiles within the context of the MFT. We consider a system of size L in contact with boundary reservoirs at densities ρ_L and ρ_R. Let $Q_\tau = \int_0^\tau dt \int_0^1 dx j(x,t)$ be the integrated current up to a time τ, i.e., the number of particles or the energy that went through the system during a time τ. Hence, the time-averaged current in which we are interested is $J = Q_\tau/\tau$. The whole current distribution, $P(J)$, depends only on two microscopic parameters $D[\rho]$ and $\sigma[\rho]$ defined as follows: Assuming that for $\rho_L = \rho + \Delta\rho$ and $\rho_R = \rho$ with $\Delta\rho$ small, we know that the Fick's (or Fourier's) law holds in the steady state,

$$\frac{\langle Q_\tau \rangle}{\tau} = \langle J \rangle = \frac{1}{L} D[\rho] \Delta\rho. \tag{A.1}$$

For $\rho_L = \rho_R = \rho$ (in which case $\langle Q_\tau \rangle = 0$) and large t the variance is

$$\frac{\langle Q_\tau^2 \rangle}{\tau} = \langle J^2 \rangle \tau = \frac{1}{L} \sigma[\rho]. \tag{A.2}$$

We are interested in $\mathrm{P}_L(J, \rho_L, \rho_R, \tau)$, which is the probability of observing a time-averaged current J during a long time τ. We have done explicit the dependence on ρ_L and ρ_R for convenience. This probability obeys a *large deviation principle* for large τ,

$$\mathrm{P}_L(J, \rho_L, \rho_R) \sim \exp[\tau F_L(J, \rho_L, \rho_R)], \tag{A.3}$$

where $F_L(J, \rho_L, \rho_R)$ is the current LDF. Bodineau and Derrida assumed that, for large L and J of order $1/L$, the large deviation function $F_L(J, \rho_L, \rho_R)$

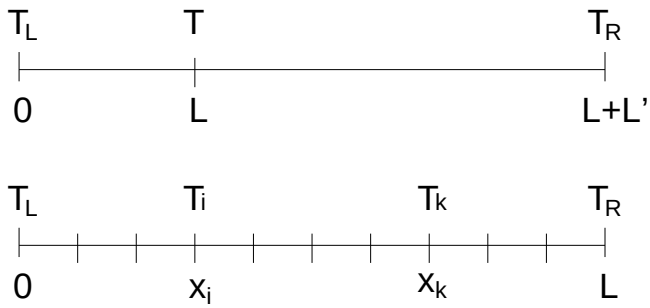

Figure A.1: ($T \equiv \rho$) Iterative slicing procedure used in the Additivity Principle

satisfies the following *additivity principle*

$$F_L(J, \rho_L, \rho_R, \tau) \simeq \max_{\rho} \{F_{L-\ell}(J, \rho_L, \rho, \tau) + F_\ell(J, \rho, \rho_R, \tau)\}. \tag{A.4}$$

This property simply means that the two subsystems are independent, except that they try to adjust the density ρ at their contact to maximize the following product

$$P_L(J, \rho_L, \rho_R, \tau) \sim \max_{\rho} [P_{L-\ell}(J, \rho_L, \rho, \tau) \times P_\ell(J, \rho, \rho_R, \tau)]. \tag{A.5}$$

Notice that we are assuming that the time-averaged integrated current J is the same for the two subsystems, i.e, J is constant across the space. That is why in Eqs. (A.4,A.5) one only maximizes over the density at their contact. As this is a 1D system, the constancy of the current implies for the density to be time independent because of the continuity equation. The additivity principle is then equivalent for 1D diffusive systems to assume the above hypothesis (1), i.e., $\rho(x,t) = \rho(x)$ and $j(x,t) = J$.

It is also necessary to make the following *scaling hypothesis*:

$$F_L(J, \rho_L, \rho_R) \simeq L^{-1} G(LJ, \rho_L, \rho_R), \tag{A.6}$$

which has been shown to be valid,in particular, for the symmetric simple exclusion process [82]. If we split the system of macroscopic unit length into two parts of lengths x and $1-x$, i.e., if we write $\ell = L(1-x)$, then (A.4) and (A.6), lead to

$$G(\tilde{J}, \rho_L, \rho_R) \simeq \max_{\rho} \left\{ \frac{G(\tilde{J}x, \rho_L, \rho)}{x} + \frac{G(\tilde{J}(1-x), \rho, \rho_R)}{1-x} \right\}, \tag{A.7}$$

where $\tilde{J} = LJ$ is the time-averaged current independent of the size. If we keep dividing the system into N smaller (macroscopic) subsystems of size Δx with $L = N\Delta x$ (see figure A.1), the LDF is given by

$$F_{N\Delta x}(J, \rho_L, \rho_R) \simeq \max_{\tilde{\rho}_i : i=1,\ldots,N-1} \left\{ \sum_{i=1}^{N} F_{\Delta x}(J, \tilde{\rho}_{i-1}, \tilde{\rho}_i) \right\}, \tag{A.8}$$

which is equivalent to

$$\frac{1}{N\Delta x}G(N\Delta x J,\rho_L,\rho_R)\simeq \max_{\tilde{\rho}_i:i=1,\dots,N-1}\left\{\sum_{i=1}^{N}\frac{1}{\Delta x}G(\Delta x J,\tilde{\rho}_{i-1},\tilde{\rho}_i)\right\}, \quad \text{(A.9)}$$

being $\tilde{\rho}_0=\rho_L$, $\tilde{\rho}_N=\rho_R$ and $\tilde{\rho}_i-\tilde{\rho}_{i-1}=\Delta\rho$. Assuming locally-Gaussian current fluctuations in each subsystem, i.e.,

$$\frac{1}{\Delta x}G(\Delta x J,\tilde{\rho}_i,\tilde{\rho}_i+\Delta\tilde{\rho})\simeq -\frac{(J\Delta x+D[\tilde{\rho}_i]\Delta\tilde{\rho}_i)^2}{2\sigma[\tilde{\rho}_i]\Delta x}, \quad \text{(A.10)}$$

we get in the continuum limit the following variational form for G,

$$G(J,\rho_L,\rho_R)=-\min_{\rho(x)}\left\{\int_0^1\frac{[J+D[\rho]\rho'(x)]^2}{2\sigma[\rho]}dx\right\}, \quad \text{(A.11)}$$

which is just the 1D counterpart of Eq. (3.1) for $Q[\rho]=-D[\rho]\rho'(x)$ without external field. We emphasize that, equivalently to the MFT, we can get the whole distribution of the current fluctuations kowing only the two macroscopic parameters $D[\rho]$ and $\sigma[\rho]$.

Appendix B

AppendixB

B.1 Evaluation of Large-Deviation Functions: Cloning Algorithm

Large deviation functions are very hard to measure in experiments or simulations because they involve by definition exponentially-unlikely events. Recently, Giardinà, Kurchan and Peliti [41] have introduced an efficient algorithm to measure the probability of a large deviation for observables such as the current or density in stochastic many-particle systems. The algorithm is based on a modification of the underlying stochastic dynamics so that the rare events responsible of the large deviation are no longer rare, and it has been extended for systems with continuous-time stochastic dynamics [42]. Let $U_{C'C}$ be the transition rate from configuration C to C'. The probability of measuring a time-integrated current $\mathbf{Q}_t$ after a time t starting from a configuration C_0 can be written as

$$P(\mathbf{Q}_t, t; C_0) = \sum_{C_t..C_1} U_{C_t C_{t-1}}..U_{C_1 C_0}\, \delta(\mathbf{Q}_t - \sum_{k=0}^{t-1} \mathbf{J}_{C_{k+1}C_k})\,, \tag{B.1}$$

where $\mathbf{J}_{C'C}$ is the elementary current involved in the transition $C \to C'$. For long times we expect the information on the initial state C_0 to be lost, $P(\mathbf{Q}_t, t; C_0) \to P(\mathbf{Q}_t, t)$. In this limit $P(\mathbf{Q}_t, t)$ obeys the usual large deviation principle $P(\mathbf{Q}_t, t) \sim \exp[+t\mathcal{G}(\mathbf{J} = \mathbf{Q}_t/t)]$. In most cases it is convenient to work with the moment-generating function of the above distribution

$$\begin{aligned} \Pi(\boldsymbol{\lambda}, t) &= \sum_{\mathbf{Q}_t} \mathrm{e}^{\boldsymbol{\lambda}\cdot\mathbf{Q}_t} P(\mathbf{Q}_t, t) \\ &= \sum_{C_t..C_1} U_{C_t C_{t-1}}..U_{C_1 C_0}\, \mathrm{e}^{\boldsymbol{\lambda}\cdot\sum_{k=0}^{t-1}\mathbf{J}_{C_{k+1}C_k}}\,. \end{aligned} \tag{B.2}$$

For long t, we have $\Pi(\boldsymbol{\lambda}, t) \to \exp[+t\mu(\boldsymbol{\lambda})]$, with $\mu(\boldsymbol{\lambda}) = \max_{\mathbf{J}}[\mathcal{G}(\mathbf{J}) + \boldsymbol{\lambda}\cdot\mathbf{J}]$. We can now define a modified dynamics, $\tilde{U}_{C'C} \equiv \mathrm{e}^{\boldsymbol{\lambda}\cdot\mathbf{J}_{C'C}}\, U_{C'C}$, so

$$\Pi(\boldsymbol{\lambda}, t) = \sum_{C_t...C_1} \tilde{U}_{C_t C_{t-1}} \ldots \tilde{U}_{C_1 C_0}\,. \tag{B.3}$$

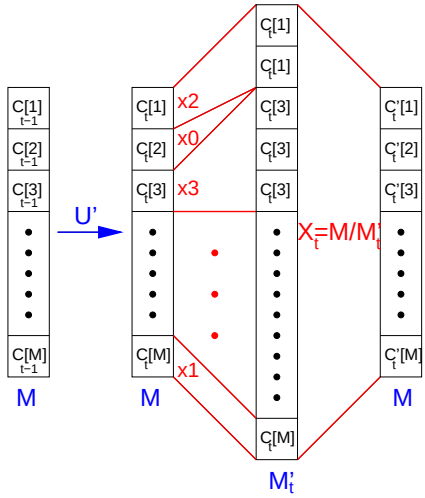

Figure B.1: Sketch of the evolution and cloning of the copies during the evaluation of the large deviation function.

This dynamics is however not normalized, $\sum_{C'} \tilde{U}_{C'C} \neq 1$.

We now introduce Dirac's bra and ket notation, useful in the context of the quantum Hamiltonian formalism for the master equation [84, 85], see also [41, 86]. The idea is to assign to each system configuration C a vector $|C\rangle$ in phase space, which together with its transposed vector $\langle C|$, form an orthogonal basis of a complex space and its dual [84, 85]. For instance, in the simpler case of systems with a finite number of available configurations (which is not the case for the KMP model), one could write $|C\rangle^T = \langle C| = (\ldots 0 \ldots 0, 1, 0 \ldots 0 \ldots)$, i.e. all components equal to zero except for the component corresponding to configuration C, which is 1. In this notation, $\tilde{U}_{C'C} = \langle C'|\tilde{U}|C\rangle$, and a probability distribution can be written as a probability vector

$$|P(t)\rangle = \sum_C P(C,t)|C\rangle\,,$$

where $P(C,t) = \langle C|P(t)\rangle$ with the scalar product $\langle C'|C\rangle = \delta_{C'C}$. If $\langle s| = (1 \ldots 1)$, normalization then implies $\langle s|P(t)\rangle = 1$.

With the above notation, we can write the spectral decomposition $\tilde{U}(\boldsymbol{\lambda}) = \sum_j \mathrm{e}^{\Lambda_j(\boldsymbol{\lambda})}|\Lambda_j^R(\boldsymbol{\lambda})\rangle\langle\Lambda_j^L(\boldsymbol{\lambda})|$, where we assume that a complete biorthogonal basis of right and left eigenvectors for matrix $\tilde{U}$ exists, $\tilde{U}|\Lambda_j^R(\boldsymbol{\lambda})\rangle = \mathrm{e}^{\Lambda_j(\boldsymbol{\lambda})}|\Lambda_j^R(\boldsymbol{\lambda})\rangle$ and $\langle\Lambda_j^L(\boldsymbol{\lambda})|\tilde{U} = \mathrm{e}^{\Lambda_j(\boldsymbol{\lambda})}\langle\Lambda_j^L(\boldsymbol{\lambda})|$. Denoting as $\mathrm{e}^{\Lambda(\boldsymbol{\lambda})}$ the largest eigenvalue of $\tilde{U}(\boldsymbol{\lambda})$, with associated right and left eigenvectors $|\Lambda^R(\boldsymbol{\lambda})\rangle$ and $\langle\Lambda^L(\boldsymbol{\lambda})|$, respectively, and writing $\Pi(\boldsymbol{\lambda},t) = \sum_{C_t}\langle C_t|\tilde{U}^t|C_0\rangle$, we find for long times

$$\Pi(\boldsymbol{\lambda},t) \xrightarrow{t\gg 1} \mathrm{e}^{+t\Lambda(\boldsymbol{\lambda})}\langle\Lambda^L(\boldsymbol{\lambda})|C_0\rangle\left(\sum_{C_t}\langle C_t|\Lambda^R(\boldsymbol{\lambda})\rangle\right). \tag{B.4}$$

In this way we have $\mu(\boldsymbol{\lambda}) = \Lambda(\boldsymbol{\lambda})$, so the Legendre transform of the current LDF is given by the natural logarithm of the largest eigenvalue of $\tilde{U}(\boldsymbol{\lambda})$. In

order to evaluate this eigenvalue, and given that dynamics $\tilde{U}$ is not normalized, we introduce the exit rates $Y_C = \sum_{C'} \tilde{U}_{C'C}$, and define the normalized dynamics $U'_{C'C} \equiv Y_C^{-1} \tilde{U}_{C'C}$. Now

$$\Pi(\boldsymbol{\lambda}, t) = \sum_{C_t \dots C_1} Y_{C_{t-1}} U'_{C_t C_{t-1}} \dots Y_{C_0} U'_{C_1 C_0} \tag{B.5}$$

This sum over paths can be realized by considering an ensemble of $M \gg 1$ copies (or clones) of the system, evolving sequentially according to the following Monte Carlo scheme [41]:

I Each copy evolves independently according to modified normalized dynamics $U'_{C'C}$.

II Each copy $m \in [1, M]$ (in configuration $C_t[m]$ at time t) is cloned with rate $Y_{C_t[m]}$. This means that, for each copy $m \in [1, M]$, we generate a number $K_{C_t[m]} = \lfloor Y_{C_t[m]} \rfloor + 1$ of identical clones with probability $Y_{C_t[m]} - \lfloor Y_{C_t[m]} \rfloor$, or $K_{C_t[m]} = \lfloor Y_{C_t[m]} \rfloor$ otherwise (here $\lfloor x \rfloor$ represents the integer part of x). Note that if $K_{C_t[m]} = 0$ the copy may be killed and leave no offspring. This procedure gives rise to a total of $M'_t = \sum_{m=1}^{M} K_{C_t[m]}$ copies after cloning all of the original M copies.

III Once all copies evolve and clone, the total number of copies M'_t is sent back to M by an uniform cloning probability $X_t = M/M'_t$.

Fig. B.1 sketches this procedure. It then can be shown that, for long times, we recover $\mu(\boldsymbol{\lambda})$ via

$$\mu(\boldsymbol{\lambda}) = -\frac{1}{t} \ln (X_t \cdots X_0) \qquad \text{for } t \gg 1 \tag{B.6}$$

To derive this expression, first consider the cloning dynamics above, but without keeping the total number of clones constant, i.e. forgetting about step III. In this case, for a given history $\{C_t, C_{t-1} \dots C_1, C_0\}$, the number $\mathcal{N}(C_t \dots C_0, t)$ of copies in configuration C_t at time t obeys $\mathcal{N}(C_t \dots C_0, t) = Y_{C_{t-1}} U'_{C_t C_{t-1}} \mathcal{N}(C_{t-1} \dots C_0, t-1)$, so that

$$\mathcal{N}(C_t \dots C_0, t) = Y_{C_{t-1}} U'_{C_t C_{t-1}} \dots Y_{C_0} U'_{C_1 C_0} \mathcal{N}(C_0, 0)\,. \tag{B.7}$$

Summing over all histories of duration t, see eq. (B.5), we find that the average of the total number of clones at long times shows exponential behavior, $\langle \mathcal{N}(t) \rangle = \sum_{C_t \dots C_1} \mathcal{N}(C_t \dots C_0, t) \sim \mathcal{N}(C_0, 0) \exp[+t\mu(\boldsymbol{\lambda})]$. Now, going back to step III above, when the fixed number of copies M is large enough, we have $X_t = \langle \mathcal{N}(t-1) \rangle / \langle \mathcal{N}(t) \rangle$ for the global cloning factors, so $X_t \cdots X_1 = \mathcal{N}(C_0, 0) / \langle \mathcal{N}(t) \rangle$ and we recover expression (B.6) for $\mu(\boldsymbol{\lambda})$.

In this thesis we used the above method to measure the current LDF for the Kipnis-Marchioro-Presutti model in two dimensions, described in chapters 2 and 3. For this model the transition rate from a configuration $C = \{e_1 \dots e_N\}$ to another configuration $C'_k = \{e_1 \dots e'_k, e'_{k+1} \dots e_N\}$, with $k \in [0, N]$ and the pair (e'_k, e'_{k+1}), being $N = L \times L$ the number of sites and

k the kind of par selected ($k \in$ bulk or $k \in$ boundaries) , can be written as

$$U_{C'_k C} = \begin{cases} (2N+L)^{-1}\,, & k \in \text{ bulk} \\ \dfrac{\beta_L \mathrm{e}^{\beta_L e_k}}{2N+L} \mathrm{E}_1\left[\beta_L \max(e_k, e'_k)\right], & k \in \text{ left bath} \\ \dfrac{\beta_R \mathrm{e}^{\beta_R e_k}}{2N+L} \mathrm{E}_1\left[\beta_R \max(e_k, e'_k)\right], & k \in \text{ right bath}\,. \end{cases}$$

where $\beta_L = \rho_L^{-1}$ and $\beta_R = \rho_R^{-1}$. Here $\mathrm{E}_1(x) = -\mathrm{Ei}(-x)$, where $\mathrm{Ei}(x)$ is the exponential integral function, or

$$\mathrm{E}_1(x) = \int_x^\infty \mathrm{d}u \frac{\mathrm{e}^{-u}}{u}\,. \tag{B.8}$$

It appears when integrating over all possible pairs $(p, \tilde{e}_{L,R})$ that can result on a given $e'_{1,N}$, respectively . It is easy to show that $U_{C'_k C}$ is normalized as it should, so $\sum_{C'_k} U_{C'_k C} = 1$.

In order to measure current fluctuations we need to provide a microscopic definition of the energy current involved in an elementary move. There are many different ways to define this current: the energy exchanged per unit time with one of the boundary heat baths, the current flowing between two given nearest neighbors, or its spatial average, etc. Assuming that energy cannot accumulate in the system *ad infinitum*[14, 83, 86], all these definitions give equivalent results for the current large deviation function in the long time limit. However, this is not so for some observables different from the large deviation function (e.g. for average profiles measured *at the end* of the large deviation event; see Ref. [38]). In our case, the following choice turns out to be convenient

$$\mathbf{J}_{C'_k C} = (J^x_{C'_k C}, J^y_{C'_k C}) = \begin{cases} \left(\dfrac{e_k - e'_k}{N-L}, 0\right), & k \in \text{ bulk (horizontal exchange)} \\ \left(0, \dfrac{e_k - e'_k}{N}\right), & k \in \text{ bulk (vertical exchange)} \\ 0\,, & k \in \text{ boundary baths} \end{cases}$$

That is, we measure the energy current flowing through the bulk of the system. Using this current definition and eq. (B.9), we may write the

modified normalized dynamics $U'_{C'_kC} \equiv Y_C^{-1} U_{C'_kC} \exp[\boldsymbol{\lambda}\cdot\mathbf{J}_{C'_kC}]$, which reads

$$U'_{C'_kC} = \begin{cases} \dfrac{e^{\bar{\lambda}_x(e_k - e'_k)}}{Y_C(2N+L)}\,, & k \in \text{ bulk (horizontal exchange)} \\ \dfrac{e^{\bar{\lambda}_y(e_k - e'_k)}}{Y_C(2N+L)}\,, & k \in \text{ bulk (vertical exchange)} \\ \dfrac{\beta_L e^{\beta_L e_1}}{Y_C(2N+L)} \mathrm{E}_1\left[\beta_L \max(e_k, e'_k)\right], & k \in \text{ left bath} \\ \dfrac{\beta_R e^{\beta_L e_N}}{Y_C(2N+L)} \mathrm{E}_1\left[\beta_R \max(e_k, e'_k)\right], & k \in \text{ right bath} \end{cases}$$

with $\bar{\boldsymbol{\lambda}} = (\bar{\lambda}_x, \bar{\lambda}_y) = (\lambda_x/(N-L), \lambda_y/N)$. The exit rate is given by

$$Y_C = \frac{2L}{2N+L} + \sum_{k=1}^{2N-L} \frac{\mathrm{e}^{\bar{\lambda}e_k} - \mathrm{e}^{-\bar{\lambda}e_{k+1}}}{\bar{\lambda}(2N+L)(e_k + e_{k+1})}\,, \tag{B.9}$$

where $2N-L$ are the total number of pairs in the bulk, $\bar{\lambda} = \bar{\lambda}_x$ if the chosen k-pair corresponds to a horizontal bulk pair and $\bar{\lambda} = \bar{\lambda}_y$ if the chosen k-pair corresponds to a vertical bulk pair. In chapter 3 we simulated a system of size $N = 20$, with $\rho_L = 2$ and $\rho_R = 1$, using $M = 10^3$ copies of the system and a maximum time of $t = 10^4$ Monte Carlo steps. For a given initial condition, we averaged the measured $\mu(\boldsymbol{\lambda})$ for different times once in the steady state, after a relaxation time of 2×10^3 Monte Carlo steps. In addition, we averaged results over many independent initial conditions, in which local initial energies e_i are randomly drawn according to the Gibbs distribution with temperature parameter $\rho_{\mathrm{st}}[x = i/(L+1)]$ corresponding to the linear, steady energy density profile.

B.2 Time Reversibility and Statistics during a Large Fluctuation

In this section we use the time reversibility of the underlying stochastic dynamics to study the system statistics during a large deviation event and the symmetries of the large deviation function and the associated optimal profiles, using the previously described formalism. In particular, we describe a relation between system statistics at the end of the large deviation event and for intermediate times. First, consider the probability $P(C_t, \mathbf{Q}_t, t)$ that the system is in configuration C_t at time t with a total time-integrated current $\mathbf{Q}_t$. As previously, we drop the dependence of this probability on the initial state C_0, which we assume lost for long enough times. This probability obeys the following master equation

$$P(C_t, \mathbf{Q}_t, t) = \sum_{C'} U_{C_tC'} P(C', \mathbf{Q}_t - \mathbf{J}_{C_tC'}, t-1)\,. \tag{B.10}$$

which by iterating in time leads to

$$P(C_t, \mathbf{Q}_t, t) = \sum_{C_{t-1}..C_1} U_{C_t C_{t-1}}..U_{C_1 C_0}\, \delta(\mathbf{Q}_t - \sum_{k=0}^{t-1} \mathbf{J}_{C_{k+1}C_k})\,, \qquad \text{(B.11)}$$

and it is clear that $P(\mathbf{Q}_t, t) = \sum_{C_t} P(C_t, \mathbf{Q}_t, t)$, see eq. (B.1) in the previous section. Now, $P_q^{\rm end}(C_t) \equiv P(C_t, \mathbf{Q}_t, t)/P(\mathbf{Q}_t, t; C_0)$ is the probability of having a configuration C_t *at the end* of a large deviation event associated to a current $q = \mathbf{Q}_t/t$. Defining $\Pi(C_t, \boldsymbol{\lambda}, t) = \sum_{\mathbf{Q}_t} \exp(\boldsymbol{\lambda}\mathbf{Q}_t) P(C_t, \mathbf{Q}_t, t)$ so that

$$\Pi(C_t, \boldsymbol{\lambda}, t) = \sum_{C_{t-1}...C_1} \tilde{U}_{C_t C_{t-1}} \dots \tilde{U}_{C_1 C_0}\,, \qquad \text{(B.12)}$$

with $\tilde{U}_{C'C}(\boldsymbol{\lambda}) = U_{C'C} \exp(\boldsymbol{\lambda}\mathbf{J}_{C'C})$, one can easily show that, for long times t, $P_{\boldsymbol{\lambda}}^{\rm end}(C_t) \equiv \Pi(C_t, \boldsymbol{\lambda}, t)/\Pi(\boldsymbol{\lambda}, t) = P_{q_o(\boldsymbol{\lambda})}^{\rm end}(C_t)$, where $q_o(\boldsymbol{\lambda})$ is the current conjugated to parameter $\boldsymbol{\lambda}$, and $\Pi(\boldsymbol{\lambda}, t)$ is defined in eq. (B.3). Using the previous spectral decomposition, it is simple to show that $P_q^{\rm end}(C_t) \propto \langle C_t|\Lambda^R(\boldsymbol{\lambda})\rangle$, so the right eigenvector $|\Lambda^R(\boldsymbol{\lambda})\rangle$ associated to the largest eigenvalue of *matrix* $\tilde{U}(\boldsymbol{\lambda})$ gives the probability of having any configuration *at the end* of the large deviation event. Noticing that, for the Monte Carlo algorithm described in the previous section, the fraction of clones or copies in state C_t is proportional to $\langle C_t|\Lambda^R(\boldsymbol{\lambda})\rangle$ for long times, see eq. (B.7), we deduce that the the average profile among the set of clones yields the mean temperature profile *at the end* of the large deviation event, $\rho_{\boldsymbol{\lambda}}^{\rm end}(x)$.

The initial and final time regimes during a large deviation event show transient behavior which differs from the behavior in the *bulk* of the large deviation event, i.e. for intermediate times [14]. In particular, as we will show here, midtime and endtime statistics are different, though intimately related as a result of the time reversibility of the microscopic dynamics. Let $\bar{P}(C_\tau, \boldsymbol{\lambda}, \tau, t)$ be the probability that the system was in configuration C_τ at time τ when at time t the total integrated current is $\mathbf{Q}_t$. Timescales are such that $1 \ll \tau \ll t$, so all times involved are long enough for the memory of the initial state C_0 to be lost. We can write now

$$\bar{P}(C_\tau, \mathbf{Q}_t, \tau, t) = \sum_{C_t...C_{\tau+1}C_{\tau-1}...C_1} U_{C_t C_{t-1}} \cdots U_{C_{\tau+1}C_\tau} \qquad \text{(B.13)}$$
$$U_{C_\tau C_{\tau-1}} \cdots U_{C_1 C_0}\, \delta\Big(\mathbf{Q}_t - \sum_{k=0}^{t-1} \mathbf{J}_{C_{k+1}C_k}\Big)\,,$$

where we do not sum over C_τ. Defining the moment-generating function of the above distribution, $\bar{\Pi}(C_\tau, \boldsymbol{\lambda}, \tau, t) = \sum_{\mathbf{Q}_t} \exp(\boldsymbol{\lambda}\mathbf{Q}_t)\bar{P}(C_\tau, \mathbf{Q}_t, \tau, t)$, we can again check that the probability weight of configuration C_τ at intermediate time τ in a large deviation event of current $q = \mathbf{Q}_t/t$, $P_q^{\rm mid}(C_\tau) \equiv \bar{P}(C_\tau, \mathbf{Q}_t, \tau, t)/P(\mathbf{Q}_t, t)$, is also given by $P_{\boldsymbol{\lambda}}^{\rm mid}(C_\tau) \equiv \bar{\Pi}(C_\tau, \boldsymbol{\lambda}, \tau, t)/\Pi(\boldsymbol{\lambda}, t)$ for long times such that $1 \ll \tau \ll t$, with $q = q_o(\boldsymbol{\lambda})$. In this long-time limit one thus finds

$$P_{\boldsymbol{\lambda}}^{\rm mid}(C_\tau) \propto \langle \Lambda^L(\boldsymbol{\lambda})|C_\tau\rangle\langle C_\tau|\Lambda^R(\boldsymbol{\lambda})\rangle\,, \qquad \text{(B.14)}$$

in contrast to $P^{\rm end}_{\boldsymbol{\lambda}}(C)$, which is proportional to $\langle C|\Lambda^R(\boldsymbol{\lambda})\rangle$, see above. Here $|\Lambda^R(\boldsymbol{\lambda})\rangle$ and $\langle\Lambda^L(\boldsymbol{\lambda})|$ are the right and left eigenvectors associated to the largest eigenvalue $\mathrm{e}^{\Lambda(\boldsymbol{\lambda})}$ of modified transition rate $\tilde{U}(\boldsymbol{\lambda})$, respectively. They are different because $\tilde{U}$ is not symmetric. In order to compute the left eigenvector, notice that $|\Lambda^L(\boldsymbol{\lambda})\rangle$ is the *right* eigenvector of the transpose *matrix* $\tilde{U}^{\rm T}(\boldsymbol{\lambda})$ with eigenvalue $\mathrm{e}^{\Lambda(\boldsymbol{\lambda})}$. This right eigenvector of $\tilde{U}^{\rm T}(\boldsymbol{\lambda})$ can be in turn related to the corresponding right eigenvector of $\tilde{U}(-\boldsymbol{\lambda}-2\mathcal{E})$ by noticing that the local detailed balance condition holds for the KMP model, guaranteeing the time reversibility of microscopic dynamics. This condition states that $U_{C'C}p_{\rm eq}(C) = U_{CC'}p_{\rm eq}(C')\mathrm{e}^{2\mathcal{E}\mathbf{J}_{C'C}}$, where $p_{\rm eq}(C)$ is an effective equilibrium weight which for the KMP model takes the value $p_{\rm eq}(C) = \exp(-\sum_{y=1}^{N}\beta_y e_y)$ with $C=\{e_y, y=1\dots N\}$ and $\beta_y = \rho_L^{-1}+2\mathcal{E}\frac{y-1}{N-1}$. Local detailed balance then implies a symmetry between the forward modified dynamics for a current fluctuation and the time-reversed modified dynamics for the negative current fluctuation, i.e. $\tilde{U}_{CC'} = p_{\rm eq}^{-1}(C')\tilde{U}(-\boldsymbol{\lambda}-2\mathcal{E})p_{\rm eq}(C)$, or in matrix form

$$\tilde{U}^{\rm T}(\boldsymbol{\lambda}) = \mathbf{P}_{\rm eq}^{-1}\tilde{U}(-\boldsymbol{\lambda}-2\mathcal{E})\mathbf{P}_{\rm eq}\,, \tag{B.15}$$

where $\mathbf{P}_{\rm eq}$ is a diagonal *matrix* with entries $p_{\rm eq}(C)$. Eq. (B.15) implies that all eigenvalues of $\tilde{U}(\boldsymbol{\lambda})$ and $\tilde{U}(-\boldsymbol{\lambda}-2\mathcal{E})$ are equal, and in particular the largest, so $\mu(\boldsymbol{\lambda}) = \mu(-\boldsymbol{\lambda}-2\mathcal{E})$ and this proves the Gallavotti-Cohen fluctuation relation. Moreover, if $|\Lambda_j^R(-\boldsymbol{\lambda}-2\mathcal{E})\rangle$ is a right eigenvector of $\tilde{U}(-\boldsymbol{\lambda}-2\mathcal{E})$, which can be expanded as $|\Lambda_j^R(-\boldsymbol{\lambda}-2\mathcal{E})\rangle = \sum_C\langle C|\Lambda_j^R(-\boldsymbol{\lambda}-2\mathcal{E})\rangle|C\rangle$, then

$$|\Lambda_j^L(\boldsymbol{\lambda})\rangle = \sum_C (p_C^{\rm eq})^{-1}\langle C|\Lambda_j^R(-\boldsymbol{\lambda}-2\mathcal{E})\rangle|C\rangle \tag{B.16}$$

is the right eigenvector of $\tilde{U}^{\rm T}(\boldsymbol{\lambda})$ associated to the same eigenvalue. In this way, by plugging this into eq. (B.17) we find

$$P^{\rm mid}_{\boldsymbol{\lambda}}(C) \propto (p_C^{\rm eq})^{-1}\langle C|\Lambda^R(-\boldsymbol{\lambda}-2\mathcal{E})\rangle\langle C|\Lambda^R(\boldsymbol{\lambda})\rangle\,,$$

where we assumed real components for the eigenvectors associated to the largest eigenvalue. Equivalently

$$P^{\rm mid}_{\boldsymbol{\lambda}}(C) = A\,\frac{P^{\rm end}_{\boldsymbol{\lambda}}(C)P^{\rm end}_{-\boldsymbol{\lambda}-2\mathcal{E}}(C)}{p_C^{\rm eq}}\,, \tag{B.17}$$

with A a normalization constant. This relation implies that configurations with a significant contribution to the average profile at intermediate times are those with an important probabilistic weight at the end of both the large deviation event and its time-reversed process. Supplementing the above relation with a local equilibrium hypothesis, one can obtain average temperature profiles at intermediate times in terms of profile statistics at the end of the large deviation event.

List of figures

Bibliography

[1] A. Einstein, *Annalen der Physik* **324**, 289 (1906)

[2] J.J. Binney, N.J. Dowrick, A.J. Fisher and M.E.J. Newman, *The Theory of Critical Phenomena: An Introduction to the Renormalization Group* (Oxford University Press, Oxford) (1998)

[3] *Dynamical Heterogeneities in Glasses, Colloids and Granular Materials*, L. Berthier et al (Editors), Oxford University Press, Oxford (2011)

[4] S. Weinberg, *Cosmology*, Oxford University Press, Oxford (2008)

[5] B. Derrida, E. Domany and D. Mukamel, *J. Stat. Phys.* **69**, 667 (1992)

[6] B. Derrida, M. R. Evans, V. Hakim and V. Pasquier, J. Phys. A **26** 1493 (1993)

[7] G. Schtz and E. Domany, *J. Stat. Phys.* **72**, 277 (1993)

[8] Gallavotti G, Cohen EGD *Phys. Rev. Lett.* **74**, 2694 (1995)

[9] D.J. Evans, E.G.D. Cohen and G.P. Morriss, *Phys. Rev. Lett.* **71**, 2401 (1993)

[10] P.I. Hurtado, C. Pérez-Espigares, J.J. del Pozo and P.L. Garrido, *Proc. Natl. Acad. Sci* USA **108**, 7704 (2011)

[11] S. Lepri, R. Livi and A. Politi, *Phys. Rep.* **377**, 1-80 (2003)

[12] J. Kurchan, *J. Phys. A: Math. Gen.* **31**, 3719 (1998)

[13] J.L. Lebowitz and H. Spohn, *J. Stat. Phys.* **95**, 333 (1999)

[14] B. Derrida, *J. Stat. Mech.* P07023 (2007); T. Bodineau and B. Derrida, *C. R. Physique* **8**, 540 (2007).

[15] L. Bertini, A. De Sole, D. Gabrielli, G. Jona-Lasinio and C. Landim, *Phys. Rev. Lett.* **87**, 040601 (2001); *J. Stat. Phys.*, **107**, 635 (2002)

[16] L. Bertini, A. De Sole, D. Gabrielli, G. Jona-Lasinio and C. Landim, *Phys. Rev. Lett.* **94**, 030601 (2005); *J. Stat. Phys.*, 123, 237 (2006)

[17] L. Bertini, A. De Sole, D. Gabrielli, G. Jona-Lasinio and C. Landim, *J. Stat. Mech.* P07014 (2007)

[18] L. Bertini, A. De Sole, D. Gabrielli, G. Jona-Lasinio and C. Landim,*J. Stat. Phys.* **135**, 857 (2009)

[19] G. Jona-Lasinio, Prog.Theor.Phys.Supp. 184, 262 (2010)

[20] G. Jona-Lasinio, Prog. Theor. Phys. 124, 731 (2010)

[21] P.L. Garrido, J.L. Lebowitz, C. Maes, H. Spohn, *Phys. Rev. A* **42**, 1954 (1990)

[22] L. Bertini, A. De Sole, D. Gabrielli, G. Jona-Lasinio and C. Landim, *arXiv*:0705.2996. (2007)

[23] R.S. Ellis, *Entropy, Large Deviations and Statistical Mechanics* (Springer, New York, 1985).

[24] H. Touchette, *Phys. Rep.* **478**, 1 (2009).

[25] C. Jarzynski, *Phys. Rev. Lett.* **78**, 2690 (1997); *Phys. Rev. E* **56**, 5018 (1997).

[26] G. E. Crooks, *J. Stat. Phys.* **90**, 1481 (1998); G. E. Crooks, *Phys. Rev. E* **61**, 2361 (2000).

[27] T. Hatano, S. I. Sasa, *Phys. Rev. Lett.* **86**, 3463 (2001).

[28] L. Bertini, A. De Sole, D. Gabrielli, G. Jona-Lasinio y C. Landim, arXiv: 1206.2412 (2012); L. Bertini, A. De Sole, D. Gabrielli, G. Jona-Lasinio y C. Landim, arXiv: 1208.1872 (2012);

[29] C. Pérez-Espigares, A. B. Kolton and J. Kurchan, *Phys. Rev. E* **85** 031135 (2012)

[30] C. Kipnis, S. Olla and S. Varadhan, *Commun. Pure Appl. Math.* **42**,115 (1989)

[31] C. Kipnis and C. Landim, *Scaling Limits of Interacting Particle Systems* (Springer-Verlag, Berlin) (1991)

[32] B. Derrida, J.L. Lebowitz and E. R. Speer, *J. Stat. Phys.* **107** 599-634 (2002)

[33] H. Spohn, *Large Scale Dynamics of Interacting Particles* (Springer-Verlag, Berlin) (1991)

[34] T. Bodineau and B. Derrida, *Phys. Rev. Lett.* **92**, 180601 (2004).

[35] C. Kipnis, C. Marchioro and E. Presutti, *J. Stat. Phys.* **27**, 65 (1982).

[36] P.I. Hurtado and P.L. Garrido, *Phys. Rev. Lett.* **102**, 250601 (2009);

[37] P.I. Hurtado and P.L. Garrido, *Phys. Rev. E* **81**, 041102 (2010).

[38] P.I. Hurtado and P.L. Garrido, *J. Stat. Mech.* (2009) P02032.

[39] T. Bodineau and B. Derrida, *Phys. Rev. E* **72**, 066110 (2005).

[40] P.I. Hurtado and P.L. Garrido, *Phys. Rev. Lett.* **107**, 180601 (2011).

[41] Giardinà C, Kurchan J, Peliti L, *Phys. Rev. Lett.* **96**, 120603 (2006)

[42] V. Lecomte and J. Tailleur, *J. Stat. Mech.* P03004 (2007).

[43] C. Pérez-Espigares, P. L. Garrido, P. I. Hurtado, *AIP Conf. Proc* **1332**, 204 (2011)

[44] F. Ritort, *Advances in Chemical Physics* **137**, 31 (2008)

[45] A. Dhar, *Adv. Phys.* **57**, 457 (2008)

[46] P.L. Garrido, P.I. Hurtado and B. Nadrowski, *Phys. Rev. Lett.* **86**, 5486 (2001)

[47] P.I. Hurtado, *Phys. Rev. Lett.* **96**, 010601 (2006)

[48] D.J. Gross, *Proc. Natl. Acad. Sci.* **93**, 14256 (1996)

[49] D.G. Luchinsky and P.V.E. McClintock, *Nature*, **389** 463 (1997)

[50] P.L. Garrido and G. Gallavotti, *J. Stat. Phys.* **126**, 1201 (2007)

[51] D. Andrieux and P. Gaspard, *J. Stat. Mech.*, P02006 (2007)

[52] D. Collin, F. Ritort, C. Jarzynski, S. B. Smith, Jr.I. Tinoco and C. Bustamante, *Nature* **437**, 231 (2005)

[53] M. Gorissen and C. Vanderzande, *arXiv*:1201.6264 (2012)

[54] J. Liphardt, S. Dumont, S. B. Smith, I. Tinoco, and C. Bustamante, *Science* **296**, 1832 (2002)

[55] D. Collin, F. Ritort, C. Jarzynski, S. B. Smith, I. Tinoco and C. Bustamante, *Nature* **437**, 231 (2005)

[56] E. H. Trepagnier, C. Jarzynski, F. Ritort, G. E. Crooks, C. J. Bustamante and J. Liphardt, *Proc. Natl. Acad. Sci.* U.S.A. **101**, 15038 (2004)

[57] S. F. Edwards, in: *Granular Matter: An Interdisciplinary Approach*, A. Mehta, Ed. (Springer-Verlag, New York, 1994), and references therein.

[58] J. Kurchan, *J. Phys. A*, **12**, 6611 (2000).

[59] D. Loi, S. Mossa and LF Cugliandolo, *Soft Matter*, Advance Article (2011).

[60] S. Wang and P. G. Wolynes, *Proc. Natl. Acad. Sci.*, USA **108**, 15184 (2011).

[61] A broad review with an emphasis in experimental results and applications is: F. Ritort, Séminaire Poincare (6 Dec 2003), p.63; A more technical one specialized in the Fluctuation Relation is: D. Evans and D. Searles, *Adv. Phys.* **51**, 1529 (2002); See also G. Gallavotti, *Statistical Mechanics A Short Treatise* Series Texts and Monographs in Physics, Springer Verlag (1999).

[62] The Hatano-Sasa, together with Seifert [67] and Speck-Seifert relations [68] were very recenlty unified in three detailed fluctuation theorems through particular two-fold decompositions of the total entropy production, either using single [69, 70, 71] or joint [74] probability distributions for the entropy production contributions.

[63] Hoover W.G.,Molecular Dynamics, *Lecture Notes in Physics*, **258**, Springer.

[64] J. L. Lebowitz and P. G. Bergmann, *Annals of Physics*, **1**, 1 (1957).

[65] R. Kawai, J. M. R. Parrondo, and C. Van den Broeck, *Phys. Rev. Lett.*, **98**, 080602 (2007)

[66] J. M. R. Parrondo, C. Van den Broeck and R Kawai, *New J. Phys.*, **11**, 073008 (2009).

[67] U. Seifert, *Phys. Rev. Lett.*, **95**, 040602 (2005).

[68] T. Speck and U. Seifert, *J. Phys. A*, **38**, L581 (2005).

[69] M. Esposito and C. Van den Broeck, *Phys. Rev. E*, **82** 011143 (2010);

[70] C. Van den Broeck and M. Esposito, *Phys. Rev. E*, **82**, 011144 (2010);

[71] M. Esposito and C. Van den Broeck, *Phys. Rev. Lett.*, **104**, 090601 (2010).

[72] N. Merhav and Y. Kafri, *J. Stat. Mech.*, P12022 (2010).

[73] G. Verley, R. Chetrite and D. Lacoste, *J. Stat. Mech.*, P10025 (2011).

[74] R. García-García, D. Domínguez, V. Lecomte, and A. B. Kolton, *Phys. Rev. E*, **82**, 030104 (2010); arXiv:1111.5369v2.

[75] H. Risken; *The Fokker-Planck equation*, Springer-Verlag, 1984.

[76] See, for example: R. Monasson and S. Cocco, *Journal Computational Neuroscience*, **31** 199 (2011); S. Cocco, R. Monasson and V. Sessak, *Phys. Rev. E*, **83** 051123 (2011)

[77] J. Nocedal, *Mathematics of Computation*, **35** 773-782 (1980)

[78] C. Pérez-Espigares, A. B. Kolton and J. Kurchan, to be published.

[79] A. B. Kolton, R. Exartier, L. F. Cugliandolo, D. Dominguez and N. Gronbech-Jensen, *Phys. Rev. Lett.* **89**, 227001 (2002).

[80] V. Y. Chernyak, M. Chertkov and C. Jarzynski, *J. Stat. Mech.*, P08001 (2006).

[81] This seems to be related to the expression, valid for systems that satisfy detailed balance, obtained in: T. Sagawa and M. Ueda, *Phys. Rev. Lett.*, **104**, 090602 (2010). Here the difference is that we are trying to approximate driven systems whose stationary measure we do not know.

[82] B. Derrida, B. Douout and P.-E, Roche, *J. Stat. Phys.* **115**, 717 (2004)

[83] T. Bodineau and B. Derrida, C. R. Physique **8**, 540 (2007).

[84] R.J. Harris and G.M. Schütz, J. Stat. Mech. P07020 (2007).

[85] G.M. Schütz, in *Phase Transitions and Critical Phenomena* vol. 19, ed. C. Domb and J.L. Lebowitz, London Academic (2001).

[86] A. Rákos and R.J. Harris, J. Stat. Mech. P05005 (2008).